CHARACTERIZING TEMPERATURE INDUCED STRENGTH DEGRADATION AND EXPLOSIVE SPALLING IN ULTRA HIGH PERFORMANCE CONCRETE

By

Mahmood A. Sarwar

A THESIS

Submitted to
Michigan State University
in partial fulfillment of the requirements
for the degree of

Civil Engineering—Master of Science

2017

ABSTRACT

CHARACTERIZING TEMPERATURE INDUCED STRENGTH DEGRADATION AND EXPLOSIVE SPALLING IN ULTRA HIGH PERFORMANCE CONCRETE

By

Mahmood A. Sarwar

Significant research and development in concrete technology have led to the evolution of ultra-high-performance concrete (UHPC). UHPC possesses excellent durability and ductility characteristics, and exemplary tensile and compressive strength properties. Therefore, owing to its superlative properties UHPC is being progressively used in infrastructure and must satisfy fire resistance requirements. Yet, evaluating fire resistance requires knowledge of elevated temperature mechanical properties, and unfortunately such properties are lacking. Furthermore, exploratory investigations reveal UHPC's composition and construct precipitate the temperature engendered dilapidation of its strength, and it is highly susceptible to fire induced spalling.

To fulfill this integral gap, a comprehensive experimental study was undertaken to develop temperature induced degradation in compressive strength, along with the fire induced spalling behavior of UHPC. Variables were introduced to the testing program through varying the content and type of fibers, and varying the application of heating rate. Furthermore, UHPC's results were compared to four conventional concretes tested, and recommendations as prescribed in ASCE (1992) and Eurocode 2 (2004). Results from the experimental testing reveal the compressive strength and stress-strain behavior of UHPC deviates from conventional concretes, and there is a vast disconnect amongst the experimental results and recommendations prescribed in codes. Moreover, successful testing of UHPC at and above 300°C, was only possible through drastically reducing the heating rate to less than 0.75°C/min. Otherwise, employing higher heating rates induces explosive spalling at temperatures as low as 190°C.

To my Beevee, our three babies, Baby Girl, Iman and Afreen, and to all the children who have suffered through war and tragedy.

ACKNOWLEDGEMENTS

Sincere thanks go in particular to my supervisor Prof. Venkatesh Kodur for his valuable guidance and constructive suggestions he provided in undertaking this research and in preparation of this thesis. Also, special thanks to the distinguished faculty members who served on my committee: Professors: Parviz Soroushian and Weiyi Lu. Thank you to all my committee members for their support, patience, encouragement, useful suggestions and guidance.

Most importantly, I thank God who brought my wife and I together. Her continuous love, care and patience is what keeps me on my feet. Also, I would like to thank the whole of our research group, especially Mohannad Naser, Ankit Agrawal, Xu Dong, Saleh Alogla, Puneet Kumar, Roya Solhmirzaei and Esam Aziz.

Thanks to the faculty and staff in the CEE department, Veterans Certification Team and Student Veteran Resource Center for their support and help, especially the manager of the Civil Infrastructure Laboratory Mr. Siavosh “Sia” Ravanbakhsh for his mentorship and everlasting patience. Without his guidance, I would not have been able to complete my experimental testing. Additionally, I would like to extend my thanks to Mrs. Laura Taylor, Mrs. Margaret Conner and Mrs. Laura Post for all their help.

Lastly, thank you to all my family for their love and continuing prayers.

TABLE OF CONTENTS

LIST OF TABLES

LIST OF FIGURES

CHAPTER ONE

1. INTRODUCTION

1.1 General

The use and implementation of concrete for construction can be traced as far back as over 3500 years (Hertz, 2003). Despite the extraordinary advancements in technology since then, the compulsion for builders to utilize concrete continues to endure the test of time. On both a domestic and global scale, the yearly manufacturing of concrete surpasses any other material, with 8 billion cubic meters globally, and 180 million cubic meters within the United States (Ulm, 2008; Kosmatka and Wilson, 2011). Whether dictated by consumer demand, or simply by availability of resources, the relentless global appetite for concrete continues to further research and development in its strength, durability, and sustainability properties.

In the early twentieth-century Abrams (1919) determined that water content was the critical constituent that determines the resulting compressive strength of concrete. Approximately a decade later, researchers discovered concrete's strength could be increased during placement through the application of pressure (Richard and Cheyrezy, 1995). Furthermore, it wasn't until the 1970's that concrete's density was increased by the addition of silica fume, and/or water reducing admixtures, allowing the compressive strength to drastically increase in the range between 50-120 megapascal (MPa) (Hertz, 2003; Buchanan and Abu, 2017). Such a concrete is referred to as high strength concrete (HSC), and concrete with compressive strength less than 50 MPa is commonly denoted as normal strength concrete (NSC). Finally, in the mid-1990s researchers developed a concrete with a denser microstructure, named ultra-high-performance concrete (UHPC), otherwise known as reactive powder concrete (RPC). UHPC provides compressive strength beyond 150 MPa, tensile strength (post-cracking) higher than 5 MPa, elastic modulus in the range of 40-70

gigapascal (GPa), protection from detrimental compounds (chloride or alkali silica reaction), freeze-thaw resistance, blast resistance and increased ductility with the inclusion of steel fibers (Kosmatka and Wilson, 2011; Graybeal, 2015; Gu et al., 2015; Li et al., 2015). Such supreme mechanical properties enable UHPC to be a versatile and durable material. UHPC has a surfeit amount of applications including construction of infrastructure, strengthening and rehabilitation of structures, and within military, petroleum, marine, and nuclear facilities (Kosmatka and Wilson, 2011; Zheng et al., 2014a; Gu et al., 2015). In North America UHPC is predominantly utilized for the construction of bridges to exploit its excellent compressive and tensile strength properties (Graybeal, 2014). As of 2014, 55 bridges and overpasses were constructed employing UHPC (Russell and Graybeal, 2013). The Hosokawa River Tunnel in Japan is the first in its class to be retrofitted utilizing UHPC (Gu et al., 2015).

However, UHPC's implementation is limited to certain areas due to autogenous shrinkage during the early stages of curing, high cost and its poor fire resistance characteristics. Extreme cases of autogenous shrinkage occur in very thin applications of UHPC, but can be avoided with certain admixtures. The initial high cost is due to the volume and type of ingredients used (cement, silica fume, etc.), and availability of such materials (Soliman and Nehdi, 2011; Canbaz, 2014; Yazıcı et al., 2010; So et al., 2015). Nevertheless, implementing a stronger material as UHPC allows the structural engineer to choose a reduced cross section (Russell and Graybeal, 2013). Furthermore, the cost may be driven down by implementing industrial by-products within the UHPC design mix. Contents of silica fume and cement may be reduced by substituting with ground granulated blast furnace slag (GGBFS) or fly ash, while maintaining UHPC's high mechanical properties (Gesoglu et al., 2015; Xiao et al., 2014; Yazıcı et al., 2009; Alkaysi, 2016; So et al., 2015). Whereas UHPC's reduced cross section subsides the cost, with increasing temperatures it

exacerbates the strength degradation and chance of explosive spalling (Hertz, 2003; Kodur, 2014). The spalling (Figure 1.1) process occurs when concrete is hastily heated, and the vaporized water begins to increase and build up. If there is no clear avenue to release the built-up pore pressure (due to low permeability), it will eventually surpass the concrete's tensile strength and experience explosive spalling (Khaliq, 2012; Buchanan and Abu, 2017). Depending on the type and size of fire, a structure exposed to such an extreme environment signifies one of the most dire circumstances (Kodur and Phan 2007; Zheng et al., 2012; Kodur, 2014). Given the predominant use of UHPC within North America is for transportation structures, detailed data pertaining to such structures affected by fire exposure is now presented. Transportation structures must endure higher temperatures since the source of fire is petroleum, and fire temperatures can reach 815°Celsius (°C) within the first three minutes (min), which is 66% greater than a standard temperature versus time fire curve such as ASTM E119 (Kodur and Phan, 2007).

During the last 22 years, seven fires within tunnel structures have occurred. The Channel Tunnel, connecting Britain and France was the first to suffer such a disaster while employing HSC (Hertz, 2003; Ingason, 2004; Aydin and Baradan, 2012; Bei and Zhixiang, 2016). Due to HSC's low permeability the Channel Tunnel, along with the Great Belt Tunnel in Denmark, suffered extreme damage in the form of spalling (Aydin and Baradan, 2012; Buchanan and Abu, 2017). The Channel and Great Belt Tunnels' fire reached a maximum temperature of 1,100 and 800°C, respectively (Khoury, 2000). On the other hand, bridges experience greater damage due to fires. From 1989 to 2000, 16 U.S. bridges collapsed due to fire, and from 2002 to 2015, the number jumped to 27 (Naser and Kodur, 2015; Aziz, 2015). Furthermore, records from 2014 reveal, of the 200,000 fire occurrences via motor vehicles in the United States, nearly 90% occurred while traveling on the highway resulting in 345 deaths and $1.5 billion worth of damage (NFDC, 2017).

Considering the increased desire for engineers to select UHPC as a building material, the fire behavior of UHPC must be investigated, and as per local structural provisions these structures must adhere to the fire resistance requirements. However, no requirements regarding fire resistance currently exist for bridges further increasing the consternation, and proving to be quite contrary to fire safety's main objectives (Naser and Kodur, 2015; Buchanan, and Abu, 2017).

1.2 Fire resistance properties of concrete

The fire resistance of a structural member is its ability to withstand elevated temperatures without compromising its structural integrity, stability, and the transmission of heat (Kodur, 2014). Different criteria may be utilized, but fire resistance is typically measured in time. Moreover, depending on the type of structure, it must maintain the previously mentioned conditions for a given specified duration as prescribed in local codes. Thus, for infrastructure applications, fire resistance is imperative. In addition, concrete as a material possesses excellent resistance properties because of its non-combustible nature, coupled with its low thermal conductivity, and high specific heat (Behloul et al., 2002; Kosmatka and Wilson, 2012; Kodur, 2014; Buchanan and Abu, 2017). The combination of such qualities enable concrete to experience a gradual progression of heat across the section and minimize the spread of fire throughout the structure (Kosmatka and Wilson, 2011). However, with the inclusion of silica fume and reduction of water content to achieve denser concrete, the fire resistance is inversely proportional to its strength, and explosive spalling further thwarts its resisting ability. As opposed to NSC and HSC, UHPC's rudiments are attributed to its granular elements allowing reduction of the cross section, precipitating the diminution of its fire resistance. Therefore, prior to implementing a novel material such as UHPC, understanding the potential of its material behavior with increasing temperature is preeminent. Exploiting the ambient condition mechanical properties of concrete allow the development of

varying structural arrangements. However, considering the inherent hazard a fire disaster poses and to ensure the structure meets its fire resistance requirements, the mechanical properties of concrete at elevated temperatures must be understood. The following section will discuss the constituents of concrete influencing the principle mechanical properties, and the risk of temperature induced strength dilapidation.

1.3 Mechanical properties of concrete at elevated temperature

Mechanical properties of materials experience a degradation with increasing temperatures. Nevertheless, the composition and construct of concrete can serve as a catalyst to the rate of reduction. The cement paste undergoes several decompositions and dehydration of chemically bound water, resulting in strength loss at each respective temperature. Moreover, the amount of cement can further exaggerate the decrease in strength (Klingsch, 2014). The type and size of aggregate can influence the fire resistance as well. With the former, limestone's specific heat is much greater than quartz, therefore providing a greater resistance to fire exposure (Kodur and Phan, 2007). Additionally, quartz's dramatic expansion in volume at temperatures above 500°C, results in further loss of strength (Schrefler et al., 2002; Jang et al., 2016). The latter, dictates the permeability of the concrete, thereby influencing the strength. Utilization of silica fume or the use of finer aggregates jointly with silica fume, will deliver a progressively increasing dilapidation of the concrete's mechanical properties and allow the concrete to be more vulnerable to explosive spalling (Kodur, 2014). Including polymer fibers to denser concretes may alleviate the explosive spalling but will decrease its strength.

As compared to conventional concretes, UHPC is designed on the premise to increase the fineness of its elements to capitalize on its packing density (Kosmatka and Wilson, 2011; Ju et al., 2013; Zdeb, 2013; Richard and Cheyrezy, 1995; Canbaz, 2014). The optimization of the packing

density of UHPC is achieved through minimizing the porosity of the UHPC, and exploiting any available space within the concrete's matrix (Magureanu et al., 2012; Zdeb, 2013). The dense microstructure is achieved through a combination of, (1) low water-to-cement (w/c) ratio of 0.20 or lower, (2) addition of superplasticizers, silica fume, and steel fibers, (3) employing quartz sand vice coarse aggregate (grain size is reduced by a factor of 50), and/or (4) through additional treatments, such as thermal, and/or applied pressure (Hager et al., 2013; Zdeb, 2013; Wang et al., 2015; Wang and Gao, 2016). Thereby, the mechanical properties will suffer a rapid degradation, as opposed to the conventional concretes. Additionally, though UHPC has tremendous compressive and tensile strength, the dense matrix causes it to be tremendously vulnerable to explosive spalling and the data associated to UHPC at high temperature conditions is limited. UHPC's strongest attributes conversely serve as its paramount imperfection at elevated temperatures.

1.4 Objectives of this research

The foremost aims of this research are to illustrate the variation of temperature-dependent compressive strength of different UHPC types as compared to other conventional types of concretes, and to highlight the details pertaining to explosive spalling within UHPC through an inclusive experimental study. To successfully complete these goals, the research objectives listed below were accomplished:

- Conduct a detailed state of the art literature review on the thermal and mechanical responses of concrete at elevated temperatures. Also, to enumerate the pertinent research gaps, specifically with respect to UHPC properties at elevated temperatures. The thorough literature review will incorporate experimental and analytical studies.

- Evaluate compressive strengths of three design mixes of UHPC at various temperatures (20, 100, 200, 300, 400, 600 and 700°C), immediately following exposure to elevated temperatures. Also, undertake compressive strength tests with differing design mixes of NSC and HSC for comparison.
- Trace the explosive spalling behavior of the UHPC specimens at the elevated temperatures stated previously.
- Compare the temperature dependent compressive strength and explosive spalling behavior of UHPC with other concrete types, ASCE (1992) and Eurocode 2 (2004).

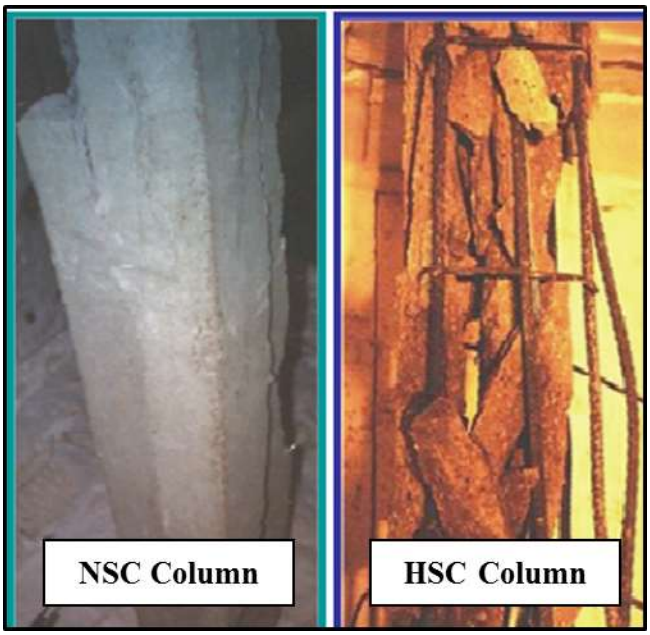

Figure 1.1: Photos depicting explosive spalling in a NSC and HSC column under elevated temperatures (Khaliq, 2012)

CHAPTER TWO

2. STATE OF THE ART REVIEW

2.1 General

UHPC's paragon properties allow the employment of such a material in diverse functions. However, with increasing temperatures, UHPC will result in a disparate degradation and associated properties given its granular microstructure; Thus posing a hindrance in reaching the required fire resistance. Therefore, for evaluating fire resistance of structural members, properties at elevated temperatures are required. Moreover, understanding the temperature induced physiochemical changes provides further insight regarding concrete's deterioration.

Klingsch (2014) presents a consolidated table that is consistent with other research conducted, providing the rising temperature with the effect on concrete (Table 2.1). The most notable points will be presented and the data is from the following research, Felicetti et al. (2000), Schrefler et al. (2002), Dehn (2004), Klingsch (2014), Way and Wille (2015), Zheng et al. (2015) and Bei and Zhixiang (2016). At temperatures above 105°C, the physical water is completely evaporated causing an increase in porosity and mechanical properties to decrease. Whereas in higher strength concretes the free water can still produce disastrous results in the form of explosive spalling. The likelihood of explosive spalling is increased at temperatures of 100-300°C upon the evaporation of the chemically bound water within the cement paste. The decomposition of the binder at the above-mentioned temperature range triggers strength loss as well.

Further strength loss is attributed to the following, (1) the formation of lime (CaO), from calcium hydroxide, $Ca(OH)_2$, and the magnitude of strength loss is contingent upon the calcium-oxide (CaO) to silica-dioxide (SiO_2) (C/S) ratio of the concrete mixture, (2) concrete with siliceous

aggregate will cause apparent expansions and result in microcracking due to the α-quartz transforming to β-quartz around 573ºC, (3) temperatures above 700°C the decarbonation of $CaCO_3$ produces additional CaO, along with carbon dioxide (CO_2), and from 800-1000°C all chemically bound water within the cement matrix evaporates. Upon cooling of the concrete, CaO rehydrates from the air and $CaCO_3$ reforms, resulting in drastic widening of the cracks (up to 40% increase). Lastly, within siliceous aggregate concrete, the β-quartz retransforms to α-quartz at 573ºC followed with a steep contraction (Khoury, 2000; Schrefler, 2002; Hertz, 2005). Though research pertaining to traditional concrete's fire behavior is ongoing, owing to UHPC's composition and construct, grasping its full depth is in its embryonic stage. The following sections will present research pertaining to concrete's thermal and mechanical properties, and the occurrence of fire induced spalling.

2.2 Thermal properties of concrete

2.2.1 General

Concrete is an inert material possessing low thermal conductivity and high specific heat. Such qualities enable it to prevent the spread of fire because it diminishes the progress of heat. However, due to the concrete undergoing physiochemical changes with increasing temperatures, the thermal properties do not remain constant, thereby inflicting change upon the mechanical behavior of concrete with increasing temperatures. Therefore, understanding the behavior of a material exposed to high temperatures, enable the designer to fully exercise the material's full potential.

2.2.2 Test methods for high temperature thermal properties

There are two methods to determine the thermal conductivity of a material. First is the hot wire method and second is the guarded heat flow meter method. The guidelines associated with

the former are presented in ASTM C1113/C1113M (2013), and for the latter in ASTM E1530-11 (2016). The hot wire method may be utilized to evaluate the thermal conductivity up to 1500°C, and utilizes an electrical current passing through a wire that is between two blocks of the material to be tested. Depending upon how fast the heat flows to the material block determines the thermal conductivity value. The second method, guarded heat flow meter method, can accurately provide the thermal conductivity up to 325°C. At temperatures beyond 325°C, it is dependent upon the calibration of the equipment. In this method, the material to be tested, along with a heat flux transducer (HFT), are placed between two controlled temperature plates. Therefore, dependent upon the heat transfer from one plate to the other determines the thermal conductivity for the material.

To determine the specific heat capacity, the guidelines prescribed in ASTM E1269-11 (2011) recommend using differential scanning calorimetry method. The test is accurate at temperatures between 100-600°C, and beyond it is dependent upon the equipment utilized. The test can be performed very quickly and is simple to conduct. Essentially, select a benchmark and measure the change in heat flow between another selected point and the benchmark.

To evaluate the linear thermal expansion of a solid material, one method is to employ a thermomechanical analysis as recommended in ASTM E831-14 (2014). The test is effective up to 900°C, and beyond it is dependent upon the equipment utilized. The specimen is exposed to a consistent heating rate and the expansion of the material is recorded with respect to temperature.

Lastly, to determine the mass loss of a material, ASTM E1868-10 (2015) recommends utilizing the thermogravimetry method. The test is valid up to 1000C and applicable to a wide range of materials. The specimen is subjected to a consistent temperature and the mass is measured for

either a specified time or once the loss attains a specified value. Following the heating process, the percent of mass loss is calculated by dividing the mass loss divided by the original mass.

2.2.3 Previous studies on thermal properties

Investigations pertaining to conventional concrete's thermal properties have been ongoing for over 4 decades. Moreover, ASCE (1992), Eurocode 2 (2004) and several researchers formulated constitutive relationships pertaining to both NSC and HSC's thermal properties with increasing temperatures. As compared to conventional concretes, UHPC's thermal properties have scarcely been researched in the last 2 decades. Furthermore, no current codes dictate the constitutive relationship of UHPC either. The following two sections will impart the notable points from literature pertaining to the effect of elevated temperatures on the thermal properties of conventional concretes and UHPC.

2.2.4 Effect of temperature on thermal properties of conventional concretes

As compared to carbonate aggregate, siliceous aggregate contributes negatively with respect to fire resistance, and except for the thermal expansion at temperatures above 700°C, NSC and HSC's thermal properties are very similar (Lie and Kodur, 1996; Kalifa et al., 2000; Sultan and Kodur, 2003). Concrete with siliceous aggregate's specific heat remains steady and only experiences a bump around 450ºC, which is attributed to the formation of CaO and H_2O from $Ca(OH)_2$. Moreover, the coefficient of thermal expansion (CTE), of siliceous aggregate concrete will abruptly rise around 550°C, due to the quartz transformation. While, the disjoining of $CaCO_3$ will cause two occurrences to transpire in carbonate aggregate concrete. At 700°C, the specific heat undergoes a drastic spike, and at 800°C the CTE deviates from a steady linear rise (So et al., 2014). The thermal conductivity experiences a steady decrease, with the siliceous concrete having

the higher values and, the mass loss progressively rises linearly but drastically reduces beyond 700°C due to all the chemically bound water evaporating.

2.2.5 Effect of temperature on thermal properties of UHPC

Aside from the thermal diffusivity, RPC's thermal conductivity, specific heat capacity and mass loss are lower than HSC. Additionally, if compared at temperature levels, the CTE is about the same (Ju et al., 2011). The thermal conductivity and thermal diffusivity decrease with increasing temperatures, while the specific heat capacity and CTE continuously rise (Behloul et al., 2002; Zheng et al., 2014b). Ju et al. (2011) examined the effects of steel fiber content and discovered altering the content of steel fiber only influences specific heat capacity and thermal diffusivity.

Behloul et al. (2002) and Wang et al. (2013) studies reported very similar results pertaining to the CTE. Both experienced a linear progression (roughly $12e^{-6}$/°C) to about 500°C and both encounter a slight bump between 300-400°C. The bump between 300-400°C is attributed to the decomposition of $Ca(OH)_2$. Beyond 500°C, the CTE experiences a dramatic increase due to the α-quartz transforming to β-quartz, followed by a decline after 700°C. Finally, Zheng et al. (2014b) exposed RPC to temperatures of 20 to 800°C and found a smooth and steady mass loss with increasing temperatures.

2.3 Mechanical properties of concrete

2.3.1 General

The major proponents of concrete's mechanical properties are compressive and tensile strength, ductility, stress-strain relationship, and elastic modulus. The preceding properties degradation dictates whether the fire resistance design is acceptable. Prior to presenting the data from literature pertaining to concrete's behavior to increased temperatures, a synopsis regarding

concrete's mechanical behavior under ambient conditions is discussed, and research investigating UHPC/RPC and ultra-high performance fiber reinforced concrete (UHPFRC) under service conditions is presented.

At room temperature, the w/c ratio coupled with the percentage of contact amid the binder with the coarse aggregate, called interface transition zones, play a crucial role regarding the concrete's strength (Kodur, 2014; So et al., 2014; Kamen et al., 2007). In very dense concretes, the strength is directly contributed by the w/c ratio, integrated with granular constituents and silica fume (Xiao et al., 2014). Specifically, superfluous amounts of silica fume (20-25% the weight of cement) make up UHPC's binder, and as cement (C_3S) mixes with water, (H_2O) the chemical reaction results in calcium silicate hydrate, C-S-H and $Ca(OH)_2$. Therefore, in addition to minimizing the voids within UHPC's matrix, silica fume contributes further by decreasing the C/S ratio, resulting in less production of $Ca(OH)_2$, and increase the production of C-S-H (Khoury, 2000; Schrefler et al., 2002; Kosmatka and Wilson, 2011; Zdeb, 2013). The C-S-H's role in dense concretes is quite significant as it serves as the chief binder directly contributing to its mechanical properties and houses majority of the chemically bound water (Burke, 2011; Jagannathan, 2013; Klingsch, 2014). Considering UHPC's very dense microstructure, it enables UHPC to have superior mechanical properties as compared to NSC and HSC at ambient conditions.

The current literature pertaining to UHPC/RPC or UHPFRC at ambient conditions predominantly explores different methods to increase the mechanical properties utilizing various treatments or with altering the main ingredients. On the contrary, research pertaining to exploring environmentally friendly and/or sustainable UHPC is quite limited. Yazıcı et al. (2010), Aydin and Baradan (2013), Gesoglu et al. (2015) and Peng et al. (2016) conducted research to develop a UHPC that maintains its mechanical properties while being environmentally conscience,

sustainable or economical. Table 2.2 provides a summation of tests regarding UHPC/RPC and UHPFRC, conducted in ambient conditions. Unless compressive strengths greater than 300 MPa are required, developing the appropriate design mix (with no treatment) will result in compressive strengths as high as 200 MPa, (Wille et al., 2011; Zdeb, 2013; Voit and Kirnbauer, 2014).

2.3.2 Testing methods for high temperature mechanical properties

Extensive research studies at ambient conditions for NSC, HSC and UHPC conducted by Elwell and Fu (1995) and Graybeal and Davis (2008) provide guidance on choosing the specimens' shape and state that choosing a cylinder or cube specimen is purely preference and does not alter the strengths. Furthermore, no ASTM standard exists to evaluate mechanical properties of concrete at elevated temperatures. Therefore, RILEM Standard (RILEM Technical Committee 200-HTC, 2007) is utilized to standardize the heating process and dimension requirements, while the respective ASTM standard is implemented for each different mechanical property test. Consolidated recommendations from the RILEM standard pertaining to the high temperature mechanical property tests are presented.

RILEM standard recommends three different steady state tests to evaluate mechanical properties at elevated temperatures, (1) unstressed, (2) stressed, and (3) residual state. The unstressed condition demands once the specimen attains its testing temperature, to remain in the furnace for a specified duration to reach complete saturation across the specimen. If a load is to be applied during the heating process, referred to as a stressed test, it must remain constant and must be a certain percentage of the at room temperature compressive strength until complete saturation is attained. Upon saturation of the specimen, the load is increased until failure of the specimen. For the residual-state, the specimen must completely cool down to the ambient condition prior to testing. The compressive strength, stress-strain behavior, and elastic modulus may be evaluated

using either of the three methods. While the tensile strength is recommended only for unstressed or residual state.

2.3.3 Previous studies on mechanical properties

Just as each element serves a purpose to contribute to concrete's facets, the constituent(s) can undesirably affect the structural member's performance with increasing temperatures. There is significant ongoing research evaluating the mechanical properties of conventional concretes. Owing to HSC's differing microstructure, literature indicates HSC's mechanical properties decrease faster as opposed to NSC (Zheng et al., 2012; Kodur, 2014). Furthermore, HSC is prone to explosive spalling and mitigation techniques must be utilized. Further discussion pertaining to fire induced spalling will be presented in section 2.4. Discordant with conventional concretes, the bulk of UHPC's studies have been conducted in the last 5 years. Attributed to UHPC's granulated elements, and superior strength, its fire performance is dissimilar as compared to the conventional concretes. UHPC's assets touted by its advocates prove to be its downfall when exposed to elevated temperatures. With increasing temperature, the multitude of physiochemical changes, dilapidation, and the inconsistency of properties between the binder and aggregate undergo, heavily contribute to UHPC's mechanical property degradation (Khoury, 2000; Zheng et al., 2015; Li and Liu, 2016). Unless proper measures are taken (for instance the addition of fibers or employ pozzolanic resources), UHPC will not be able to endure the elevated temperatures for long (Khoury, 2000; Ye et al., 2012).

Table 2.3 provides a summation of studies regarding UHPC/RPC and UHPFRC conducted at elevated temperatures, identifying the strengths, and disadvantages for each investigation. Summarizing Table 2.3 the current research pertaining to UHPC's mechanical properties exposed to increasing temperatures is dominated by residual state testing of customary UHPC design mixes.

Less than one-third explore the behavior with varying fiber type and content. Only three studies evaluate UHPC with a treatment and an additional three investigate the fire behavior of more economical and environmental design mixes of UHPC. In addition, most studies evaluate the compressive and tensile strength and only a handful cover the stress-strain relationship along with the elastic modulus. Finally, there are very few investigations proposing models to predict the explosive spalling behavior of UHPC. The following sections will impart the notable points from literature pertaining to the effect of high temperatures on the mechanical properties of conventional concretes and UHPC.

2.3.4 Compressive strength

2.3.4.1 Effect of temperature on compressive strength of conventional concretes

Investigations pertaining to conventional concretes display compressive strength decreasing with rising temperatures and HSC experiencing a steeper degradation (Arioz, 2007; Sarhat and Sherwood, 2013). However, due to the removal of free water and consolidation of concrete, the denser HSC design mixes underwent an increase in strength between 200-300ºC (Ghandehari et al., 2010). Furthermore, the 300 to 600ºC range is crucial for denser concretes, with great strength loss by 600ºC (Demirel and Keleştemur, 2010; Ghandehari et al., 2010). A handful of researchers utilized either recycled or locally available aggregate for NSC or HSC, and discovered the results are comparable to typical aggregates, and quartz dominant concrete will provide a poorer performance with increasing temperatures (Sarhat and Sherwood, 2013; Hager et al., 2016). Yet, if a pozzalanic material blend is implemented to reduce the amount of cement, the concrete's strength underwent a more rapid deterioration (Demirel and Keleştemur, 2010; Li et al., 2014). In addition, employing higher contents of cement will provide greater strengths under ambient conditions, while suffering a quicker decline with the temperature rise (Ergün et al., 2013).

A higher content of w/c ratio does not greatly affect the relative strengths, but will allow a more rapid decrease in strength (Arioz, 2007; Al-Jabri et al., 2016).

2.3.4.2 Effect of temperature on compressive strength of UHPC

UHPC is contrived to deliver high compressive strengths at ambient conditions. However, unless the proper mixture is formulated, UHPC will experience sudden degradation and/or explosive spalling. UHPC's compressive strength at elevated temperatures is dependent upon the design and Figure 2.1 illustrates the sporadic results amongst the literature for UHPC/RPC studies from the last three years (Kodur, 2014).

Behloul et al. (2002), Ye et al. (2012) and Zheng et al. (2015) were the only studies evaluating the hot-state compressive strength and two of those, Behloul et al. (2002) and Ye et al. (2012) were stressed while being heated. The non-cured UHPC mix studied by Behloul et al. (2002) performed exceptionally well, attaining 120% of its room temperature strength at 500°C. The unstressed test degraded the fastest to 50% at only 500°C (Zheng et al., 2015).

The remainder of tests evaluated the residual compressive strengths. For the most part the tests conducted attain 115-160% of their respective original strength between 100-400°C, soon followed by a steady decline. Aydin and Baradan (2012) and Bashandy (2013) studies experienced explosive spalling beyond 300°C. Aydin and Baradan (2012) design contained high volume of silica fume and cement, while Bashandy (2013) utilized locally available steel fiber and cement to produce an economic RPC. So et al. (2015), Way and Wille (2015) and Jang et al. (2016) achieved the greatest residual compressive strengths of 145, 160 and 140% at 400, 300 and 400°C, respectively. Zheng et al. (2014a) and Zheng et al. (2014b) investigated UHPC with polypropylene and steel fiber alongside UHPC with polypropylene fiber, nearly lost 40% of the compressive strength at 100°C and only increased to 80% between 500-600°C.

Aydin and Baradan (2012), So et al. (2015) and Jang et al., 2016 studied the residual compressive strength behavior of UHPC with a ternary pozzalanic material blend. All three studies conducted tests at and beyond 800°C without experiencing explosive spalling and with comparable, if not improved fire behavior than their respective typical UHPC formula. Sanchayan and Foster (2016) tested RPC with a combination of steel fiber and polyvinyl alcohol (PVA) fibers. The RPC mix with high PVA and low steel fiber content behavior was similar, save the strengths attained at 300 and 400°C. Additionally, the high PVA fiber content RPC underwent explosive spalling beyond 500°C.

Approximately 15 of the studies evaluated the effects of varying the fiber content of the UHPC. Two researchers concluded the steel and polypropylene fibers contribute positively and 0.9% polypropylene fiber content is recommended (Tai et al., 2011; Abdul-Hussain, 2013). However, Hager et al. (2013) study revealed the content of polypropylene fibers do not provide an impact to UHPC's compressive strength. Canbaz (2014), Way and Wille (2015) and Xiong and Liew (2015) investigated the effects of various curing treatments. Canbaz (2014) evaluated RPC pressure treated and cured in water at 90°C and Way and Wille (2015) oven dried the UHPFRC and both achieved improvements with respect to the compressive strength. The RPC in Canbaz (2014) study experienced an increase up to 400°C, followed by a decline. However, Xiong and Liew (2015) research did not provide any substantial effect with respect to varying curing techniques.

2.3.5 Tensile strength

2.3.5.1 Effect of temperature on tensile strength of conventional concretes

The tensile strength of conventional concretes is influenced by the following at elevated temperatures, (1) enhancement through the addition of steel or hybrid fibers, (2) undergo

dilapidation with increasing temperatures, (3) experience a dramatic decrease beyond 300°C, and (4) HSC's tensile strength sustains a greater decrease as opposed to its compressive strength (Ghandehari et al., 2010, Khaliq and Kodur, 2011). Furthermore, the alteration of the cement content alone does not pose much of a difference with respect to the relative tensile strength, but employing a ternary pozzolanic blend will result in a drastic reduction to 20% of its original tensile strength at 500°C (Li et al., 2014). As expected, the quartz aggregate concrete displayed greater reduction as opposed to limestone aggregate, and increasing the w/c ratio will decrease the tensile strength as well (Al-Jabri et al., 2016; Hager et al., 2016). Finally, similar to the compressive strength, very dense HSC's tensile strength will increase from 100 to 200ºC, followed by a decline (Ghandehari et al., 2010).

2.3.5.2 Effect of temperature on tensile strength of UHPC

Only two studies evaluated both the hot-state and residual-state tensile (direct) strength of UHPC, Felicetti et al. (2000) and Behloul et al. (2002). While Felicetti et al. (2000) results displayed very little difference between the test types, Behloul et al. (2002) study demonstrated the hot-state tensile strength was slightly higher. The remainder of the residual direct tensile tests behave very similarly with increasing temperatures and achieve 50% of original strength between 450-550 (Zheng et al., 2014a; Zheng et al., 2014b; Li and Liu, 2016).

Four separate investigations tested the residual splitting tensile strength and Peng et al. (2012), Abdul-Hussain (2013) and So et al. (2015) results are very similar. Their original strengths reduce to 50% at about 600°C. While Bashandy (2013) presented drastic degradation, 50% at 300°C, may be attributed to utilizing cheaper steel and cement. Finally, five research studies tested the residual flexural strength and Aydin and Baradan (2012) and Ali et al. (2016) tested typical RPC mixture containing silica fume could not withstand temperatures above 300 and 400°C,

respectively. Additionally, Aydin and Baradan (2012), So et al. (2015) and Ali et al. (2016) found the RPC formulation implementing ternary pozzalanic materials performed quite well at and beyond 600°C. With So et al. (2015) results were exceptionally well, attaining near 150% of original strength at 400°C, reducing to 50% around 700°C and 22% at 1000°C. Aside from Aydin and Baradan (2012) ternary pozzalanic RPC mixture, the remaining RPC's tested up to and beyond 600°C, reached 50% of their respective original strength.

Khoury (2000) claims employing the splitting tensile and flexural strength tests do not provide an accurate representation and concludes the direct tensile strength tests is supreme. However, the literature is evenly distributed amongst the 3 types of tensile strength tests. Finally, increasing the steel fiber content directly contributes to tensile strength (Abdul-Hussain, 2013; Li and Liu, 2016). Figure 2.2 depicts the tensile strengths (direct tensile, splitting tensile and flexural strengths) at elevated temperatures from literature.

2.3.6 Stress-strain relationship and elastic modulus

2.3.6.1 Effect of temperature on stress-strain relationship and elastic modulus of conventional concretes

With increasing temperatures conventional concretes' peak strain increases, the ascension portion is near linear, the descent portion becomes progressively recumbent at temperatures of 500ºC and above, and the compressive strength and elastic modulus lessen (Chang et al., 2006; Zheng et al., 2012). Additionally, the elastic modulus degrades the fastest with rising temperatures amongst the mechanical properties. Finally, the elastic modulus is further reduced utilizing a ternary pozzolanic mixture to reduce the cement content. A study conducted by Li et al. (2014) discovered the addition of high contents of GGBFS hastily declines the elastic modulus at 500°C to nearly a tenth of its original elastic modulus.

2.3.6.2 Effect of temperature on stress-strain relationship and elastic modulus of UHPC

Only 3 of the studies evaluated the stress-strain relationship, of which two were residual. Zheng et al. (2012) demonstrated residual stress-strain curve attains the peak strain at 600°C, minimal change is seen up to 300°C and beyond 300°C, the curve becomes more flattened. While Tai et al. (2011) found the residual stress-strain curve's slope steadily decreases with progressing temperature. Greater steel fiber content improved the peak strain between 200-800°C for Tai et al. (2011) but only up to 600°C for Zheng et al. (2015) study. Moreover, Zheng et al. (2015) determined 2% steel fiber content to be most optimum for increasing ductility.

Three tests evaluated the hot-state elastic modulus, Behloul et al. (2002) research indicated UHPC decreasing to 50% of its original stiffness beyond 600°C, while Zheng et al. (2015) experienced a sudden degradation at 200°C. Behloul et al. (2002) conducted residual elastic modulus tests as well and found the residual elastic modulus to perform exceptionally well. The UHPC studied maintained within its original stiffness up to 600°C, only to reduce to 80% at 700°C. Hager et al. (2013) was the only other study to reach 50% decline around 800°C. Aside from Behloul et al. (2002) and Hager et al. (2013), the bulk of the remainder elastic modulus results, declined to 50% of its stiffness between 350-500°C.

Xiong and Liew (2015) test consisted of various curing methods and heating rates. Their findings displayed the curing techniques did not influence the stiffness and the UHPC exposed to higher heating rates degraded much sooner. Hager et al. (2013) tested various polypropylene fiber content and concluded the addition of polypropylene fiber does not contribute to RPC's stiffness. Figure 2.3 depicts the elastic modulus at elevated temperatures from literature for UHPC/RPC studies from the last two years.

2.4 Fire induced spalling

2.4.1 General

Hertz (1984) encountered explosive spalling and hypothesized ultra-high strength concretes developed utilizing silica fume, to densify the concrete's matrix, have a greater risk to experience explosive spalling. The explosive spalling was attributed to the obstruction of the vaporized water attempting to evacuate the heated specimen. Following further research, Hertz (2003) concluded the increased strength does not necessarily correlate to explosive spalling as much as the exorbitant dense medium attained with silica fume. Although HSC is more susceptible to explosive spalling than NSC, HSC tested with no silica fume proved to be tolerable of increasing temperatures and did not explode (Phan, 1996; Hertz, 2003; Kodur, 2014). Additionally, a comprehensive study conducted by Klingsch (2014) determined UHPC lacking silica fume exposed to extreme heating rates to survive without exploding either. Silica fume maintains a stout link with explosive spalling but there are other crucial factors as well. The following sections will present data from literature pertaining to the foremost causes of spalling and methods to minimize the occurrence.

2.4.2 Causes of spalling

Minimal permeability, temperature gradients, migration of moisture and pore pressure build-up, and thermal dilation contribute to explosive spalling (Zheng et al., 2013; Kodur, 2014; Xiong and Liew, 2015; Jang et al., 2016). Additionally, the threat is further augmented by the type of aggregate, specimen dimensions, low tensile strength, type of fire exposure and contents of silica fume, cement (w/c ratio) and limestone filler (Hertz, 2003; Zheng et al., 2013; Klingsch, 2014; Kodur, 2014). Consequently denser concretes experience explosive spalling mainly due to the development of temperature gradients and pore pressure build-up. Furthermore, UHPC is

formulated implementing granular constituents and may not adhere to the same mechanisms of explosive spalling as HSC, and regrettably UHPC's design foundation is concocted upon most of the risks previously listed (Ju et al., 2015; Ali et al., 2016). Therefore, UHPC will experience explosive spalling at a lower temperature and shorter time period (or much sooner) than HSC (Phan, 1996). According to literature, several researchers determined explosive spalling can occur at temperatures of 250°C and above (Khoury, 2000; Burke, 2011; Zheng et al., 2013).

2.4.2.1 Rate of heat and thermal stresses induced by thermal gradient

Attributed to concrete's low thermal conductivity, fire exposure causes thermal gradients to develop resulting in a fluctuation of physiochemical variations across the cross section and thermal stresses (Hertz, 1984). The result is further compounded with applications of excessive heating rates (type of fire). Hertz (1984) research determined the critical rate of heat to avoid explosive spalling with immensely dense concretes is as low as 1ºC/min. Klingsch and Frangi (2011) precursory investigation determined the same value (1ºC/min) for UHPC. However, decreasing the heating rate does not necessarily correspond to mitigation of explosive spalling, because it only minimizes the thermal gradients (Felicetti et al., 2000; Klingsch, 2014). Thermal gradients vastly impact the development of pore pressure and will be discussed further in the next section (Phan, 2008; Khaliq, 2012).

2.4.2.2 Pore pressure build-up

Current literature correlates the built-up pore pressure within concrete to be the pivotal cause leading to explosive spalling (Klingsch, 2014; Sanchayan and Foster, 2016). The complication is further exacerbated with low permeability and extreme heating rates (Burke, 2011). In addition, various studies conducted found chemically bound water alone can cause explosive spalling (Hertz, 1984; Hertz, 2003; Sanchayan and Foster, 2016). Therefore, it is no

question due to UHPC's exceptionally dense matrix coupled with high amount of cement, explosive spalling occurs.

With increasing temperatures, thermal gradients within the concrete's cross section will develop and covert the moisture into a vapor. Since concrete maintains a certain amount of permeability, the water nearest to the surface will evaporate, however some of the moisture will follow the pressure gradient and travel inwards and condensate due to encountering cooler temperatures (Ju et al., 2013; Klingsch, 2014). Eventually a saturated barrier will form resulting in increasing pore pressure and soon followed by explosive spalling (Burke, 2011; Klingsch, 2014; Kodur, 2014). To withstand such a pressure increase, it is paramount for low permeability concrete to have great tensile strength (Klingsch, 2014; Kodur, 2014). The process is referred to as moisture clog and is well documented within the literature (Kalifa et al., 2000; Phan, 2008; Dwaikat and Kodur, 2009; Felicetti and Lo Monte, 2013).

Explosive spalling can be predicted because the point of explosion will have a much higher pressure than amongst the remaining specimen (Ju et al., 2013). In addition, the moisture clog will occur at a greater temperature with decreasing permeability. However, inclusion of polypropylene fibers within a UHPC design mix reduces the temperature corresponding to the melting point of the fibers, 170°C (Klingsch, 2014; Ju et al., 2015).

2.4.3 Previous studies on fire induced spalling

Previous studies by researchers resulted in various measures for evaluating the explosive spalling within HSC and UHPC. The investigations implemented preventive measures such as the use of organic fibers, diminish the contents of cement and/or silica fume, and numerical models. Existing research overwhelmingly utilizes organic fibers, such as polypropylene fiber to alleviate explosive spalling, with only a handful utilizing pozzolanic constituents to reduce the silica fume

and cement contents, or the use of locally available material. Moreover, Klingsch (2014) and Ju et al. (2015) developed numerical models to predict the explosive spalling behavior of UHPC with compressive strengths greater than 150 MPa. Though, numerical models require sufficient facets and validation, they provide an immense capability to efficiently determine whether explosive spalling may occur (Dwaikat and Kodur, 2009; Klingsch and Frangi, 2011).

2.4.4 Methods for minimizing explosive spalling

A simple and cost-effective method to mitigate the occurrence of fire induced spalling is with the inclusion of polypropylene fibers (Behloul et al., 2002; Bei and Zhixiang, 2016). Polypropylene fibers melt at a temperature between 150-170°C creating pathways to release the built-up pore pressure, and alleviate the rise of thermal gradients (Klingsch and Frangi, 2011; Ju et al., 2015; Xiong and Liew, 2015). Moreover, various studies utilized mercury intrusion porosimetry (MIP) and scanning electron microscopy (SEM) to confirm pathways created by the melting of the polypropylene fibers and the total pore volume increasing between 2-7 times following heating up to 600°C (Hager et al., 2013; Zheng et al., 2014b; Bei and Zhixiang, 2016). The amount of polypropylene fibers required to avoid explosive spalling is dependent upon the entire UHPC design mix and literature displayed values as low as 0.9 kg/m^3 to greater than 2.0 kg/m^3 (So et al., 2014; Zheng et al., 2014a). Research conducted by Klingsch (2014) and Bei and Zhixiang (2016) went further to assert the individual polypropylene fibers' dimension is paramount. The length must be of appropriate size to allow a continuous path for the vapor pressure to follow and the diameter must be kept minimal. Lastly, polypropylene fibers diminish the workability and strength of UHPC and must be implemented proficiently, and researchers advise their use may prove to be ineffective for encapsulated structures (Behloul et al., 2002; Hertz, 2003; Klingsch and Frangi, 2011; Aydin and Baradan, 2012).

An alternate method alleviate explosive spalling is to increase the tensile strength of the concrete with the incorporation of steel fibers. Though studies have displayed the effectiveness of steel fibers with HSC, the literature is not in total agreement with their use in UHPC (Klingsch, 2014; Kodur, 2014; Xiong and Liew, 2015; Bei and Zhixiang, 2016). Furthermore, implementing a hybrid fiber (steel and polypropylene fibers) UHPC design mix displayed an improved performance regarding the mitigation of the explosive spalling. Although polypropylene and steel fibers serve an elementary method to reduce the explosive spalling hazard, researchers are evaluating other lucrative techniques as well.

To utilize RPC in marine applications to avoid corrosion, while satisfying a tolerance to elevated temperatures, Sanchayan and Foster (2016) conducted a study to determine if PVA fibers can be utilized as an effective substitute for steel. By varying the different fiber contents, the research developed a RPC design mix mitigating the explosive spalling risk through combining PVA fibers along with a small amount of steel fibers, and oven drying the specimens. Although inclusion of PVA fibers reduces the compressive strength, the stiffness comparatively remains the same. Finally, Aydin and Baradan (2012), So et al. (2015) and Jang et al. (2016) successfully utilized ternary pozzolanic materials consisting of GGBFS, fly ash and silica fume to avoid explosive spalling.

2.5 Research gaps

As per the state of the art literature review, only few studies evaluating the residual-state mechanical properties of UHPC have been conducted in the past five years. Furthermore, data supporting the thermal properties of UHPC with increasing temperatures are severely sparse. Although the residual-state mechanical properties are important, it is quite evident the high temperature properties are lacking. To facilitate evacuation of occupants and allow the first responders an opportunity to fight the fire, the structure must remain standing for the duration it was designed for. Thus, the high temperature mechanical properties are imperative and the following research gaps remain:

- No standard exists to evaluate the properties of a cementitious composite such as UHPC/RPC or UHPFRC, at elevated temperatures.
- Thermal properties of UHPC with increasing temperature are deficient.
- Higher temperature mechanical properties of UHPC are gravely scarce.
- Detailed data and modelling of the fire induced spalling nature of UHPC is lacking.
- Impact to UHPC's high temperature mechanical properties with varying steel fiber content.
- Impact to UHPC's high temperature mechanical properties with a hybrid (steel and polypropylene) fiber content.
- Impact to sustainable and lucrative design mixes of UHPC's high temperature and residual-state properties.

Table 2.1: Temperature rise and effect on concrete, adapted from Klingsch (2014)

Temperature, °C	Resulting change to concrete
20-100	Concrete loses free and physical water (begins to dry)
105	Start of hydrothermal reaction
120-150	C-S-H phase decomposes
150	C-S-H's first peak
270	C-S-H's second peak
>300	Porosity and micro cracking drastically intensify
374	Complete evaporation of free and physically bound H_2O (critical point)
400-600	Detachment of calcium hydroxide, $Ca(OH)_2 \rightarrow CaO + H_2O$
535	Decomposition of $Ca(OH)_2$ maximum point
573	α-quartz transforms to β-quartz (reversible), leading to pronounced expansion
>700	Within cement paste and limestone decarbonation of calcium carbonate; $CaCO_3 \rightarrow CaO + CO_2$
710-720	C-S-H's decomposition, third peak
>800	Full evaporation of all water chemically bound
1200	Melting of concrete ensues

Table 2.2: Survey of UHPC/RPC and UHPFRC studies conducted at ambient conditions

Study/Investigation	Mechanical Property Tested	Type of Treatment	Strengths Recorded
Richard and Cheyrezy (1995)	Compressive strength of RPC	Pressure and thermal curing	Compressive strength 275 MPa
Reda et al. (1999)	Compressive strength of UHPC	Hot water bath (HW), oven-cured (OV), and pressure applied to fresh concrete	Compressive strength – 240 MPa (OV with pressure of 80 MPa), 140 MPa (HW)
Rahman, Molyneaux, and Patnaikuni (2005)	Compressive strength of UHPC	None – various mixtures	Compressive strength 155 MPa
Kamen et al. (2007)	Compressive and bending strength, and modulus of elasticity of UHPFRC	Varying curing temperature	Compressive strength 290 MPa Bending strength 2 MPa Modulus of elasticity 48 GPa
Graybeal and Davis (2008)	Compressive strength of UHPFRC	Temperature and RH	240 MPa
Yang et al. (2009)	Compressive and flexural strength of UHPFRC	Cured in water, 20 and 90°C	Compressive strength 160-180 MPa Flexural strength 24 MPa
Yazıcı et al. (2009)	Compressive strength of RPC	Steam and autoclave curing	Compressive strength – 234 and 250 MPa
Yazıcı et al. (2010)	Compressive and flexural strength, and fracture energy of RPC	Standard, autoclave, and steam curing, and pressure treatment	Compressive strength 403 MPa Flexural strength 33 MPa Fracture energy 7200 J/m^2
Soliman and Nehdi (2011)	Compressive strength of UHPC	Varying curing conditions – RH, and Temperature, and mixtures to mitigate shrinkage	Compressive strength 160 MPa
Wille et al. (2011)	Compressive strength of UHPC	None – adjust the content of cement, silica fume and high-range water reducer to maximize its strength	Plain UHPC – 190 MPa UHPC with steel fiber – 200 MPa

Table 2.2 (cont'd)

Aydin and Baradan (2013)	Compressive, flexural, and splitting tensile strength, modulus of elasticity, and fracture energy of RPC and alkali-activated cement (CRPC)	Steam cured	Compressive strength – 215 MPa, Flexural strength – RPC 42 MPa, ARPC 35 MPa Splitting tensile strength – 19 MPa Modulus of Elasticity – RPC 114 GPa, ARPC 84 GPa Fracture energy – RPC 14 kJ/m^2, ARPC 16 kJ/m^2
Hassan et al. (2012)	Compressive, direct tensile strength and modulus of elasticity of UHPFRC	None	Compressive strength – 151 MPa Direct tensile strength – 9 MPa Modulus of Elasticity – 46 GPa
Magureanu et al. (2012)	Compressive, flexural, and splitting tensile strength, and modulus of elasticity of UHPC	Temperature and RH	Compressive strength – 180 MPa Flexural strength – 34 MPa Splitting tensile strength – 13 MPa Modulus of Elasticity – 52 GPa
Prem et al. (2012)	Compressive, flexural, and splitting tensile strength, and modulus of elasticity of UHPC	Water and hot air curing	Compressive strength – 180 MPa Flexural strength – 44 MPa Splitting tensile strength – 24 MPa Modulus of Elasticity – 40 GPa
Zdeb (2013)	Compressive and flexural strength, and modulus of elasticity of UHPC	Steam, and water curing, autoclave	Compressive strength – 315 MPa Flexural strength – 27 MPa Modulus of Elasticity – 50 GPa
Graybeal (2014)	Compressive, and direct tensile strength, and modulus of elasticity of UHPC	Temperature and steam curing	Compressive strength – 182 MPa Direct tensile strength – 9 MPa Splitting tensile strength – MPa Modulus of Elasticity – 53 GPa
Voit and Kirnbauer (2014)	Compressive, and splitting tensile strength and fracture energy of UHPC	Pressure, and thermal	Compressive strength – 345 MPa, Splitting tensile strength – 24 MPa Fracture energy – 2500 J/m^2

Table 2.2 (cont'd)

Xiao et al. (2014)	Compressive, and flexural strength of UHPC	Steam cured at 90°C, and with special mixtures	Compressive strength UHPC 1.4% superplasticizer – 151 MPa UHPC high w/c – 100 MPa Flexural strength UHPC 4% steel fiber – 32 MPa UHPC 1% steel fiber – 16 MPa
Gesoglu et al. (2015)	Compressive strength of UHPFRC	Water or steam cured, with varying mixtures	Compressive strength 150 MPa
Ghafari et al. (2015)	Compressive strength of UHPC	None – adjust the mixture contents to develop an eco-efficient UHPC while maximizing its strength	170 MPa
Graybeal (2015)	Compressive strength of UHPC	Steam curing	200 MPa
Kusumawardaningsih et al. (2015)	Tensile strength of UHPC and UHPFRC	Varying treatment	UHPC 4 MPa, UHPFRC 7 MPa
Alkaysi (2016)	Compressive and direct tensile strength of UHPC	None – only utilized varying types of silica fume and powder, and cement	Compressive strength 186 MPa Direct tensile strength 9 MPa
Peng et al. (2016)	Compressive strength, splitting tensile strength and fracture energy of UHPC (standard, and recycled steel fiber)	None – only utilized varying types and content of steel fiber	Average – (1) compressive strength 141 MPa, (2) splitting tensile strength 9 MPa, and (3) fracture energy 5440 J/m^2
Wang and Gao (2016)	Compressive and flexural strength of UHPC	Steam curing at 90°C	Compressive strength 110-230 MPa Flexural Strength 20-45 MPa
Zdeb (2017)	Compressive, and flexural strength of RPC	Steam and autoclave curing	Compressive strength 200 MPa Flexural strength 19 MPa

Table 2.3: Survey of UHPC/RPC and UHPFRC studies conducted at elevated temperatures

Study/Investigation	Study Objectives/Detail	Features and Methodology	Observations/Conclusions	Strengths/Drawbacks
Hertz (1984)	Explosive spalling of ultra high strength concretes	▪ Observation of explosive spalling with high dense concretes ▪ Heating rate as low as 1ºC/min	▪ At room temperature compressive strength 170 MPa ▪ Explosive spalling occurred with lower moisture content and rate of heating as compared to conventional concretes	▪ Explosive spalling is solely due to the low permeability, i.e. high density, achieved through addition of silica fume ▪ Further research will be conducted to better understand behavior
Felicetti et al. (2000)	Mechanical properties of HPC and UHPC (hot and residual) are investigated	▪ Residual and hot-state direct tension, Young's modulus and fracture energy ▪ 20-600°C, with a rate of (1) residual, 1ºC/min, and (2) hot-state, 2ºC/min	▪ UHPC at room temperature compressive strength 160 MPa, tensile strength 10-11 MPa ▪ The hot-state and residual strengths are very similar	▪ The Young's modulus is lower with respect to the hot-state tests ▪ The fracture energy of UHPC experiences a dramatic increase up to 250-300°C ▪ The test method exhibits an important role
Khoury (2000)	Mechanical properties of HSC, UHPC are investigated at elevated temperatures	▪ Residual compressive strength ▪ 20-700°C, with rate of 2ºC/min	▪ At room temperature compressive strength 115-170 MPa	▪ Mechanical properties fire performance are dependent upon the design mix ▪ Be mindful of the ratio consisting of CaO/SiO_2

Table 2.3 (cont'd)

Behloul et al. (2002)	Mechanical and thermal properties of UHPC (stressed hot-state and residual) are investigated at elevated temperatures	▪ Compressive, and direct tensile strengths, elastic modulus, thermal conductivity, specific heat, and coefficient of thermal expansion (CTE) ▪ 20-750°C, with rate of 2ºC/min	▪ At room temperature compressive strength 140-200 MPa, and tensile strength 8-12 MPa, elastic modulus 45-50 GPa ▪ Thermal conductivity and specific heat steadily decline with increasing temperatures, however experience a sudden increase at 200°C ▪ CTE increases linearly up to ~550°C, then a sudden spike closer to 575 C, followed by a decline, and then an increase around 800°C	▪ Residual compressive strength, and elastic modulus mechanical properties outperformed the hot-state values ▪ Hot-state direct tensile strengths produced slightly higher values than their residual counterparts ▪ Based off the formulation of UHPC, no spalling was observed
Schrefler et al. (2002)	Investigate the overall behavior of UHPC and conventional concretes at elevated temperatures with respect to developing a model	▪ Model encompasses the thermal, hydral and mechanical behavior ▪ 20-1000°C, with a rate of 2ºC/min	▪ UHPC at room temperature compressive strength 118 MPa (input data for model) ▪ Mechanical and chemical (microstructure) behavior inputted via experimental testing	▪ Two examples are provided within the report to display the validity of said model

Table 2.3 (cont'd)

Hertz (2003)	Explosive spalling limits of concrete at elevated temperatures	▪ Consolidation of information and recommendations pertaining to explosive spalling phenomenon based off author's experience and knowledge	▪ Concrete will have a lesser chance of spalling if silica fume is not used, coupled with if the moisture content is 3-4%	▪ Explosive spalling is correlated to 374 C, approximately the pertinent temperature of steam ▪ Explosive spalling can be alleviated via either thermal cracks, and/or PP fiber, if and only if there is no immediate external deterrent
Heinz et al. (2004)	Explosive spalling behavior of UHPC of varying content of steel and PP fibers, at elevated temperatures	▪ Cylindrical specimens ▪ 20-1050°C, standardized ETK curve (DIN 4102-2)	▪ All specimens without PP fiber, exploded	▪ Steel (3.5%) and PP (0.66%) fiber by volume produce the best results for fire resistance
Liu and Huang (2009)	Mechanical properties of RPC are investigated and compared to with HPC and NSC	▪ Residual compressive strength tests ▪ Thermogravimetric analysis ▪ Fire exposure (500°C) durations were altered (0-120 min, 30 min increments)	▪ RPC at room temperature compressive strength 75 MPa ▪ The RPC's fire endurance is greater versus conventional concretes ▪ The RPC's displayed a larger residual compressive strength	▪ RPC displays greater resistance when affected by increasing temperature ▪ RPC experienced explosive spalling at 790°C

Table 2.3 (cont'd)

Burke (2011)	The compressive strength of UHPC is studied with varying PP fiber content	▪ Conducted compressive cylinder and cube specimen tests ▪ 20 to 600°C, with rate of 5ºC/min	▪ At room temperature compressive strength, (1) cylinder – 137-152 MPa, and (2) cube – 140-180 MPa ▪ PP fibers alleviated explosive spalling	▪ UHPC's residual compressive strength with respect to increasing temperature is like other concretes ▪ The exposure duration of the heat affected the cube specimens, but not the cylinder specimens
Ju et al. (2011)	The thermophysical properties of RPC are evaluated at elevated temperatures	▪ Thermophysical properties, thermal conductivity, thermal diffusivity, specific heat capacity and linear thermal expansion with four varying steel fiber volume ▪ 20 to 250°C (in 50°C increments), with rate of 5ºC/min	▪ Minimal mass loss at 250°C ▪ Only specific heat capacity increases with higher temperatures ▪ The steel fiber content effects the specific heat capacity and thermal diffusivity values ▪ RPC's thermal conductivity, and specific heat capacity are lower than HSC	▪ Due to the differing microstructure, RPC's thermophysical properties vary as compared to HSC
Tai et al. (2011)	Study the compressive stress-strain relationship of RPC with varying steel fiber content at elevated temperatures	▪ Residual compressive strength, and stress-strain relationship ▪ 20-800°C, with rate of 2ºC/min	▪ The compressive strength increases slightly up to 300°C, soon followed by a decrease with increasing temperatures ▪ The peak strain increases with higher temperatures	▪ RPC with 1% steel fiber content behave differently than with 2 and 3% steel fiber content ▪ The slope decreases of the stress-strain curve with increasing temperatures

Table 2.3 (cont'd)

Aydin and Baradan (2012)	The mechanical properties of RPC with a Portland cement replacement at elevated temperatures is investigated	▪ Cement is replaced with alkali-activated-slag (ARPC), and results are compared with cement based RPC (CRPC) ▪ Residual flexural, compressive strength and toughness ▪ 20-800°C, with rate of 10°C/min	▪ The CRPC strength changes very little up to 300°C and undergoes explosive spalling beyond 300°C ▪ The ARPC's strength steadily decreases with decreasing temperature ▪ ARPC can withstand temperatures up to 800°C	▪ CRPC's increasing temperature resistance is greater than ARPC up to 300°C ▪ Beyond 300°C, ARPC is better ▪ ARPC with 20% silica fume did not experience explosive spalling
Peng et al. (2012)	The residual mechanical properties of RPC with varying content of steel and PP fibers and the explosive spalling behavior were studied	▪ Residual compressive, splitting tensile strength and fracture energy ▪ 20-600°C, with rate of 10°C/min	▪ At room temperature compressive strength 70-100 MPa, splitting tensile strength 13-16 MPa, and fracture energy 12,000-15000 J/m^2 ▪ The compressive strength increases up to 400°C, while the splitting tensile strength and fracture energy only up to 200°C	▪ The use of PP fiber is a method to avoid explosive spalling ▪ RPC with water-cement ratio from 0.16-0.20 has a higher chance to experience explosive spalling ▪ Increase of mechanical properties between 200-400°C may be attributed to hydration of the cementitious materials, but further research is required

Table 2.3 (cont'd)

Ye et al. (2012)	Study the compressive strength of UHPC with varying PP fiber, and with and without steel bar reinforcement at elevated temperatures	▪ Stressed at 30% of the ultimate strength, hot-state compressive strength ▪ 20-400°C	▪ Many cracks were observed with increasing temperature up to 300°C ▪ Specimen heated to 400°C experienced explosive spalling	▪ Adding PP fiber, 2 kg/m^3, alleviated the cracks and spalling
Zheng et al. (2012)	Study the compressive stress-strain relationship of RPC with varying steel fiber content at elevated temperatures	▪ Residual compressive strength, stress-strain relationship and elastic modulus ▪ 20-900°C, with rate of 4ºC/min ▪ Specimens are heat treated	▪ The compressive strength increase with initial temperature increase, however begin to decrease soon after ▪ The peak strain increases with higher temperatures	▪ Minimum compressive strength reached at 700°C ▪ Very little changes with respect to the stress strain relationship up to 300°C; following 300°C, the curves begin to flatten
Abdul-Hussain (2013)	Various mechanical properties of fiber RPC, and explosive spalling were studied	▪ Residual compressive, flexural and splitting tensile strength on cubes, cylinders and prisms ▪ 20-600°C, with slow heating rate	▪ At room temperature (with increasing PP fiber content) compressive strength 97-122 MPa, flexural strength 6-23 MPa, and splitting tensile strength 5-15 MPa	▪ All mechanical properties tested decrease at temperatures above 400°C ▪ Tensile strengths suffered the most following exposure of 600°C

Table 2.3 (cont'd)

Jagannathan (2013)	To study and understand the C-S-H in concrete at elevated temperatures	▪ Utilizing experimental data, compare the C-S-H in UHPC versus conventional concretes	▪ At the micro-level, the drastic difference in stiffness between the C-S-H phase and steel fiber, cause the packing density of the C-S-H to lessen, and capillary porosity within the matrix is formed	▪ UHPC's C-S-H phase is quite durable up to 400°C, and dramatically firmer than conventional concretes
Zheng et al. (2013)	Various mechanical properties of steel fiber RPC were studied	▪ Residual compressive and tensile strength tests ▪ 20-800°C, with rate of 5ºC/min	▪ The critical temperatures for explosive spalling are from 260-520°C, and the risk rises with larger dimensions ▪ The compressive strength decreases at 100°C, rises up to 500°C, and followed by a decline ▪ The tensile strength decreases at 200°C, rises only up to 300°C, and followed by a decline	▪ 2% steel fibers can prevent RPC to undergo explosive spalling ▪ Based off study implementation of codes for RPC design is conservative for temperatures between 400-800°C, and not recommended for temperatures under 400°C

Table 2.3 (cont'd)

Bashandy (2013)	Various mechanical properties of fiber RPC, with varying cement and steel fiber content, and differing fire exposure times	▪ Residual compressive (cube specimens of 100 x 100 x 100 mm) and splitting tensile strength (cylinder specimens of 200 mm length and 100 mm diameter) ▪ 20-500°C, with a rate of 10°C/min ▪ Heating durations of 2 and 4 hours	▪ At room temperature compressive strength 85-150 MPa, splitting tensile strength 7-11 MPa ▪	▪ Increasing the heating duration, decreases the residual strengths ▪ Increase in cement improves only the at room temperature strengths ▪ Steel fibers enhance the strengths only up to 150°C
Hager et al. (2013)	The compressive strength and modulus of elasticity of RPC are studied with varying PP fiber content	▪ Residual compressive strength tests on prism specimens 40 x 40 x 80 mm ▪ 20 to 1000°C, with rate of 0.5ºC/min ▪ Spalling tests to 600°C, with rates of 0.5, 1, 2, 4 and 8ºC/min ▪	At room temperature compressive strength 180-220 MPa, and elastic modulus 48 GPa	▪ 2.0 kg/m3 PP fibers prevented explosive spalling ▪ PP fibers do not drastically alter the relative compressive strength as a function of temperature ▪ Modulus of elasticity is not affected by the addition of PP fibers ▪ Porosity increases from 0.02 to 0.14 cm3/cm3, when temperature is heated to 600°C

Table 2.3 (cont'd)

Ju et al. (2013)	In order to better understand the spalling behavior of RPC, the microstructure along with the pore pressure were studied at elevated temperatures	▪ Plain RPC specimens ▪ 20-350°C ▪ Mercury intrusion porosimetry (MIP), and scanning electron microscopy (SEM) were utilized	▪ The pore characteristics increase with higher temperatures A model proposed to help analyze the pore pressure and explosive spalling	▪ Explosive spalling is mainly attributed to the lack of pathways to allow release of vapor pressure
Wang et al. (2013)	The study investigated the thermomechanical (TMA) analysis of UHPC with varying dimensions and content of steel fiber	▪ Coefficient of thermal expansion (CTE), ▪ 20-800°C, with rate of ±3ºC/min	▪ α-β quartz transformation – 570°C, reversible phase transformation ▪ Dihydroxylation transition of C-S-H – above 700°C, irreversible phase transformation	▪ Both UHPC types tested, (1) extended almost linearly up to 570°C, (2) severely contracted above 700°C, and (3) ▪ Copious amount of cracks exposed via SEM, in vicinity of phase interfaces due to thermal stresses caused by differences in CTE

Table 2.3 (cont'd)

Canbaz (2014)	Investigate the compressive strength of pressurized and accelerated curing RPC with varying PP fiber content, at elevated temperature	▪ Residual compressive strength and UPV tests ▪ 20-900°C, with rate of 10°C/min	▪ At room temperature compressive strength, 200 MPa (0% PP), and 165 MPa (1% PP) ▪ RPC with no PP fiber relatively well up to 400°C, however poor performance at high temperatures up to 900°C ▪ Addition of PP fiber improved the RPC's performance up to high temperatures	▪ 1% of PP fibers is suggested to avoid explosive spalling and to maintain its strength at elevated temperatures up to 900°C ▪ RPC with no PP fiber was not able to withstand temperatures higher than 900°C
Klingsch (2014)	Investigate the explosive spalling behavior of UHPC at elevated temperatures	▪ Vary the silica fume content and employ different heating rates	▪ At room temperature compressive strength 150 MPa ▪ Hydrothermal model is presented, which is validated via experimental testing	▪ Explosive spalling will occur if the pore pressure exceeds the concrete's tensile strength ▪ Employing a low rate of heating can still contribute to explosive spalling, due to UHPC's dense matrix
So et al. (2014)	Mechanical properties and thermogravimetric-differential thermal analysis (TG-DTA) of RPC with varying cement, silica fume and PP fiber at elevated temperatures	▪ Residual compressive and flexural strength ▪ 20-1095 C, with rate of 30°C/min (KSF 2257-1, Korean standard)	▪ At room temperature compressive strength 106-150 MPa, and flexural strength 17-27 MPa ▪ The relative residual compressive and flexural strength at 1095 C was between 0.15-0.29 and 0.20-0.33, respectively	▪ RPC is more at risk of explosive spalling with (1) increasing cement content and silica fume-cement ratio, (2) value of the pore-volume proportion, and (3) PP fiber content of at least 2.0 kg/m^3

Table 2.3 (cont'd)

Zheng et al. (2014a)	Study the mechanical properties of RPC with steel and PP fiber at elevated temperatures and varying fire exposure durations	▪ Residual compressive and tensile strength ▪ 20-800°C, with rate of 5ºC/min	▪ At room temperature compressive strength, 135-163 MPa, tensile strength, 5.5-7.5 MPa ▪ Compressive strength (PP and steel fiber) decrease at 100°C, and increases up to 500°C; followed by a decrease at 600°C and above ▪ Compressive strength increases up to 400°C with prolonged fire exposure ▪ Tensile strength (PP and steel fiber) decrease at 200°C, and increase at 300°C; followed by a decrease with higher temperatures	▪ The compressive and tensile strengths attain an initial increase, soon followed by a degradation of strength ▪ PP fibers provide avenues for the vapor pressure to release, and avoid explosive spalling

Table 2.3 (cont'd)

Zheng et al. (2014b)	Various mechanical properties of fiber RPC, the microstructure and explosive spalling were studied Objective: ▪ Evaluate the effects of differing PP fiber content ▪ Measure porosity, thermal conductivity	▪ Compressive strength tests, 70 x 70 x 70 mm cubes and 70 x 70 x 220 mm prismatic specimens ▪ Tensile strength tests, dog-bone shaped ▪ 20 to 800°C, with rate of 5ºC/min	▪ Room temperature compressive strength, (1) cube 107-137 MPa, and (2) 92-138 MPa, (3) tensile strength 4.5-5.75 MPa ▪	▪ 2.73 kg/m3 PP fibers prevented explosive spalling ▪ Cube compressive strength performed the best ▪ Compressive and tensile strength fluctuated, decreased at 100 and 200°C, respectively, increased from 200 to 600°C, and 200 to 300°C, respectively, and decreased above 600°C, and 400°C, respectively ▪ Thermal conductivity sharply decreased up to 400°C, and slowly beyond 400°C

Table 2.3 (cont'd)

Ju et al. (2015)	The residual mechanical properties and the spalling behavior of RPC were investigated Objective: To vary the PP fiber content (by volume)	▪ Compressive strength, split tensile strength, and flexural strength (up to 350°C), with rate of 3ºC/min ▪ The spalling performance and details up to 600°C, with rate of 4.8ºC/min	▪ Room temperature compressive strength 135-160 MPa ▪ Thermomechanical properties increase up to 300°C, and decrease following 300°C ▪ 0.9% PP fiber is critical dosage for ideal residual strengths ▪ Mass loss variation with respect to temperature range ▪ At 280-290°C, moisture begins to migrate towards the outside	▪ 0.9% PP fiber dosage is optimum for residual mechanical properties ▪ Above 150°C, mass loss (evaporation of water) increases very rapidly ▪ Moisture migration occurs around 280-290°C
So et al. (2015)	▪ Study the mechanical properties of a more economical mixture of RPC at elevated temperatures	▪ The contents of silica fume and cement are drastically reduced ▪ In return, developed a mixture that contains silica fume, blast furnace slag and fly ash ▪ Residual strength tests at 20-1000°C with a rate of 10°C/min	▪ Room temperature compressive strength 140-190 MPa, tensile strength 15-22 MPa, and flexural strength 35-42 MPa ▪ Modified RPC residual compressive, flexural, and splitting tensile strengths were 36%, 22%, and 29% of the ambient strength, following exposure to 1000°C	▪ The modified RPC outperformed the more traditional RPC mixture ▪ 30% fly ash, 10% blast furnace slag, and with the lowest silica fume content proved to be the best combination ▪ Substantial strength loss experienced from 400-800°C

Table 2.3 (cont'd)

Way and Wille (2015)	▪ Investigate the effect of chemical degradation (DSC/TGA) of the mechanical properties of UHPFRC	▪ Residual compressive strength and stress-strain relationship ▪ 20-900°C with a rate of 0.1ºC/min	▪ At room temperature 206-233 MPa (with thermal treatment ▪ Oven drying the specimens provided an increase in compressive strength and elastic modulus over the control (90°C)	▪ UHPFRC experienced a rise in strength at 135 and 200°C, followed by a decrease ▪ The elastic modulus decreased following 300°C and above ▪ The peak strain increased with increasing temperature ▪ The thermomechanical analysis provided reasoning to decrease in strength at respective temperatures
Xiong and Liew (2015)	Investigate mechanical properties of UHPC with varying fiber type, dosage, heating rate and curing condition at elevated temperatures	▪ Residual compressive strength and elastic modulus ▪ 20-800°C, with rates of 5 and 30°C/min	▪ At room compressive strength 160-185 MPa ▪ Steel fibers are not effective to avoid explosive spalling ▪ Compressive strength experiences an increase at 200°C – attributed to water removal; not seen with elastic modulus	▪ PP fiber with dosages of 0.1% is effective to avoid explosive spalling ▪ The compressive strength and elastic modulus reduce more rapidly with higher heating rates ▪ Curing conditions do not effect the compressive strength and elastic modulus

Table 2.3 (cont'd)

Zheng et al. (2015)	Mechanical properties at hot-state of RPC with steel fiber at elevated temperatures	▪ Hot-state compressive strength, stress-strain relationship, elastic modulus and energy absorption ▪ 20-800°C, with rate of 5ºC/min	▪ At room temperature compressive strength 142-165 MPa ▪ With increasing temperatures, (1) the thermal expansion, peak strain, and energy absorption (up to 400°C) escalate, (2) compressive strength, and Gismodine progressively decreases	▪ Increasing the steel fiber content will not improve the compressive strength, however will intensity the ductility ▪ Following temperatures up to 800C C-S-H decomposes (pores and cracks appear), and C_2S and C_3S formulate ▪ The mechanical properties dilapidation is due to the pores and microcracks
Ali et al. (2016)	Investigate the use of waste glass powder to enhance the mechanical properties at elevated temperature of HSC and compare to RPC	▪ Residual compressive, and flexural strengths, modulus of elasticity and stress strain relationship ▪ 20-800°C with rate of 13ºC/min	▪ RPC (HSC with waste glass powder, no silica fume, HSC-GP) at room temperature compressive strength 142 MPa (81 MPa), modulus of elasticity 52.8 GPa (40.4 GPa) and flexural strength 6.7 MPa (5.9 MPa)	▪ RPC experiences a sudden decline in compressive and flexural strengths with increasing temperature, while HSC-GP experiences a steady decline ▪ RPC (HSC-GP) experienced partial spalling at 400°C (500°C) and full spalling at and above 500°C (800°C)
Bei and Zhixiang (2016)	Investigate the explosive spalling behavior of UHPC (with varying fiber mix and content) at elevated temperatures	▪ Place UHPC specimen in a preheated furnace (1000°C) for a short duration, followed by sudden exposure to a 25 C environment	▪ At room temperature, compressive strength 168-198 MPa ▪ Steel fiber merely postpones the time to spall	▪ PP fiber content greater than 0.20%, and length of 12 and 19 mm prevent explosive spalling

Table 2.3 (cont'd)

Li and Liu (2016)	Investigates the tensile properties of RPC with steel and PP fibers at elevated temperatures	▪ Residual flexural and direct tensile strength ▪ 20-900°C, with rate of 4ºC/min	▪ At room temperature, flexural strength 22-31 MPa, and direct tensile strength is between 6-8 MPa ▪ The flexural and direct tensile strength experience a steady decline with increasing temperature	▪ Only the steel fibers can increase the tensile strength and the tensile strength increases with higher steel fiber content
Jang et al., 2016	The residual mechanical properties and the spalling behavior of RPC were investigated Objective: ▪ To vary the fiber content (by volume) ▪ Alter the admixture with a combination of ternary pozzolanic materials	▪ Compressive, flexural and splitting tensile strength ▪ 20 to 1000°C, with a rate of 10°C/min ▪ Thermogravimetric and microstructure analysis	▪ Room temperature compressive strength 150 MPa, and flexural strength 25-32 MPa, ▪ Modified RPC contained only 765 kg/m3 of cement, and an increase in compressive and flexural strength as a function of temperature ▪ Compressive strength increased up to 400°C, and then decreased ▪ Flexural strength increased up to 200°C, and then decreased	▪ A decrease in table flow as the fiber content was increased ▪ PP fiber is effective to inhibit explosive spalling, so long as the volume is 0.2% of the binder content ▪

Table 2.3 (cont'd)

Peng et al. (2016)	Study the explosive spalling behavior and ambient condition mechanical properties of UHPC with varying types of steel fiber at elevated temperature	▪ Utilize standard steel fiber and sustainable (recycled) steel fiber to reinforce UHPC ▪ 20-800°C, rate of 10°C/min (for explosive spalling tests only)	▪ At room temperature compressive strength 130-154 MPa, splitting tensile strength 7-12 MPa, and fracture energy 260-13,828 J/m^2 ▪ The recycled steel fiber compressive strength ranged from the lowest to about the average of compressive strengths ▪ While the splitting tensile strength, and the fracture energy of the recycled steel fiber proved to be the most favorable	▪ The steel fiber with the least diameter proved to be the most effective to avoid explosive spalling ▪ Additionally, the recycled steel fiber UHPC provided explosive spalling relief as well
Sanchayan and Foster (2016)	The residual and hot state mechanical properties and the spalling behavior of RPC (6 different mixes) were investigated Objective: If PVA fibers would alleviate the explosive spalling behavior	▪ Residual compressive strength, and elastic modulus, with a rate of 5ºC/min ▪ Hot state elastic modulus, free thermal strain and transitional thermal creep, with a rate of 5ºC/min	▪ Room temperature compressive strength 134-170 MPa ▪ Utilizing PVA fibers alone reduced the compressive strength, elastic modulus remained constant ▪ Elastic modulus and ultrasonic pulse velocity drop following exposure to 300°C ▪ Transitional thermal creep very high above 250°C ▪ Surfeit amount of mass loss for tests conducted to 300, and 400°C	▪ 1% of steel and PVA fibers design mix provided the best results ▪ Increase of compressive strength up to 300°C, followed by a drop ▪ Hot state elastic modulus of RPC 1% steel and PVA fibers decreased almost linearly

Table 2.3 (cont'd)

Nazri et al. (2017)	The residual mechanical properties and the spalling behavior of UHPFRC were investigated	▪ Residual compressive strength on cube specimens of 40 x 40 x 50 mm ▪ 20-600°C with a rate of 15ºC/min	▪ At room temperature compressive strength 157-161 MPa ▪ UHPFRC experienced explosive spalling at temperatures above 400°C ▪ Did not contain any PP fiber	▪ Due to undergoing explosive spalling only conducted compressive strength up to 200°C with very little reduction in strength ▪ Fire Propagation Index of 0.0, under BS476 Part 6, Class 1 fire rating under Part 7

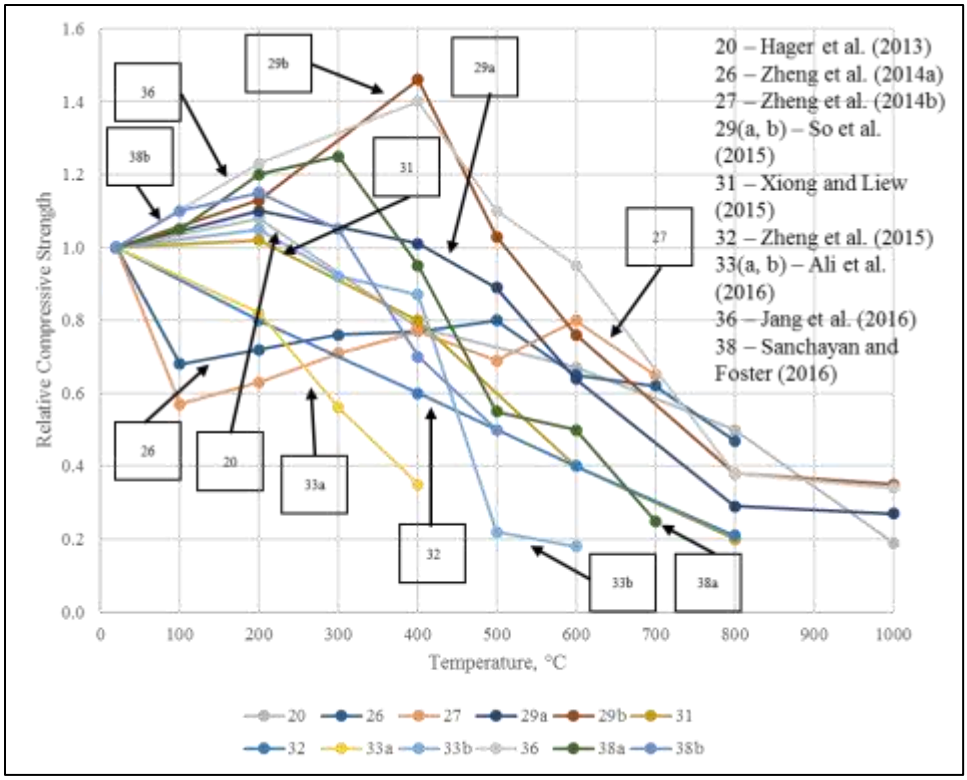

Figure 2.1: Relative compressive strength versus temperature as per literature from the past 3 years

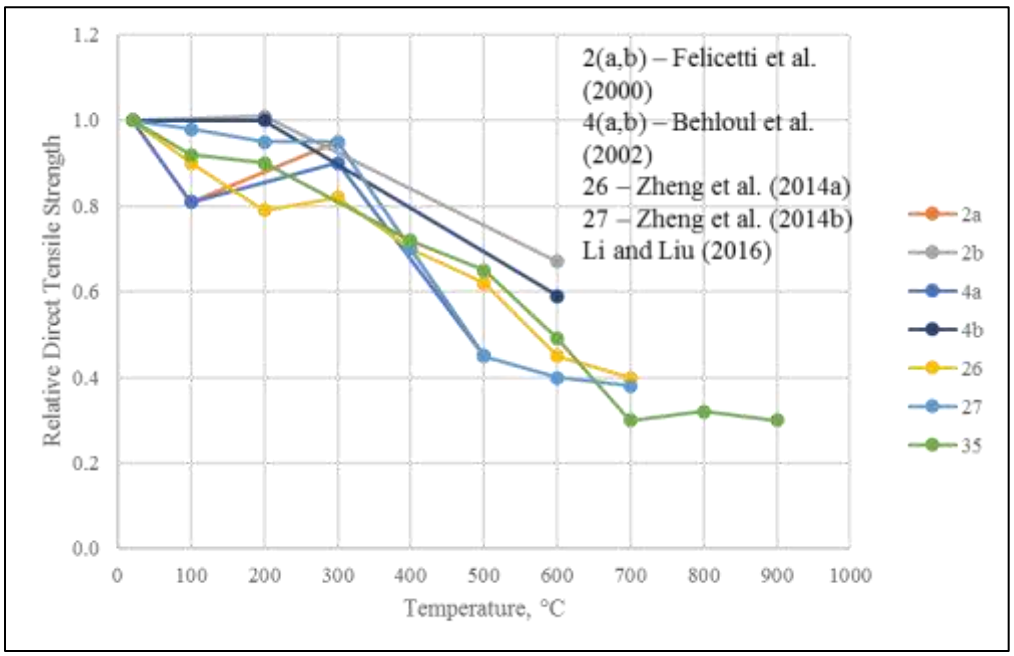

(a) Relative direct tensile strength

Figure 2.2 Relative tensile strength versus temperature as per literature

Figure 2.2 (cont'd)

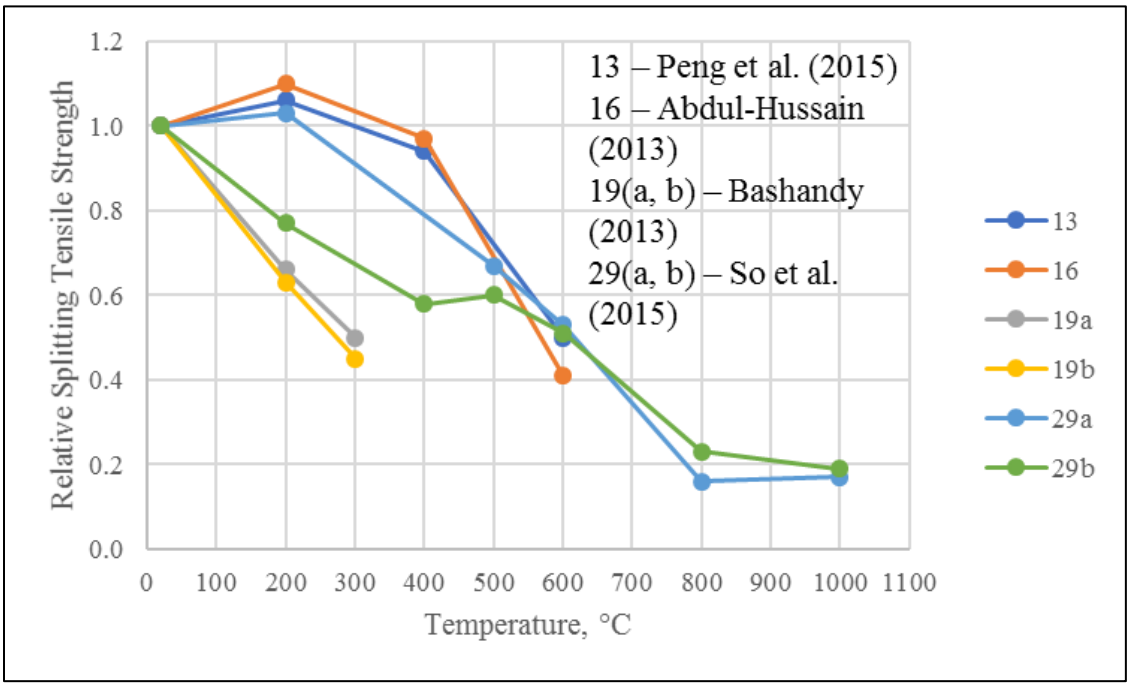

(b) Relative splitting tensile strength

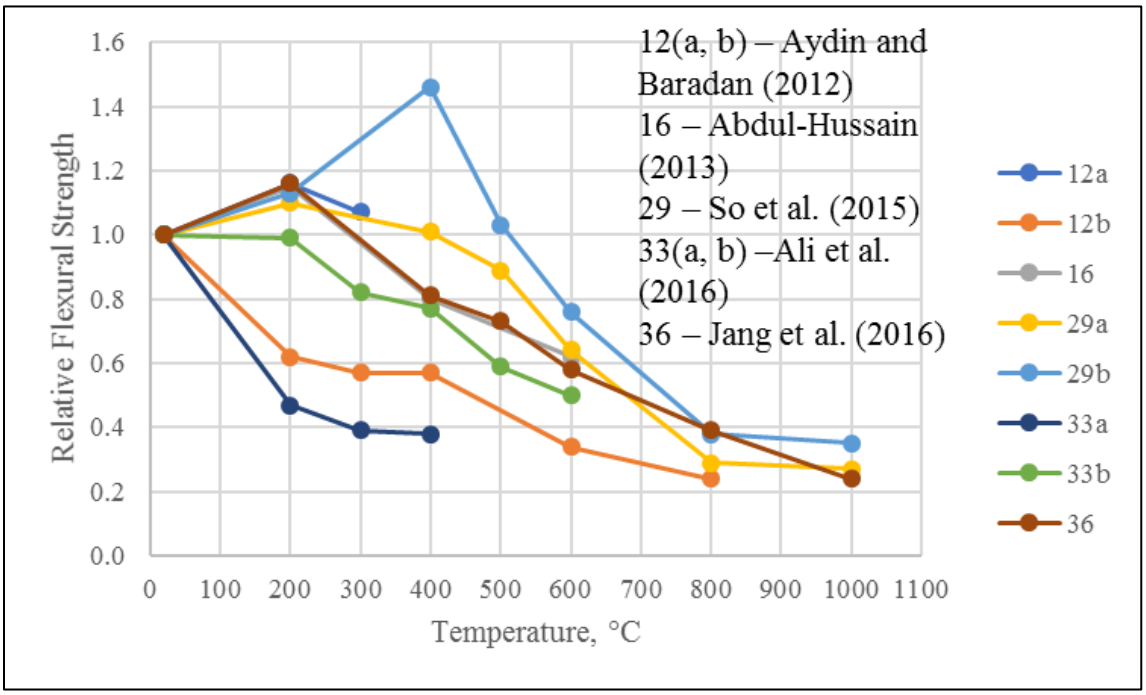

(c) Relative flexural strength

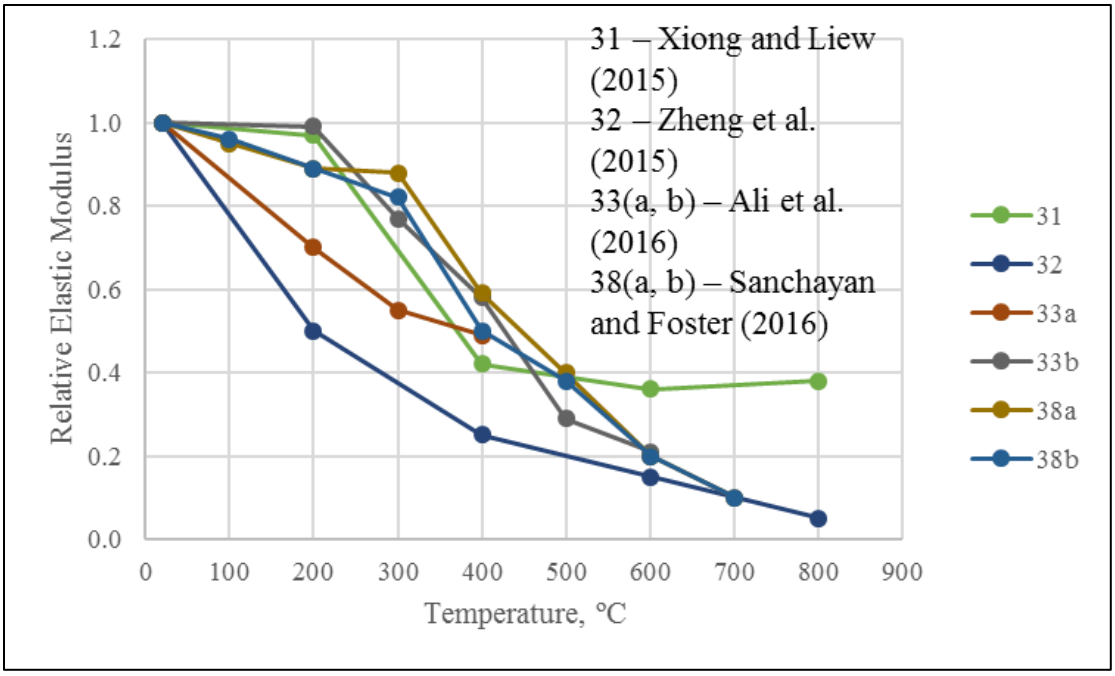

Figure 2.3 Relative elastic modulus versus temperature as per literature from the past 2 years

CHAPTER THREE

3. EXPERIMENTAL STUDIES ON COMPRESSIVE STRENGTH AND EXPLOSIVE SPALLING OF UHPC AT ELEVATED TEMPERATURES

3.1 General

Data pertaining to the mechanical properties of UHPC at elevated temperatures are needed to evaluate concrete structural members' fire response. Thus, grasping the degradation of compressive strength, stress-strain relationship, and elastic modulus with increasing temperatures, enable designers to achieve the fire resistance requirements dictated by code provisions. As presented in the previous chapter, it is apparent data on high temperature mechanical properties and temperature induced explosive spalling behavior of UHPC are lacking.

To fulfill this integral gap, a comprehensive experimental study was undertaken to investigate UHPC's compressive strength, stress-strain relationship, and elastic modulus with increasing temperatures. From the collected data, an empirical relation was formulated showing the variation of the 3 mechanical properties of UHPC with respect to temperature (20-700^{o}C), and highlights pertaining to explosive spalling. The following sections will impart the experimental design and details, procedures followed, and the findings will be discussed.

3.2 Design of mechanical property experiments

The experimental study evaluated the unstressed mechanical properties of 3 different design mixes of UHPC. Each UHPC design mix incorporated a varying mixture of fiber(s), to investigate their influence on the respective mechanical properties, and effect of mitigating the explosive spalling occurrence. Specifically, two mixes of UHPC with varying content of steel fibers and one UHPC mix with a combination of steel and polypropylene fibers (hybrid) were

tested. The cylinders were tested under compressive loads at various temperatures (20, 100, 200, 300, 400, 600 and 700°C) in a elevated temperature state as opposed to testing under conventional residual-state regime.

For comparative purposes, in addition to the UHPC 4 other conventional types of concretes, NSC, NSC with steel fiber (NSC-SF), HSC, and HSC with polypropylene fibers (HSC-PP) were also tested (at similar temperature ranges). Additionally, in the absence of an ASTM standard dictating guidelines for material properties at elevated temperatures, to regulate the testing procedure a combination of published standards was followed. The mechanical property tests were carried out as outlined in each respective ASTM standard, coupled with the heating regiment delineated in RILEM Standard (RILEM Technical Committee 200-HTC, 2007) were applied.

3.3 Mechanical properties tests

The mechanical properties investigated as part of this study were compressive strength, stress-strain relationship, and elastic modulus. Table 3.1 displays the type and number of tests conducted for each respective type of concrete.

3.3.1 Batch mix proportions

Four batches of UHPC were cast to prepare needed test specimens for evaluating the mechanical properties. Batch mix proportions for the UHPC mixes have been developed by Metna Co. Furthermore, 4 conventional concrete design mixes were cast as well, NSC, NSC-SF, HSC, and HSC-PP. All concrete types evaluated contained Portland cement, Type I, but with varying quantities. The conventional concrete mixes incorporated 9.5-millimeter (mm) limestone-coarse aggregate, and natural sand. The HSC mixes contained nearly 2.5 times the cement as the NSC mixes, and silica fume. All 3 UHPC design mixes contained 2.38 mm limestone-coarse aggregate, silica and natural sand, over 5 times the silica fume as compared to the HSC mixes, limestone

powder, and a superplasticizer, Chryso. The two UHPC design mixes with steel fibers are UHPC A, B, and D. UHPC A and B (A & B) are the same mixture proportions, however due to logistical constraints at the time of casting, two concrete batches were made. UHPC D has the same components but in lesser quantity, as compared to UHPC A & B. Namely, there is less steel fiber content in UHPC D, vice UHPC A & B. UHPC F is the hybrid design mix with steel and polypropylene fibers, and the other components are very similar as to design mix UHPC D. Furthermore, UHPC D and F were casted in Metna Co. laboratory, and therefore in a more controlled environment. The mix proportions in each type of UHPC design mix, and conventional concretes tested are given in Table 3.2, and Table 3.3, respectively. Additionally, the conventional concretes 28-day compressive strength range from 29-110 MPa, while UHPC's from 132-182 MPa. The 28-day compressive strengths, along with the densities of all concretes tested, are provided in Table 3.4.

3.3.2 Test specimens

The test specimens comprised of 75 mm in diameter by 150 mm in length cylinders as shown in Figure 3.1 and were cast using paper molds. Paper molds were used for casting UHPC cylinders to facilitate the placement of type K thermocouples in the cylinder for temperature measurement. Prior to casting, each paper mold is drilled from the side at mid-height and thermocouples are inserted from the side exactly at the center (75 mm from the side) of the cylinder. However, center thermocouples were not employed with the conventional concretes, thereby allowing the use of reusable plastic molds. When each respective concrete mixture was ready, the molds were filled with concrete and placed on a shaking table at high frequency for about 2 min.

The casted specimens are covered with plastic sheets to minimize moisture loss and left to set slowly for 24 hours. After 24 hours, the hardened UHPC specimens are demolded and immediately placed in a steam chamber for curing at 90°C for 48 hours. After steam curing, the specimens are air dried in Michigan State University Civil Infrastructure Laboratory (MSU CIL) for at least 90 days before conducting high-temperature tests.

Since the cylinder's top and bottom surfaces are originally rough from casting, a table saw (Figure 3.2) is utilized to create a smooth and leveled finish on both end surfaces (Figure 3.1). This smooth finished surface was performed for high-temperature testing since the available capping material melt at low temperatures of less than 127ºC. However, if an excellent level finish is not attained using the electrical saw, the results for compressive strength will not be accurate and this can be observed from the failure mode of the specimen as described in ASTM-C39/C39M (ASTM C39/C39M, 2016). The smooth leveled surface is achieved through slowly cutting the specimen, and repeatedly smoothing the surface until it achieves a leveled finish. The finished surface is finally checked utilizing a magnetic level.

For each heated UHPC specimen in the furnace, three thermocouples are utilized to monitor temperature rise. Figure 3.1(a) depicts the thermocouple locations when the specimen is placed within the electrical furnace. Thermocouple (1) monitors the furnace temperature, nearest to the specimen, (2) the specimen's surface temperature and (3) specimen's core temperature. In addition, the electrical furnace has its own temperature gauges which are compared with the thermocouple readings. Contrary to UHPC specimens, the four conventional concretes did not have a center thermocouple, and the surface thermocouple is utilized to monitor the temperature rise. The arrangement of thermocouples for the conventional concretes is shown in Figure 3.1(b).

3.3.3 Test apparatus

The test apparatus for compressive strength tests at various temperatures is composed of an electrical furnace to heat the specimens to the target temperature, loading machine to conduct the compressive strength test, and compressometer equipped with two high accuracy linear variable displacement transducers (LVDT), to track the deformations. The electric furnace shown in Figure 3.3 is specially designed for simulating high-temperature conditions and can produce maximum temperatures up to 925°C. It is equipped with internal heating electric elements, a ramp and a hold temperature controller that can generate different heating rates. Along with attaining the compressive strength, the 1800 kN load-controlled strength testing machine shown in Figure 3.4, combined with the compressometer shown in Figure 3.5, provide the stress-rate controlled stress-strain relationship by monitoring the load and deformation with respect to time. The elastic modulus can be extracted from the stress-strain relation utilizing equation 1, as prescribed in ASTM-C469/C469M (ASTM C469/C469M, 2014).

$$E = (S_2 - S_1)/(\varepsilon_2 - 0.000050) \quad (1)$$

Where E, is the chord modulus of elasticity (GPa), S_1, is the stress corresponding to a longitudinal strain, S_2, is the stress corresponding to 40% of ultimate load (MPa), ε_1, of 50 millionths, (MPa), and ε_2, is the longitudinal strain produced by stress, S_2, (mm/mm). The LVDTs are part of the compressometer, thus providing more local and accurate deformation measurements.

3.3.4 Test procedure

3.3.4.1 General procedure

The specimen was evaluated at the elevated target temperature, and the applied load commenced following the heating of the specimen to the appropriate temperature. RILEM

standard considers such a procedure as an unstressed test. Furthermore, a steady-state method is adopted for determining the compressive strength utilizing the electric furnace (Figure 3.3). In the steady-state testing method, the specimen is heated to a predetermined target temperature, and then the specimen is immediately transferred to the strength testing machine for applying stress. Figure 3.6(a) depicts the desired regime of heating in this kind of test and Figure 3.6(b) summarizes the desired rate of heating for each type of concrete evaluated. The RILEM standard recommends a heating rate of 2ºC/min for specimens with a maximum diameter of 80 mm and a temperature recording interval of 4 min. For the testing conducted, a rate of heating of 2ºC/min was utilized for the four conventional types of concretes. Unfortunately, due to UHPC's lower permeability as compared to conventional concretes, unless a lower heating regime was employed, tests at and above 300°C would result in explosive spalling. The spalling of this nature reduces the UHPC specimens into fragments and a compressive strength test cannot be conducted. Therefore, to improve the understanding of the explosive spalling behavior of UHPC, a heating rate ranging from 0.25 to 4ºC/min were employed. For all tests conducted, temperature recordings were taken every thirty seconds. Furthermore, due to the constraints of the electric furnace (Figure 3.3), coupled with the installation of the compressometer (Figure 3.5), the core temperature is taken 30°C beyond the target temperature. As seen in Figure 3.6(a), the increased temperature facilitates the additional time required to install the compressometer. Plus, as recommended by RILEM standard the additional 30°C permits the specimen to saturate for 30-45 min before removal from the furnace. Since the surface thermocouple is utilized to track the heating rate for the conventional concretes, the specimen is ready once the surface temperature reaches 60°C beyond the target temperature. The thermocouples are attached to a data acquisition device (Figure 3.7) that continuously monitor and records the temperature.

3.3.4.2 Compressive strength, stress-strain relationship, and elastic modulus

Once concrete specimen attains the targeted temperature, it is removed from the furnace, Figure 3.6(b), and while the center thermocouple remains intact (UHPC specimens only), the surface thermocouple is removed prior to weighing the specimen. However, since the conventional concretes do not have a center thermocouple, the surface thermocouple remains in place to monitor the temperature while conducting the strength test. Preceding to place the specimen within the Forney strength machine (Figure 3.4), the compressometer (Figure 3.5) is installed upon the cylinder. As seen in Figure 3.5, there are two rods that hold the apparatus together, and once the compressometer is installed upon the concrete specimen, the rods are removed prior to commencing the compressive strength test. Tests conducted at 20ºC follow the steps outlined in this section, excluding the placement of thermocouples and heating within the furnace.

When the specimen is set up within the Forney strength test machine, as per ASTM C39/C39M, a load rate of 0.25 ± 0.05 MPa/sec is applied and must be maintained for the duration of the test. Once the concrete specimen reaches its maximum load and depending on the temperature at which the test is being conducted and type of concrete, the specimen may fail in an explosive and brittle way, thus the test is concluded. Upon hearing the explosion, the test of specimens with steel fiber is continued briefly to ensure the specimen has in fact completely failed; Further discussion will be provided in section 3.4.2. The maximum load along with the load versus displacement data collected is used to develop the stress versus strain curves, along with the modulus of elasticity.

Unless there was a poor failure as per ASTM-C39/C39M (ASTM C39/C39M, 2016), one conventional concrete specimen was evaluated at each respective temperature. While 3-4 repetition tests were conducted for UHPC A & B, and F up to 400°C, unfortunately, due to limited specimens cast and explosive spalling, only 1 specimen was tested for UHPC F above 400°C and

UHPC D. UHPC A & B and D's compressive strengths were evaluated at 20, 100, 200, 300, and 400ºC, but for UHPC F, tests were conducted similarly as UHPC A & B and D, plus at 600 and 700°C. NSC tests were at 20, 400, 600, 700, and 750 ºC, NSC-SF at 20, 200, 400, 600, and 700ºC, HSC at 20. 200, 400, and 600ºC, and HSC-PP at 20, 200, 400, 600, 700, and 750ºC.

3.4 Results and discussion

Results from the compressive strength tests are presented in this section. This section will discuss each type of concrete's results individually. Chapter four will discuss the UHPC results as compared to the conventional concretes tested.

3.4.1 Sectional temperatures

As illustrated in Figure 3.1, thermocouples are mounted in the electrical furnace and on the cylinders to record the temperature data with respect to time. The thermocouples ensured the appropriate rate of heat is being applied to the specimen while it is in the electric furnace and the proper temperature is reached. The temperature data acquisition device (Figure 3.7) records the temperatures via the thermocouples every 30 seconds. Following the completion of the test, the data is analyzed and the actual average rate of heat is calculated by plotting the temperature versus time (Figures 3.8), and enumerating the average slope developed during the heating of the concrete specimen. In each respective figure, the targeted rate of heat is shown via a dashed dark grey line as annotated by the legend. Additionally, the temperature versus time data, depicts the thermal gradients experienced by the UHPC specimen while being heated within the electric furnace. The thermal gradient is calculated utilizing equation (2).

$$thermal\ gradient = \frac{T_s - T_c}{r_{spec}} \qquad (2)$$

Where, T_s, is the surface temperature (C), T_c, is the center temperature (C), and r_{spec}, is the radius of the concrete cylinder, i.e. distance from the surface to the placement of the center thermocouple within the specimen (centimeter, cm). Therefore, employing equation (2) with the temperature rise data with respect to time, the thermal gradient is graphed with respect to time as well. The thermal gradient data is pertinent regarding UHPC's explosive spalling behavior and will be discussed further in section 3.4.3.2.

The desired heating rate utilized for the conventional concretes tests was 2ºC/min and to avoid explosive spalling, the rate of heat for UHPC testing depended upon the target temperature, Figure 3.6(b). Tests conducted at temperatures of 300ºC and above employed a heating rate of 0.50°C/min, while the remaining UHPC tests employed the same heating rate as the conventional concretes. Figure 3.8 illustrates the rise in temperature to 600°C for each type of concrete. Due to concrete's low thermal conductivity and high specific heat, as expected the surface temperatures increase more rapidly as compared to the temperature within the core of the cylinder (Figure 3.8).

Although the equipment is tested prior to each test, at times during a test, a thermocouple would begin providing erroneous data. While each thermocouple is essential, the surface and center thermocouples, Figure 3.1(a), are more critical for they provide vital data with respect to explosive spalling. If the surface thermocouple was reporting erroneous values, the average between the furnace, and center thermocouples was taken to be the surface values. Additionally, if the center thermocouple experienced damage, the recorded surface temperatures were utilized for the average rate of heat and the thermal gradient was not calculated. Furthermore, in case a similar test was performed previously, i.e. same UHPC type, and furnace input, the respective value from the preceding test were utilized. Table A1, A2, and A3 in Appendix A will provide further details associated with each UHPC design mix test.

The conventional concretes (Figure 3.8(a) and (b)) temperature rise to 600°C is very similar. However, due to the lower thermal conductivity of UHPC, as compared to the conventional concretes, the time required to reach 600°C is over three times greater. There was a smaller learning curve with the conventional concretes as opposed to UHPC, to calibrate the furnace to provide the desired rate of heating. Therefore, the same average rate of heat were not utilized for the conventional concretes depicted in Figure 3.8. However, regarding the tests conducted at the other temperatures, NSC-SF and HSC both required greater time to reach their target temperatures as opposed to NSC and HSC-PP, respectively. The additional time for NSC-SF is due to the steel fibers and the lack of polypropylene fibers for HSC. Regarding Figure 3.8(c) the desired rate of heating to allow UHPC F9 to reach 600°C was 0.5ºC/min and as seen in the figure it took over 17 hours to do so. Furthermore, similar to HSC, the design mixes of UHPC containing no polypropylene fibers required a greater time versus design mix UHPC F. Moreover, due to explosive spalling, temperatures above 400°C were not attainable for UHPC A & B and D. Finally, as seen in Figure 3.8(c) no visible moisture induced plateau was seen in any UHPC F temperature versus time curve (Klingsch, 2014; Ju et al., 2015). The rate of heating for UHPC will be discussed in detail in section 3.4.3.

3.4.2 Compressive strength, elastic modulus, and stress-strain relationship

The compressive strength, and modulus of elasticity with respect to temperature are presented in Figures 3.9 and 3.10, accordingly. All the tests were load-controlled and stopped as soon as the specimen experienced failure. The stress-strain relationship will be presented in the following subsequent sections for each respective type of concrete, along with the discussion of all three mechanical properties. Details pertaining to each UHPC test are given in Tables 3.5, 3.6 and 3.7; While the conventional concretes respective data are in Table 3.8 and 3.9. Chapter Four

will compare and discuss the 3 UHPC design mixes, with the 4 conventional concretes and ASCE (1992) and Eurocode 2 (2004).

3.4.2.1 NSC

Figure 3.11 and 3.13 provide the stress-strain relationship for NSC and NSC-SF, respectively. Additionally Figure 3.12 and 3.14 display the type of failure modes for NSC and NSC-SF, following the compressive strength tests. Both types of concretes were evaluated from 20-750°C and the ambient temperature tests for both NSC and NSC-SF were conducted utilizing rubber caps. Due to the limited capability of the electrical furnace (Figure 3.3), 800°C tests could not be conducted. The maximum temperature attained were 750 and 700°C for NSC and NSC-SF, respectively. The NSC-SF specimens' slightly lower temperature is attributed to the steel fiber content and the higher specific heat of the concrete at temperatures above 400°C (Kodur and Khaliq, 2011). The compressive strength tests conducted up to 400°C resulted in a thunderous explosion. However, the tests conducted at, and above 600°C did not produce any sound upon failure. The concrete's hue (Figure 3.12 and 3.14) begins to change following exposure to 600°C, and above.

The compressive strength (Figure 3.9) of NSC and NSC-SF reduces to about 50% at 600°C. Such a decrease may be attributed to the severance of calcium-hydroxide between 400 and 600°C (Schrefler et al., 2002; Klingsch, 2014). Furthermore, the relative compressive strength of NSC at 750°C drastically decreases below 25%. The calcium-carbonate decarbonating at temperatures greater than 700°C may be the cause of the sudden loss of strength. Moreover, due to the electrical furnaces' capability, in an attempt to reach 800°C, the reduction may have been exacerbated further due to the prolonged exposure to the heat. Overall, up to 700°C, NSC's compressive strength (Figure 3.9) degradation is much smoother as compared to NSC-SF. Although the NSC-

SF test conducted at 200°C suffered a diagonal fracture (Figure 3.14), it resulted in a lower compressive strength than the 400°C test.

For the most part NSC and NSC-SF behave very similarly with respect to their stress-strain relationship (Figure 14, and 16). At ambient conditions, NSC-SF displayed 33% more ductility than NSC and with increasing temperatures NSC-SF remained more ductile. Although, steel fibers are predominantly utilized for tensile strength purposes, the additional ductility during the stress-strain curve is attributed to the fibers as well. As the specimens were exposed to elevated temperatures, the peak strain increased due to softening of the material. The elastic modulus for both, NSC, and NSC-SF regress faster as compared to their compressive strengths. NSC elastic modulus reaches down to 26% at 400°C, and NSC-SF even further to 16% as compared to their respective ambient condition stiffness. The decaying of the cement paste most likely caused the rapid stiffness decline (Kalifa et al., 2000). The addition of steel fiber to the concrete did not contribute towards its stiffness.

3.4.2.2 HSC

Figure 3.15 and 3.17 provide the stress-strain relationship for HSC and HSC-PP, respectively. Additionally Figure 3.16 and 3.18 display the type of failure modes for HSC and HSC-PP, following the compressive strength tests. HSC was evaluated from 20-600°C, and HSC-PP up to 750°C, and the ambient temperature tests for both HSC and HSC-PP were conducted utilizing rubber caps. Due to the limited capability of the electrical furnace (Figure 3.3), 800°C test for HSC-PP could not be conducted. The compressive strength tests sound upon failure for HSC and HSC-PP is equivalent to NSC and NSC-SF, and the concrete's hue (Figure 3.16 and 3.18) begins to change following exposure to 400°C, and above.

Due to the denser microstructure achieved through the addition of silica fume and high content of cement, coupled with the reduction in w/c ratio, the compressive strength's (Figure 3.9) reduction is much more drastic. The HSC and HSC-PP design mixes tested, employ over two times the amount of cement as compared to the NSC and NSC-SF. Therefore, at temperatures between 100-300°C, the decomposition of the hydration products of cement contribute greatly to the strength loss (Dehn, 2004; Klingsch, 2014). As seen in Figure 3.9, at 400°C the compressive strength is reduced to a third of its original strength. However, HSC and HSC-PP maintain around 30% of their original strength at 600°C. The minimal strength loss is attributed to the reduction of calcium-hydroxide formation accomplished with the addition of silica fume. Though it is only 7% of the cement, it is enough to relatively maintain its strength (Khoury, 2000; Zdeb, 2013). The decreasing strength of HSC-PP beyond 600°C is owed to the analogous factors that influenced NSC's strength.

Beyond 200°C, HSC-PP (Figure 3.17) displayed greater ductility as opposed to HSC (Figure 3.15), and excluding the HSC test at 600°C, the peak strain increased with elevated temperatures due to softening of the material. The HSC at 20°C and HSC-PP at 200°C, were repeated due to erroneous results and poor compressive failure mode of the cylinder. Furthermore, below temperatures of 600°C, the addition of polypropylene fibers improved the stiffness. While, HSC's stiffness degraded below 50% at 200°C, it wasn't until 400°C for HSC-PP. Finally, at 600°C, both concretes stiffness degraded to about 15% of its original elastic modulus. Therefore, the addition of polypropylene fibers with HSC assists its ductility and stiffness with increasing temperatures.

3.4.2.3 UHPC

Figure 3.19, 3.21 and 3.23 provide the stress-strain relationship for design mixes UHPC A & B, D, and F, respectively. Additionally Figure 3.20, 3.22 and 3.24 display the type of failure modes for each UHPC design mix, following the compressive strength tests. Due to UHPC A & B and D undergoing explosive spalling, both design mixes' mechanical properties were only evaluated up to 400°C; while the addition of polypropylene fibers granted UHPC F to be tested up to 700°C. Moreover, due to explosive spalling and limited resources, only design mixes UHPC A & B and F allowed repetition of tests (3-4), conducted at temperatures of 20-400°C and tests at and beyond 300°C could only be performed utilizing an heating rate of less than 1ºC/min. The data provided for the remaining UHPC tests, consisted of a singular test. There are 4 UHPC A & B tests in Table 3.5, conducted at 20, 100, 200 and 200°C, that did not adhere to the method according to ASTM-C469/C469M, but followed ASTM-C39/C39M. Therefore only their respective compressive strengths were attained, and their corresponding data is incorporated in Figure 3.9. The compressive strength tests sound upon failure and the concrete's hue (Figure 3.20, 3.22 and 3.24) are similar to the design mixes of HSC.

The ambient temperature data collected for UHPC A & B and F were conducted utilizing caps and with no cap. Unfortunately, due to the limited number of specimens of design mix UHPC D, no 20°C test could be conducted utilizing a cap. The cap removes any imperfections upon the horizontal surfaces and provides a higher value. Therefore, though UHPC D's 28-day compressive strength is 10% greater than UHPC F, from Figure 3.9 UHPC D and F have the same compressive strength at ambient conditions.

All the UHPC design mixes tested experienced a decrease in strength at 100°C, with UHPC A & B experiencing the greatest reduction of 18%. The degradation of strength is attributed to the

evaporation of the non-chemically bound water within the UHPC, causing increased permeability and loss of strength (Dehn, 2004; Klingsch, 2014). However, following exposure of 200°C, UHPC F was the only design mix that did not increase in strength. The increase in strength is owed to shrinkage of the concrete following the water evaporation (Xiong and Liew, 2015). UHPC F did not experience an intensification until 300°C. The delayed response of the surge of strength may be caused by the melting of polypropylene fibers around 150-170°C and further increasing the permeability (Klingsch and Frangi, 2011; Bei and Zhixiang, 2016).

At 300 and 400°C, UHPC D and F maintain strengths close to their respective original strength, with UHPC D achieving strengths greater than the original at 110 and 104% at 300 and 400°C, respectively, while UHPC design mix A & B deviate from the group beyond 200°C. The nonconformity seems to be caused by either the specimen was not properly prepared, resulting in a poor break, or higher heating rates deteriorated the strength. The former was the cause for one test and the latter for the remaining four. The greatest compressive strengths attained for UHPC A & B at 300 and 400°C employed heating rates that were on average 30% lower than the lower compressive strengths, with on average 16% greater duration of heating. Moreover, the supreme strength attained from all UHPC design mixes, was by UHPC D8 tested at 300°C with an average heating rate of 0.25ºC/min and total heat exposure duration of 18 hours. Although nearly reducing the average rate of heating to 50%, UHPC F sustained a 16% increase in compressive strength at 200°C, dramatically increasing the duration in the furnace and employing extremely slow heating rates, at 300 and 400°C negatively effects UHPC design mix F. When employing a heating rate like UHPC D8 (0.25ºC/min), on average the duration within the furnace was increased and strength decreased, 2.5 times and 8%, accordingly.

UHPC F9 decays to 70% of its original strength at 600°C and experiences a drastic deterioration at 700°C (UHPC F13). The inordinate amount of silica fume as compared to the cement content in UHPC F provides a very low C/S ratio, thus resulting in minimal calcium-hydroxide (Khoury, 2000; Zdeb, 2013). Therefore, the sudden decrease experienced by UHPC F9 and F13, is dominated by the α-quartz to β-quartz transformation occurring around 570°C coupled with the continual dilapidation of the cement paste (Dehn, 2004; Klingsch, 2014).

At ambient conditions (Figure 3.19, 3.21 and 3.23), save the maximum compressive strengths attained, the three UHPC design mixes tested resulted in similar peak strains. At elevated temperatures, for the most part UHPC A & B, D, and F behave very similarly, with respect to their stress-strain relationship, with increasing temperatures the peak strain increases. However, as explained previously, some of the UHPC A & B tests conducted at 300 and 400°C differed slightly. The elastic modulus for UHPC behaved quite differently as compared to their respective compressive strengths. At ambient conditions the elastic modulus for all three UHPC tested is very similar. At temperatures of 100 and 200°C, UHPC F's elastic modulus experiences the slowest degradation. However, all three UHPC tested reach half their elastic modulus around the same temperature (300°C). At 600 and 700°C design mix UHPC F elastic modulus sustained a rapid decrease to 10 and 7% from ambient conditions.

The addition of polypropylene fibers along with steel fibers, UHPC F, does improve the fire performance with respect to compressive strength, elastic modulus below 400°C and reaching temperatures above 400°C. Finally, utilization of larger volume content of steel fiber (design mix UHPC A & B) does not necessarily increase the compressive strength.

3.4.3 Fire-induced spalling behavior

The following two sections will emphasize the prominent results accumulated as part of this study corresponding to explosive spalling in UHPC. The data pertaining to the effects of rate of heating will be discussed first, followed by thermal gradients.

3.4.3.1 Spalling behavior in experiments

The results from this study indicate that employing a low rate of heating does not necessarily correlate with the mitigation of explosive spalling. Though the rate of heat and development of thermal gradients are vital, their resultant, pore pressure, seems to be the predominant trigger (Felicetti et al., 2000). The effects of rate of heat upon the three UHPC design mixes will be discussed here and information pertaining to thermal gradients will be presented in detail in the following section.

During this study, the electric furnace experienced fourteen fire induced spalling events; of those, thirteen were explosive in nature. As seen by Figure 3.25, such an explosion produces an exorbitant amount of energy, enough to expand the metal frame of the furnace. The numerous explosive spalling events experienced by the furnace caused a gap of at least 6.35 mm, for most of the height of the furnace door. Therefore, tie down straps were utilized to compensate for the gap. The explosion was usually accompanied with a very loud sound, and Figure 3.26 displays specimens from each design mix that underwent explosive spalling. Prior to utilization of the temperature acquisition data device (Figure 3.7), a handheld thermocouple reader was used, and the temperature was measured every 30 to 45 min. Therefore, the first three elevated temperature tests listed in Table 3.5, the rate of heats listed are estimates, and not exact values. Moreover, the initial goal was to maintain a rate of heat of 2ºC/min as recommended by RILEM standard. However, there was a bit of a learning curve due to testing a novel material. In the first three

elevated temperature tests as listed in Table 3.5, the actual heating rates were far below the desired 2ºC/min. Therefore, the electric furnace (Figure 3.3) was calibrated with UHPC A1, in desire to better understand the furnace behavior with UHPC, coupled with an attempt to complete a 600°C compressive test. Unfortunately, specimen UHPC A1 experienced explosive spalling with an average rate of 1.05ºC/min.

To better comprehend the explosive spalling involved with UHPC a new testing regime was devised. In short, rate of heating ranging from 2 to 4ºC/min were to be used, with temperature ranging from 200 to 400°C with design mix UHPC A & B. The data associated with this testing, along with all UHPC data for tests conducted at, and above 300°C, is given in Table 3.10. To avoid presenting redundant data, thermal gradient results are presented in Table 3.10 as well, however as stated previously, thermal gradient results will be discussed further in the following section. Table A1, A2, and A3 in Appendix A will provide further details associated with each UHPC test conducted.

As expected, the higher the rate of heat, the sooner the UHPC specimen will experience explosive spalling. UHPC B3 (Figure 3.26) experienced explosive spalling in the shortest period, 80 min, combined with the lowest center temperature, 191°C. Although specimen UHPC B8's rate of heat was higher than UHPC B3, UHPC B8 exploded at 95 min and at a greater core temperature, 248°C. The conflicting results may be attributed to differing furnace input or variance in moisture within the specimen. As opposed to design mix UHPC A & B, UHPC F contains 2.00 kg/m^3 of polypropylene fibers as prescribed by Eurocode 2 (2004), and explosive spalling was not expected. However, UHPC F1 (Figure 3.26) sustained explosive spalling with a rate of heat less than 1.50°C/min. The test was repeated and UHPC F12 underwent explosive spalling around the same temperature, 295°C. Furthermore, UHPC B3's test was repeated but with UHPC F14 and sustained

explosive spalling at the equivalent time, with an average rate of heat 2.50°C/min and core temperature slightly higher, 220°C. Item to mention, due to an experiment error, UHPC A7's test was abruptly ended and sustained mere surface spalling. However, as the rate was shy of 2ºC/min it is highly expected if the furnace was not shut down too soon, it would have experienced explosive spalling. The nine specimens to explosively spall as part of the initial testing regiment, the average rate of heat was 2.70°C/min, with the least slightly higher than 1ºC/min and average core temperature of 250°C. Therefore, it was concluded to conduct a successful 300°C or higher compressive strength test, a rate of heat lower than 1ºC/min must be utilized.

To further study the behavior of UHPC, all three design mixes were studied with a desired rate of heat of 0.50°C/min at temperatures of 300°C and above. To achieve such a rate, two different furnace inputs were utilized, a steady increase with a high target temperature (referred to as input 1) and rapid increase with a low target temperature (referred to as input 2). The former produced three (UHPC B1, B2 and D7) out of the nine tests to explode and surprisingly the latter only two (UHPC D5 and D6) out of fourteen. Employing either of these inputs, design mix UHPC F did not sustain any explosions.

UHPC D4 (average rate of heating, 0.50°C/min) was the sole specimen from design mix UHPC D to avoid explosive spalling with input 2 and UHPC D5 and D6 experienced explosive spalling with a center temperature close to 270°C. Astonishingly, the average rate of heat for the two tests were very similar to the UHPC A & B tests that did not experience explosive spalling, of around 0.95ºC/min. Following the resulting two explosions, UHPC D7 and D8 were tested employing input 1 and desired average rate of heating of 0.25ºC/min, with 50% success. UHPC D7 (Figure 3.26) sustained an explosion following a slight increase to the furnace input with core temperature of 284°C and a time to spall of 850 min. UHPC D8 avoided an explosion with an

average rate of heating of 0.25ºC/min. Additionally, UHPC B5 was the sole test to avoid explosive spalling from design mix UHPC A & B with input 1 and the core temperature was taken to 329°C. Moreover, upon removal from the furnace, there was moisture visibly escaping the specimen in numerous locations (Figure 3.27). Design mix UHPC F overall average rate of heating to avoid explosive spalling was 0.75ºC/min. The last four UHPC F tests listed in Table 3.7 were not included as part of the previous average. The tests consisted of altering the average rate of heating drastically in an attempt to evaluate the compressive strength following prolonged exposure in the furnace.

The average heating rate, core temperature and time to spall for the specimens to undergo explosive spalling for each separate design mix are: UHPC A & B, 1.75ºC/min, 250°C and 170 min, UHPC D, 0.75ºC/min, 275°C and 440 min, and UHPC F, 2.00°C/min, 270°C and 140 min. Overall amongst all UHPC to experience explosive spalling the averages are: 1.50°C/min, 265°C and 250 min. UHPC D's time to spall is very high due to UHPC D7 undergoing the explosion at 850 min. If UHPC D7 is not included, UHPC D's average time to spall is 232 min. Figure 3.28, displays the average rate of heating with respect to either, the maximum core temperature attained, or the core temperature for which the specimen experienced explosive spalling, for all the UHPC tests from Table 3.7. Each specimen is labeled in Figure 3.28 and all 14 specimens to experience explosive spalling are depicted with a red box along with their respective time to spall. It is abundantly clear, the rate of heating to avoid explosive spalling for design mixes UHPC A & B, and F is 0.75ºC/min (depicted by a pink dashed line in Figure 3.28) and design mix UHPC D is 0.25ºC/min (depicted by a red dashed line in Figure 3.28).

From this experimental study, employing a higher average rate of heating, shows that UHPC can undergo explosive spalling quicker, with core temperatures and average rate of heating

as low as 191°C and 1.50°C/min, accordingly. UHPC A & B contains 10% more steel fiber and its critical rate of heating to avoid explosive spalling is 3 times versus UHPC D. In addition, steel fiber alone and the combination with 2.00 kg/m^3 of polypropylene fibers does not mitigate explosive spalling. Moreover, tests confirmed minimal average rate of heating alone do not mitigate the explosive spalling behavior of UHPC. As seen with UHPC B5 and D7, moisture is quite relevant at temperatures above 300°C. Therefore, at lower heating rates, development of thermal gradients coupled with the release of vapor pressure are more crucial. Effect of thermal gradients will be discussed further in the following section.

3.4.3.2 Temperature gradient and rate of heat analysis

The thermal gradients development within UHPC directly affect the release of built-up pore pressure (Phan, 2008: Klingsch, 2014). Furthermore, since majority of the moisture content is chemically bound within the binder and does not completely evaporate until temperatures above 800°C, the risk of explosive spalling resulting from thermal gradients is continuously present (Klingsch, 2014). Therefore, results from this research give importance to not only high thermal gradients, but to minimal values as well (Ju et al., 2013). Table 3.11 displays the key points from the thermal gradient with respect to time graphs for each UHPC test listed in Table 3.10. Table 3.11 does not include the UHPC tests conducted employing an average heating rate less than 0.50°C/min. Furthermore, the thermal gradient with respect to time graph for each UHPC design mix (A & B, D, and F) tests, are given in Figure 3.29, 3.30 and 3.31, respectively. Table 3.12 is given to serve as a legend to Figure 3.29, 3.30 and 3.31. The legend describes the average rate of heating for each UHPC test.

Referring to Table 3.10 and 3.11, the UHPC tests that underwent high average rate of heating, of at least 1.25ºC/min, the maximum thermal gradient ranged from 14.55 to 32.00°C/cm.

The maximum thermal gradients occurred on average within 82 min of heating duration and the center temperature of the specimen did not go beyond 240°C. Eight of these tests, UHPC A13, B8, B3, A4, F1, F12 and F14 (Figure 3.29 and 3.31), underwent explosive spalling, which happened to occur on average about 40 min following the peak thermal gradient. Only UHPC F14 experienced the maximum thermal gradient and explosive spalling at the same time and UHPC F1 with the longest of 86 min. UHPC A13, B8, F1 and F14 respective thermal gradients experienced a short-lived sudden decline following the apex, and then a rapid increase which was concluded abruptly by the occurrence of explosive spalling. UHPC F1's test was not concluded following the explosive spalling, because the loud explosion was not heard. Thereby, the specimen was discovered to have exploded once opening of the furnace. UHPC B3 and F12 did not suddenly increase following the decline and underwent explosive spalling during their respective decline. Prior to the test prematurely ending, UHPC A7's (Figure 3.29) thermal gradient was at the initial stages of decreasing. Based off the data attained by the three tests that did explode, if the test were to have continued it too would have experienced explosive spalling.

The UHPC specimens that experienced explosive spalling with the slower rate of heating, of less than 1.25ºC/min, the maximum thermal gradients occurred at a much later time as compared to the higher average rate of heating. On average, the maximum thermal gradient occurred within 200 min for these five tests, and the time to spall occurred within 70 min thereafter. Three of the five tests (UHPC A1, B1 and B2) underwent explosive spalling utilizing input 1. Furthermore, the thermal gradient reached the maximum value during the latter part of the test; with each of the specimens experiencing an explosion within 20 min following the maximum thermal gradient. The remaining two tests (UHPC D5, and D6) that underwent explosive spalling, utilized input 2. The maximum thermal gradient was attained much faster (within 90 min), and the explosion occurred

144 min following the maximum thermal gradient. Specimen UHPC D6's maximum thermal gradient (20°C/cm) was as high as the specimens that underwent the higher rate of heating (at least 1.25ºC/min). Surprisingly, specimen UHPC D5's pinnacle value for its thermal gradient was under 5ºC/cm, yet it still underwent explosive spalling.

On the other hand, there were thirteen specimens that did not explode implementing the lower rate of heating. As stated in the previous section UHPC B5 is the sole test not to explode with input 1. Its maximum thermal gradient was 6.9ºC/cm and occurred during the latter part of the test. Over 90% of the remaining twelve specimens, the maximum thermal gradient occurred early (within 90 min), ranging from 6.53 to 8.83ºC/min. UHPC F13 (700°C) is the sole test where the maximum thermal gradient occurred at the end of the heating duration. In an attempt to reach 700°C, the furnace input's rate was increased towards the latter part of the heating process. Thus, if the input was not drastically increased, the maximum thermal gradient would have occurred within the first 100 min of heating.

Based off this study, UHPC inflicted with higher average rate of heating, will develop greater thermal gradients within the specimen that will occur later in the heating process. Average rate of heating greater than 1.25ºC/min coupled with thermal gradients of at least 20°C/cm for design mix UHPC A & B and 5ºC/cm for design mix UHPC F, 100% of the specimens experienced explosive spalling. Plus, the maximum thermal gradient occurred within two-thirds of the heating duration. Additionally, it makes sense UHPC F would result in a lower thermal gradient because of the presence of polypropylene fibers (Phan, 2008). However, with lower average rate of heating of less than 1ºC/min, two different scenarios occurred, (1) if the maximum thermal gradient (at least 10°C/cm) was reached towards the latter portion of the heating process, 67% of the specimens underwent explosive spalling, and (2) if the maximum thermal gradient (at least 5ºC/cm) was

reached early during the heating process, 22% of the specimens experienced explosive spalling. The lower maximum thermal gradient corresponds with UHPC D5 and the higher to UHPC B1. Given the critical average rate of heating for design mix UHPC D is lower than UHPC A & B, the values do coincide. Monitoring the thermal gradient while the UHPC specimen is being heated, can provide an inclination whether the UHPC will in fact, experience explosive spalling.

Table 3.1: Testing regime conducted as part of this study

Number	Concrete type	Room temperature	Elevated temperatures
		Cylinder size	
		75x150 mm	
1	UHPC A & B	4	24
2	UHPC D	1	7
3	UHPC F	4	17
4	HSC-PP	1	6
5	HSC	1	3
6	NSC-SF	1	5
7	NSC	1	4

Table 3.2: Mix proportions for UHPC design mixes tested as part of study

Components	UHPC A & B	UHPC D	UHPC F
Limestone No. 8, kg/m^3	526	487	488
Michigan Natural Sand, kg/m^3	553	513	514
Silica Sand, kg/m^3	304	282	283
Cement Type I, kg/m^3	519	481	482
Silica Fume, kg/m^3	228	212	212
Slag St. Lawrence, kg/m^3	104	96	96
Limestone Powder, kg/m^3	187	173	173
Steel Fiber, kg/m^3	130	118	118
Polypropylene Fiber, kg/m^3	-	-	2.00
Water, kg/m^3	153	114	115
Water Cement Ratio (w/c)	0.14	0.14	0.14
HWRA (28%) Chryso., kg/m^3	43	46	46

Table 3.3: Mix proportions for conventional concretes tested as part of study

Components	HSC	HSC-PP	NSC	NSC-SF
Cement Type I, kg/m^3	561	561	230	230
Fine aggregate, kg/m^3	641	641	930	930
Course aggregate 3/8" Limestone, kg/m^3	1089	1089	985	985
Silica Fume, kg/m^3	42	42	-	-
Steel fiber, kg/m^3	-	-	-	42
Polypropylene fibers, kg/m^3	-	1.66	-	-
Water, kg/m^3	151	151	157	154
Water cement ratio (w/c)	0.30	0.30	0.50	0.50
Superplastizer, kg/m^3	-	-	25	25
Fly Ash (Class C), kg/m^3	-	-	77	77

Table 3.4: Density and 28-day compressive strengths of concrete cylinders tested as part of study

Concrete type	28-day compressive strength, MPa	Density, kg/m^3	Density, g/cm^3
UHPC A & B	132	2500 *	2.50 *
UHPC D	182	2456	2.46
UHPC F	165	2436	2.44
HSC	111	2297	2.30
HSC-PP	100	2358	2.36
NSC	29	2256	2.26
NSC-SF	29	2231	2.23

* - Denotes an estimate

Table 3.5: Details of compressive strength tests of UHPC A & B cylinders

Specimen	T	Average rate of heat	f_c'	E	$T_{max(core)}$	$T_{max(furnace)}$
	ºC	ºC/min	MPa	GPa	ºC	ºC
UHPC B9	20	N/A	135	X	N/A	N/A
UHPC A12	20	N/A	139	39	N/A	N/A
UHPC A2	20	N/A	134	42	N/A	N/A
UHPC A7	20	N/A	138	38	N/A	N/A
UHPC A	100	0.60 *	121	X	X	X
UHPC A	100	0.40	109	30	X	X
UHPC B14	100	1.37	119	35	133	237
UHPC A3	100	0.30*	112	31	105	129
UHPC A9	100	1.00*	103	38	132	174
UHPC A14	100	2.00*	108	35	116	162
UHPC A & B	200	0.70*	118	X	X	X
UHPC A6	200	0.54	138	25	218	262
UHPC A & B	200	0.75*	135	X	X	X
UHPC B12	300	0.70	114	18	354	353
UHPC B19	300	0.65	120	11	X	443
UHPC A12	300	0.42	135	18	301	330
UHPC B4	400	0.60*	100	11	X	X
UHPC A2	400	0.69	117	14	434	339
UHPC A13	400	0.50	134	13	401	425
UHPC B11	400	0.60	124	13	X	443

* – Denotes an estimate

X – Denotes data not collected

Table 3.6: Details of compressive strength tests of UHPC D cylinders

Specimen	T	Average rate of heat	f_c'	E	$T_{max(core)}$	$T_{max(furnace)}$
	ºC	ºC/min	MPa	GPa	ºC	ºC
UHPC D-1	20	N/A	148	36	N/A	N/A
UHPC D-2	100	1.60	134	27	161	244
UHPC D-3	200	1.13	142	19	237	X
UHPC D-8	300	0.27	163	15	330	347
UHPC D-4	400	0.53	153	10	455	463

* – Denotes an estimate

X – Denotes data not collected

Table 3.7: Details of compressive strength tests of UHPC F cylinders

Specimen	T	Average rate of heat	f_c'	E	$T_{max(core)}$	$T_{max(furnace)}$
	ºC	ºC/min	MPa	GPa	ºC	ºC
UHPC F-4	20	N/A	128	38	N/A	N/A
UHPC F-11	20	N/A	170	39	N/A	N/A
UHPC F-19	20	N/A	153	X	N/A	N/A
UHPC F-21	20	N/A	140	X	N/A	N/A
UHPC F-2	100	1.64	120	36	169	229
UHPC F-6	100	2.66	125	X	X	304
UHPC F-20	100	1.65	131	X	170	317
UHPC F-3	200	1.89	115	40	230	330
UHPC F-7	200	1.76	127	24	234	300
UHPC F-10	200	0.91	133	X	238	231
UHPC F-5	300	0.75	150	16	330	360
UHPC F-15	300	0.21	136	13	319	346
UHPC F-17	300	0.25	143	10	329	344
UHPC F-8	400	0.74	151	11	433	X
UHPC F-16	400	0.23	142	13	421	433
UHPC F-18	400	0.24	132	10	421	436
UHPC F-9	600	0.74	100	4	632	629
UHPC F-13	700	0.69	38	3	731	768

* – Denotes an estimate

X – Denotes data not collected

Table 3.8: Details of compressive strength tests of NSC-SF and NSC cylinders

Specimen	T	Average rate of heat	f_c'	E	$T_{max(core)}$	$T_{max(furnace)}$
	°C	°C/min	MPa	GPa	°C	°C
NSC-SF	20	N/A	42	21	N/A	N/A
NSC-SF	200	2.36	26	10	N/A	364
NSC-SF	400	2.11	25	3	N/A	482
NSC-SF	400	3.66	30	5	N/A	526
NSC-SF	600	2.29	19	2	N/A	692
NSC-SF	700	1.48	11	2	N/A	X
NSC	20	N/A	46	24	N/A	N/A
NSC	400	1.93	30	6	N/A	482
NSC	600	2.15	26	2	N/A	691
NSC	700	1.82	24	3	N/A	742
NSC	750	1.49	11	3	N/A	777

* – Denotes an estimate

X – Denotes data not collected

Table 3.9: Details of compressive strength tests of HSC-PP and HSC cylinders

Specimen	T	Average rate of heat	f_c'	E	$T_{max(core)}$	$T_{max(furnace)}$
	°C	°C/min	MPa	GPa	°C	°C
HSC-PP	20	N/A	112	32	N/A	N/A
HSC-PP	200	1.04	82	31	N/A	277
HSC-PP	200	2.31	73	13	N/A	401
HSC-PP	400	2.29	41	10	N/A	483
HSC-PP	600	1.94	32	4	N/A	696
HSC-PP	700	1.62	24	3	N/A	741
HSC-PP	750	1.86	16	1	N/A	784
HSC	20	N/A	68	27	N/A	N/A
HSC	20	N/A	120	31	N/A	N/A
HSC	200	2.96	72	14	N/A	432
HSC	400	1.90	41	5	N/A	507
HSC	600	2.40	39	6	N/A	664

* – Denotes an estimate

X – Denotes data not collected

Table 3.10: Details pertaining to UHPC tests conducted at, and above 300°C

Specimen	T	Average rate of heat	Time to spall	T_{core}	Maximum thermal gradient	Time for maximum thermal gradient	Heating rate at time of spalling
	ºC	ºC/min	min	ºC	ºC/cm	min	ºC/min
A1	600	1.05	293	350	24	245	2.80
A13	300	2.20	125	248	32	83	3.42
B8 *	300	2.83	95	248	29	72	3.43
A7 *	400	1.87	99	185	21	96	3.89
B3	200	2.60	80	191	24	67	5.41
A4	300	2.00	102	227	X	X	2.70
A & B	300	0.42	No spalling	301	X	X	N/A
A & B	400	0.50	No spalling	401	X	X	N/A
B5	300	0.80	No spalling	329	7	290	N/A
B1	400	0.77	281	273	10	279	1.60
B2	300	0.70	290	277	14	293	1.97
B12	300	0.70	No spalling	354	9	76	N/A
B4 *	400	0.60	No spalling	430	X	X	N/A
A2	400	0.69	No spalling	434	8	81	N/A
B19	300	0.65	No spalling	340	7	83	N/A
B11 *	400	0.60	No spalling	430	X	X	N/A
D4	400	0.53	No spalling	455	7	84	N/A
D5 *	600	0.88	228	267	4	87	0.48
D6	300	0.98	236	275	20	90	0.63
D7	300	0.39	849	284	5	849	0.48
D8	300	0.27	No spalling	330	X	X	N/A
F1	600	1.42	177	295	15	91	1.51
F5	300	0.75	No spalling	330	7	90	N/A
F8	400	0.74	No spalling	433	8	87	N/A
F9	600	0.74	No spalling	632	8	85	N/A
F12	600	1.99	159	296	5	83	1.63
F13	700	0.69	No spalling	731	10	1104	N/A

Table 3.10 (cont'd)

Specimen	T	Average rate of heat	Time to spall	T_{core}	Maximum thermal gradient	Time for maximum thermal gradient	Heating rate at time of spalling
	C	ºC/min	min	ºC	ºC/cm	min	ºC/min
F14	300	2.45	81	220	13	81	5.83
F15	300	0.21	No spalling	319	2	661	N/A
F16	400	0.23	No spalling	421	X	X	N/A
F17	300	0.25	No spalling	329	1	680	N/A
F18	400	0.24	No spalling	421	3	714	N/A

* – Denotes an estimate

X – Denotes data not collected

Table 3.11: Key points from thermal gradient with respect to time graphs for UHPC tests conducted at, and above 300°C

Average rate of heat, ºC/min	Average rate of heat, ºC/min	Maximum average thermal gradient, ºC/cm	Average time for maximum average thermal gradient, min	Maximum thermal gradient, ºC/cm	% of tests to spall	Average time to spall, min	$T_{avg.(core)}$, ºC
$r \geq 1.25$	2.17	20	82	32	100	115	239
$r < 1.25$	0.71	10	212	24	27	266	389
$r < 1.25$ (No spalling)	0.65	8	220	10	N/A	N/A	431
$r < 1.25$ (Spalling)	0.88	14	199	24	100	266	288

r – Denotes average rate of heat

Table 3.12: Color legend for thermal gradient with respect to time graphs

Average rate of heat, ºC/min	Color designator
$r \leq 0.70$	**Any shade of blue**
$0.70 < r \leq 1.25$	**Any shade of green**
$1.25 < r \leq 1.75$	**Any shade of violet**
$1.75 < r \leq 2.25$	**Any shade of orange**
$2.25 < r \leq 2.75$	**Any shade of red**
$r > 2.75$	**Any shade of dark red**

r – Denotes average rate of heat

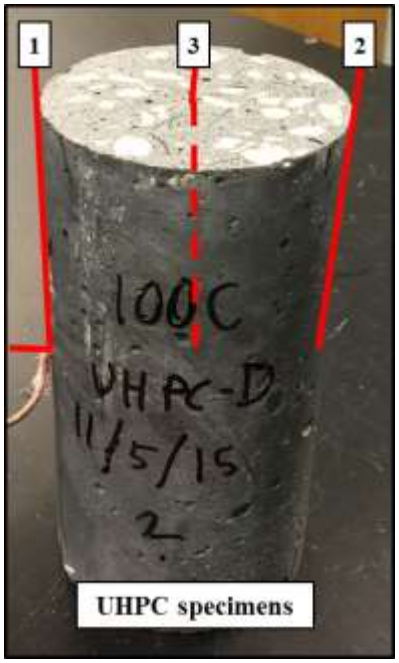

(a) UHPC specimens' thermocouple placement

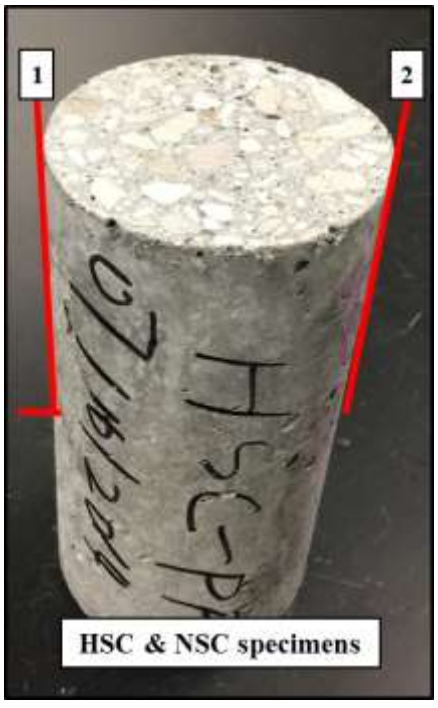

(b) HSC and NSC specimens' thermocouple placement

Figure 3.1: Prepared concrete specimens

Figure 3.1 (cont'd)

(c) Dimensions of tested cylinders

Figure 3.2: Table saw utilized to cut and prepare the concrete cylinders

Figure 3.3: Electrical furnace utilized in heating concrete cylinders

Figure 3.4: Forney load controlled strength testing machine to conduct compressive strength testing as part of this study

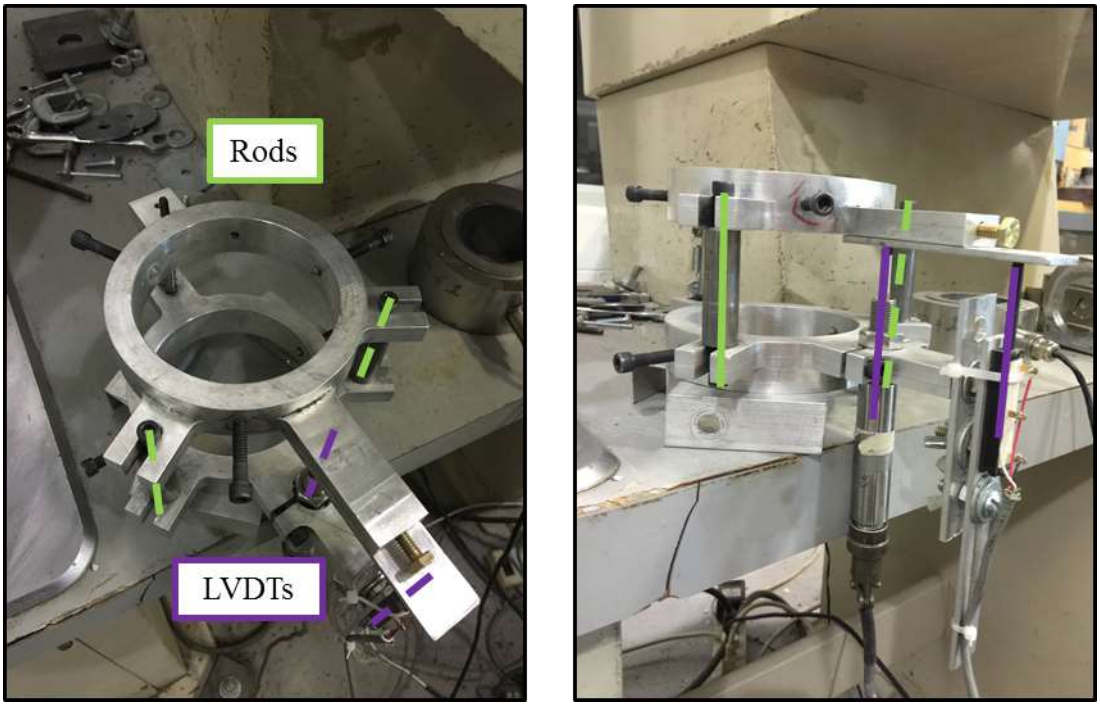

Figure 3.5: Compressometer with (2) LVDTs and (2) metal rods utilized to develop the stress-strain relationship as part of this study

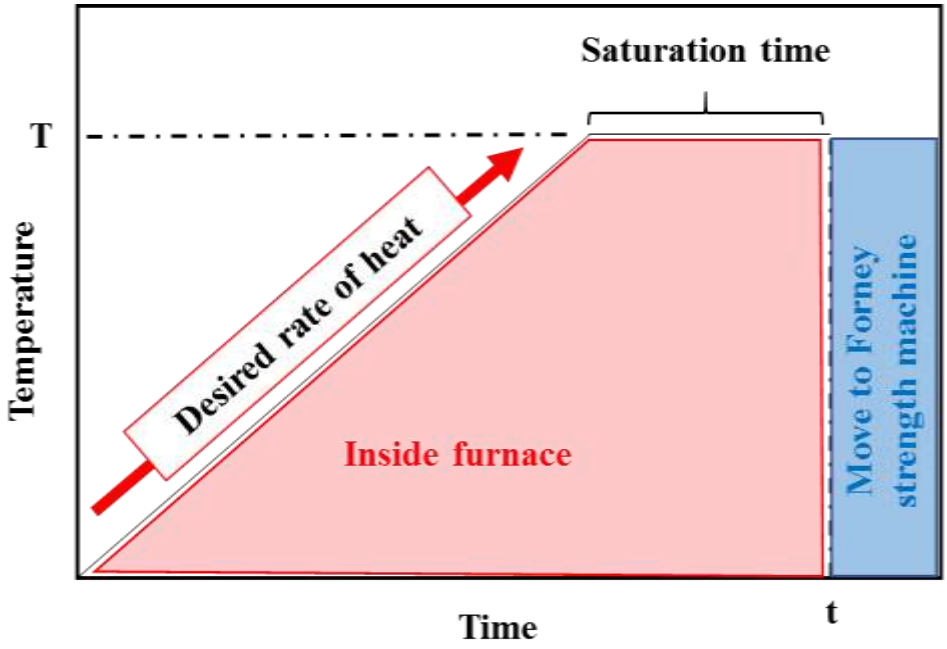

(a) Desired heating regime; Adapted from Khaliq (2012)

Figure 3.6: Desired heating rates for high temperature compression tests

Figure 3.6 (cont'd)

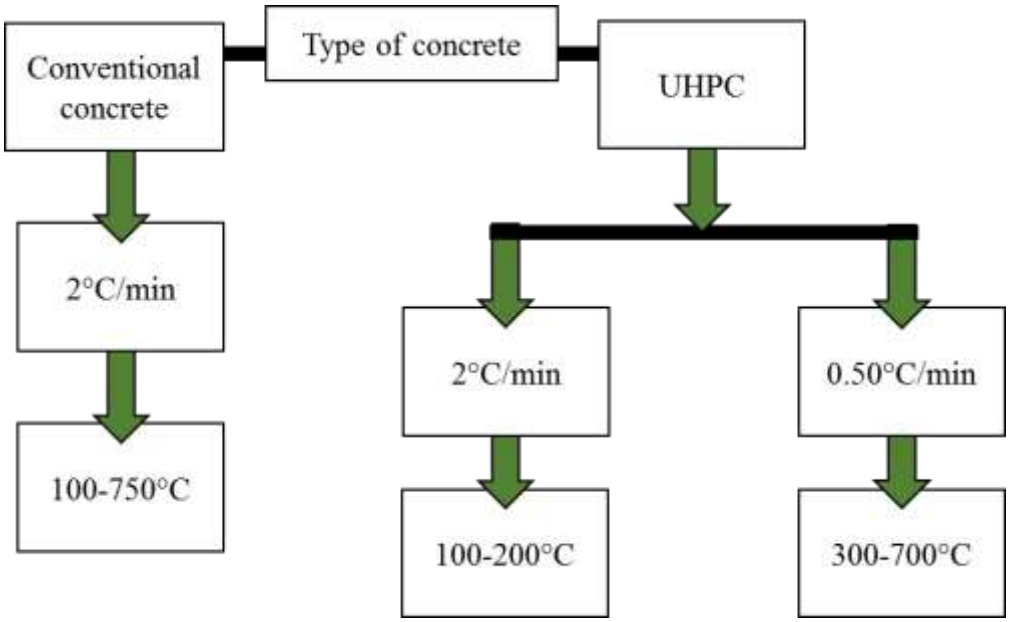

(b) Desired rate of heat by type of concrete

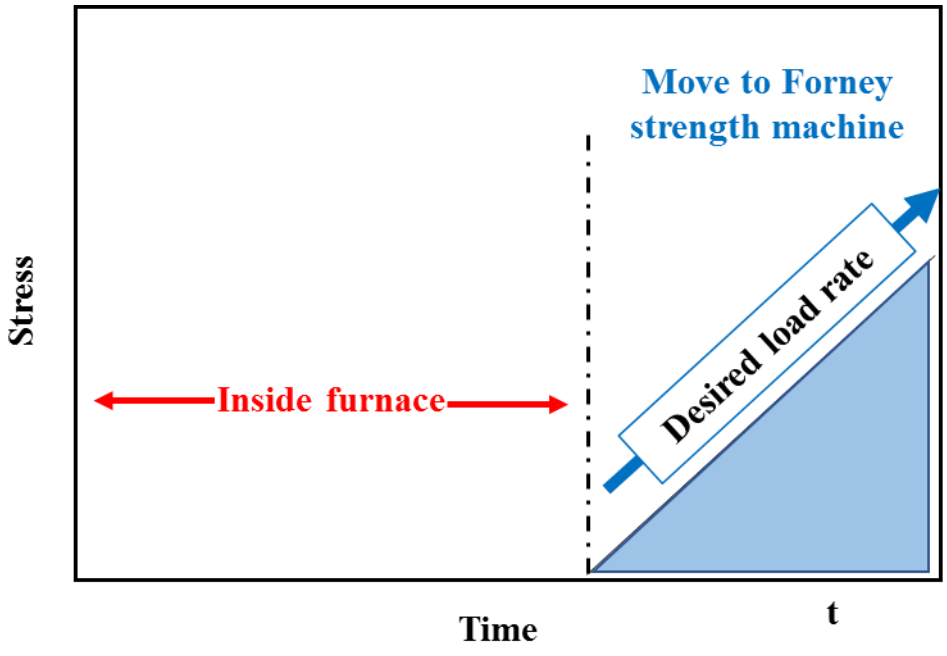

(c) Desired loading regime; adapted from Khaliq (2012)

Figure 3.7: Temperature data acquisition device utilized as part of this study

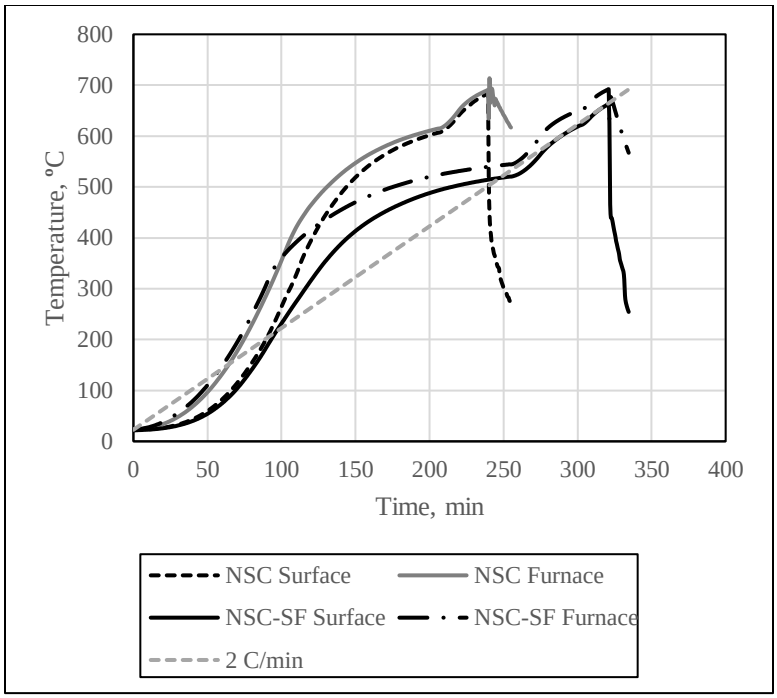

(a) NSC and NSC-SF concrete cylinders tested at 600ºC

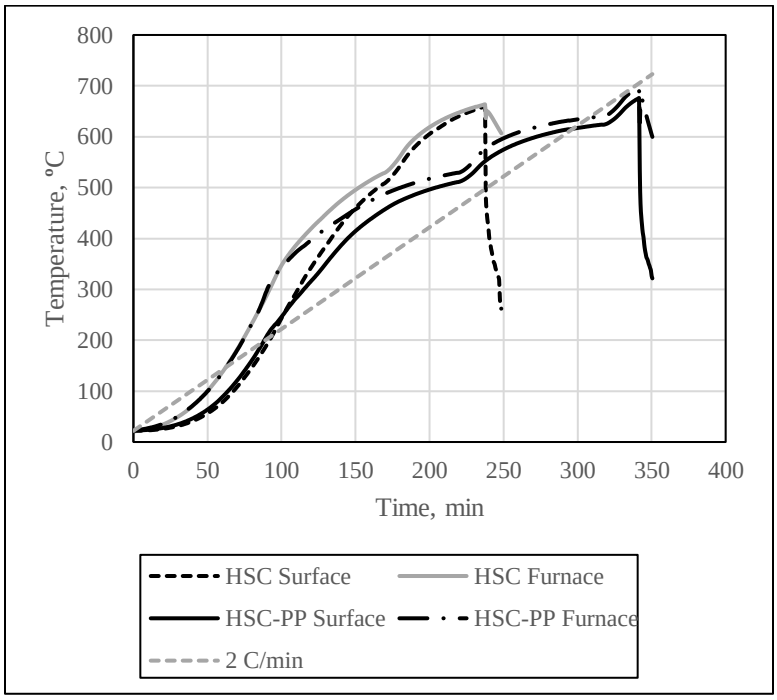

(b) HSC and HSC-PP concrete cylinders tested at 600ºC

Figure 3.8: Temperature versus time development for concrete cylinders tested at 600°C

Figure 3.8 (cont'd)

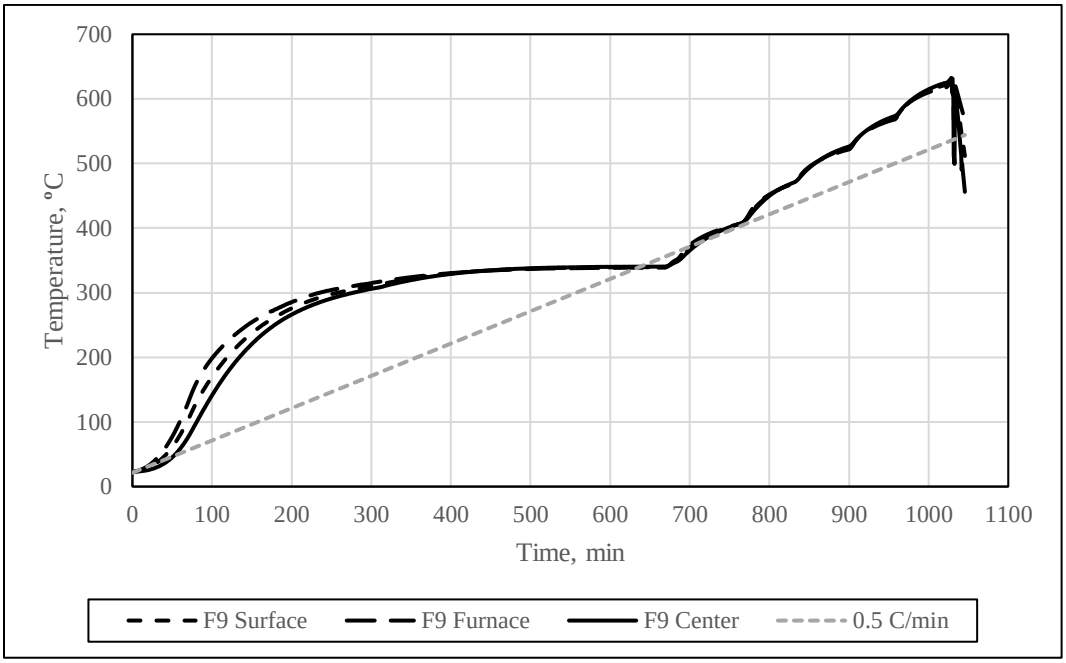

(c) UHPC F9 concrete cylinder tested at 600ºC

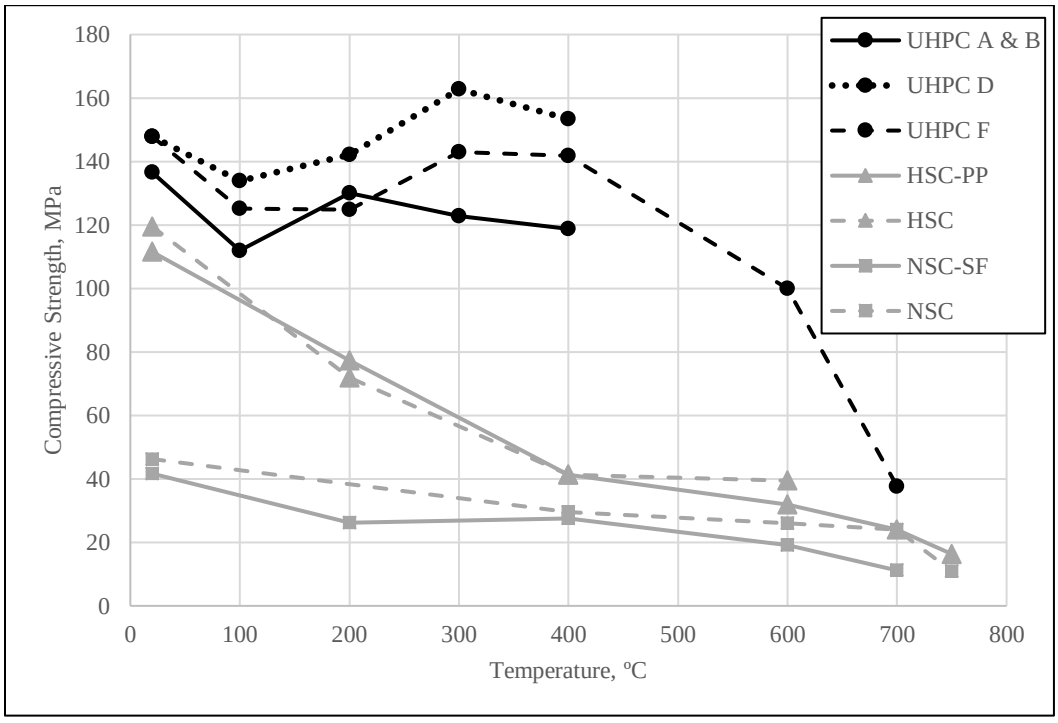

Figure 3.9: Compressive strength with respect to temperature of various concrete cylinders tested as part of research

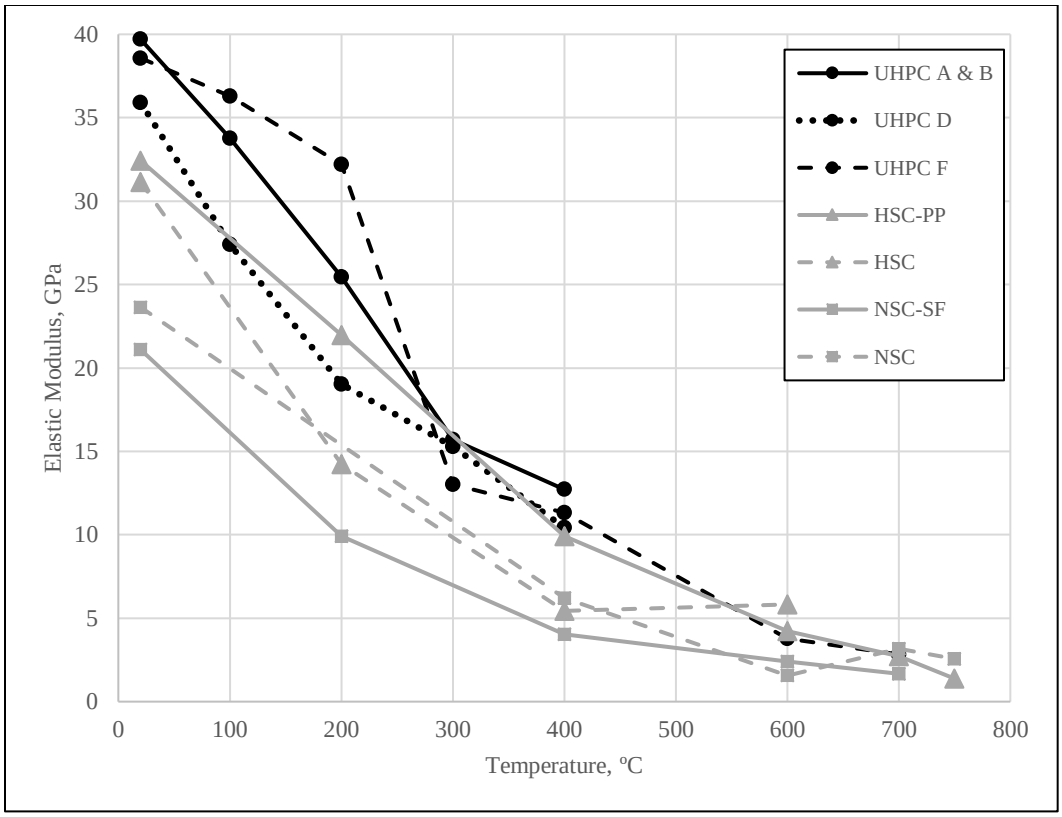

Figure 3.10: Elastic modulus with respect to temperature of various concrete cylinders tested as part of research

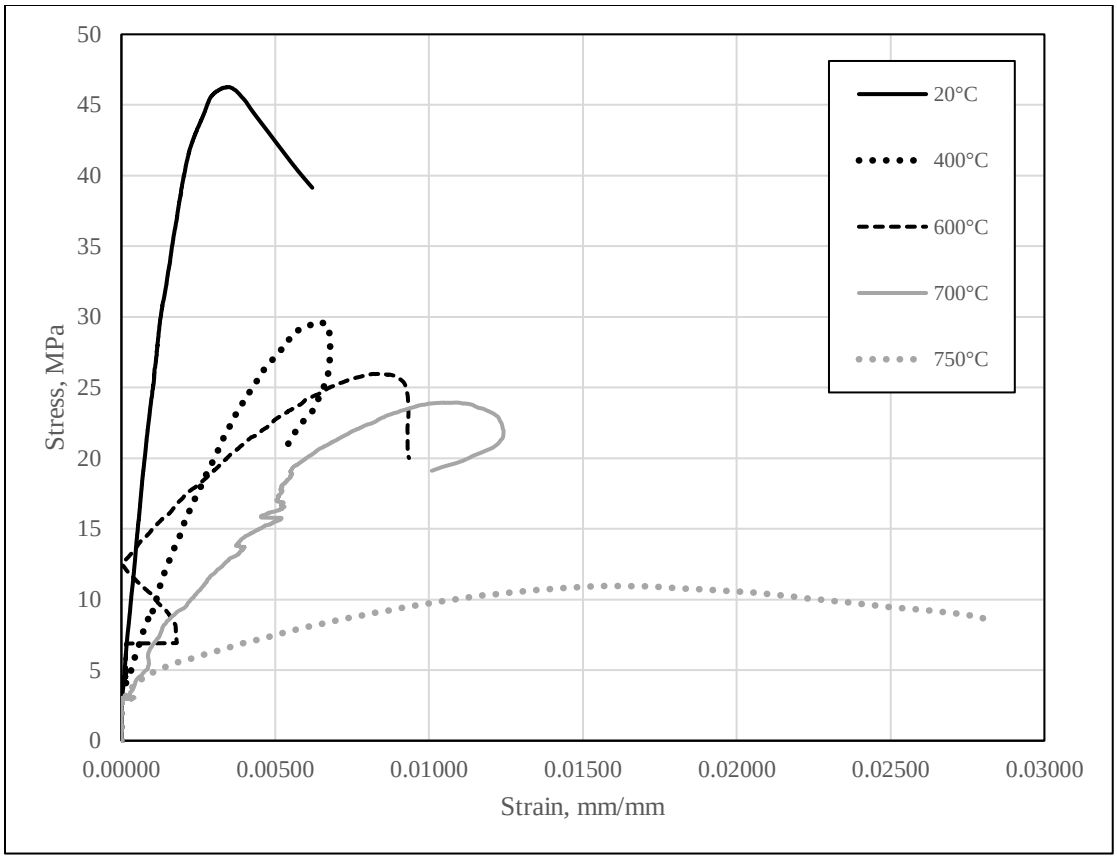

Figure 3.11: NSC stress-strain relationships with respect to temperature

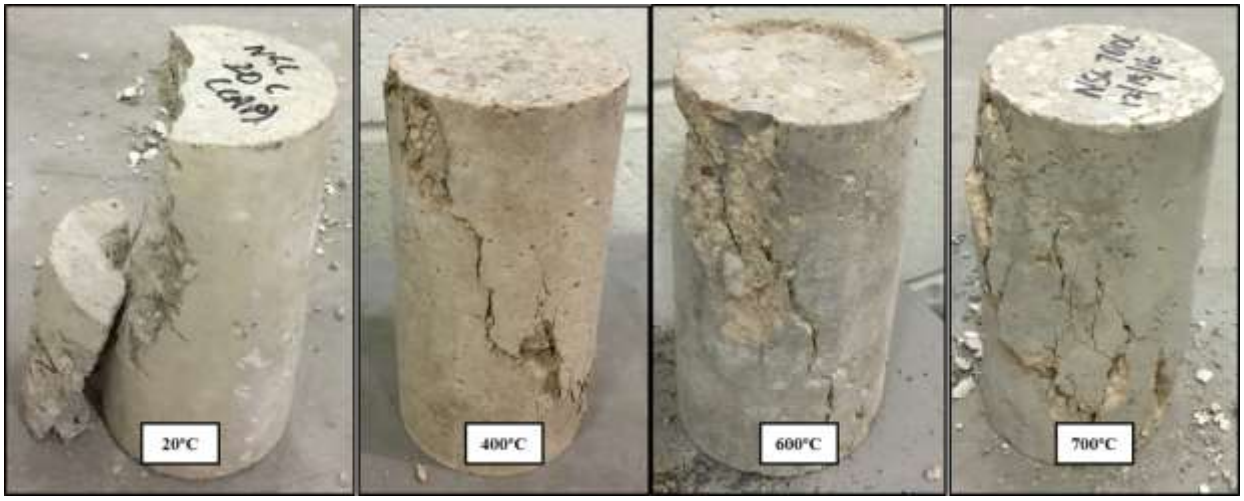

Figure 3.12: Failure modes of NSC at respective temperatures

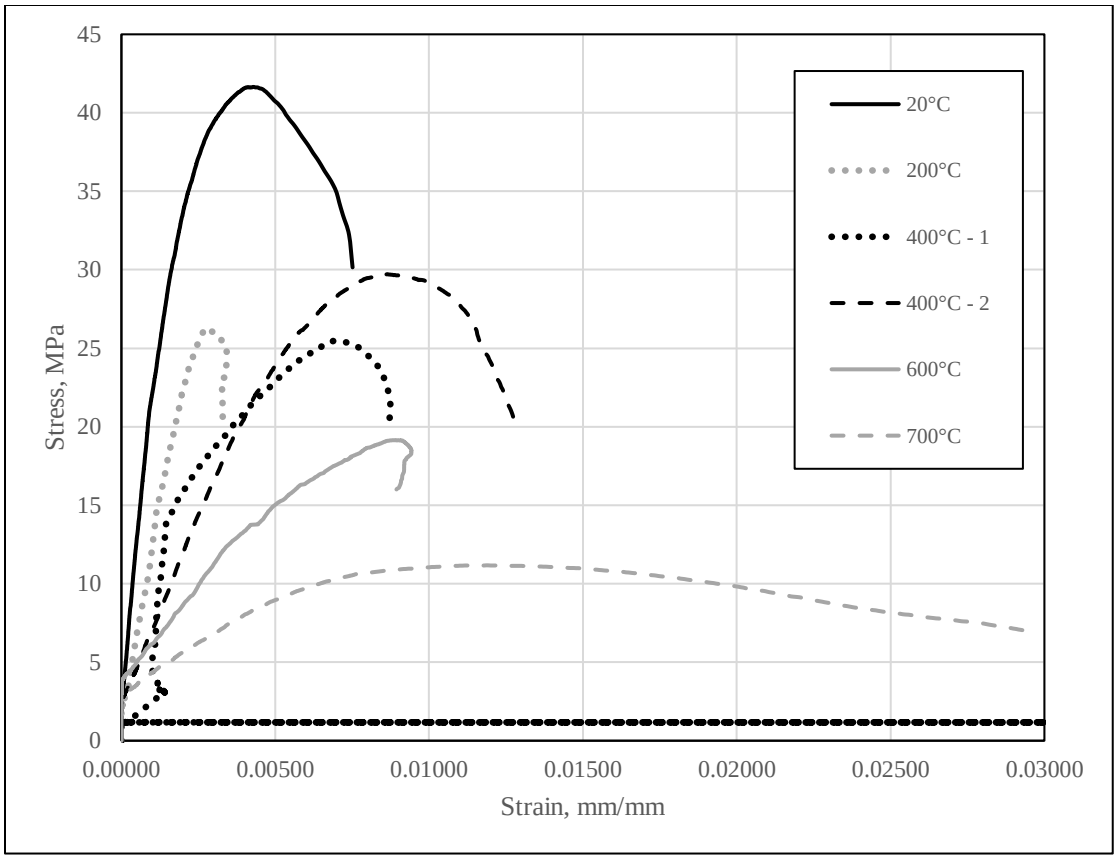

Figure 3.13: NSC-SF stress-strain relationships with respect to temperature

Figure 3.14: Failure modes of NSC–SF at respective temperatures

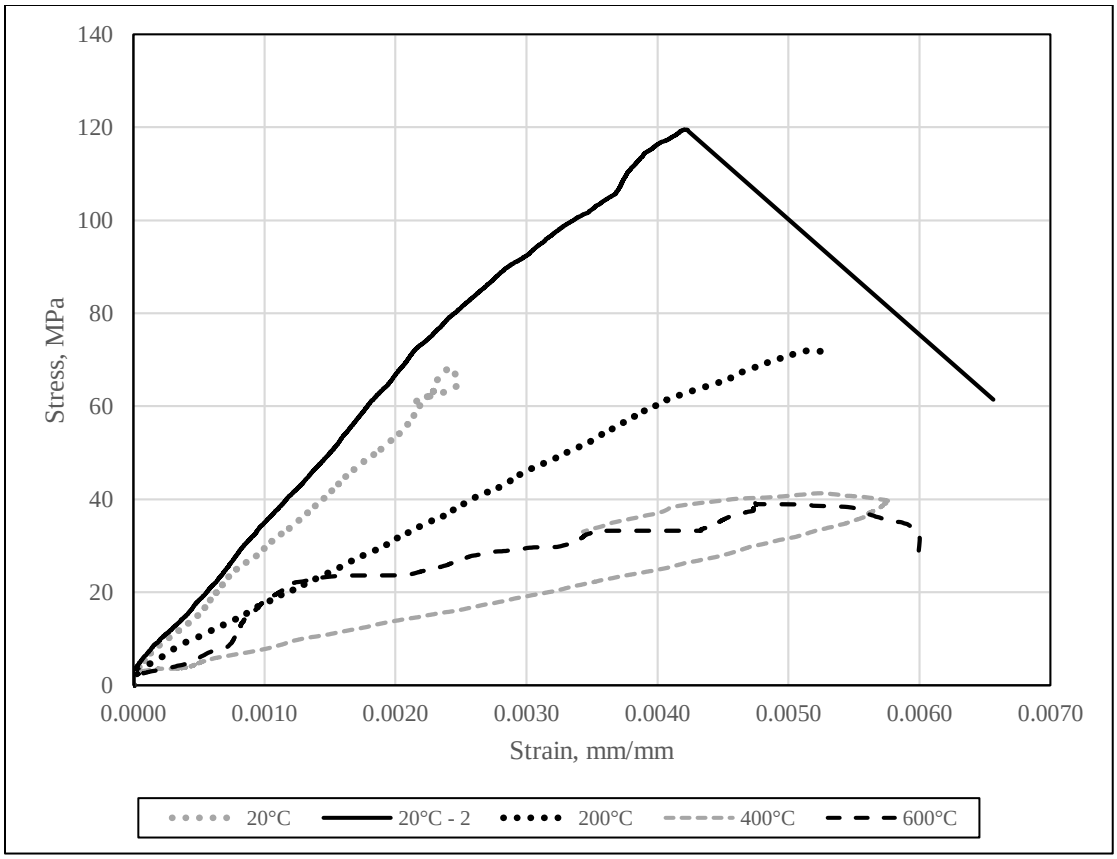

Figure 3.15: HSC stress-strain relationships with respect to temperature

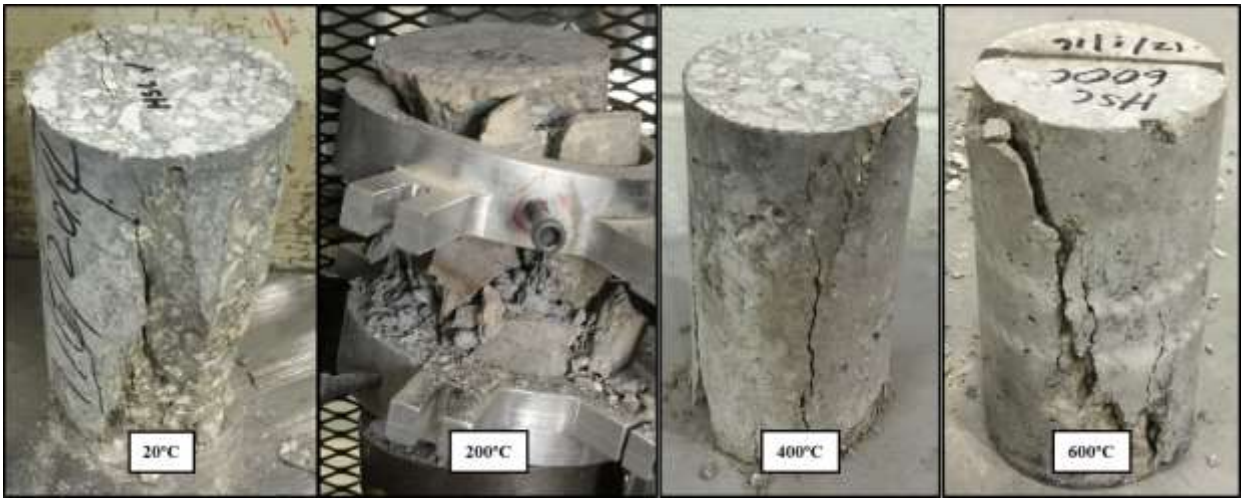

Figure 3.16: Failure modes of HSC at respective temperatures

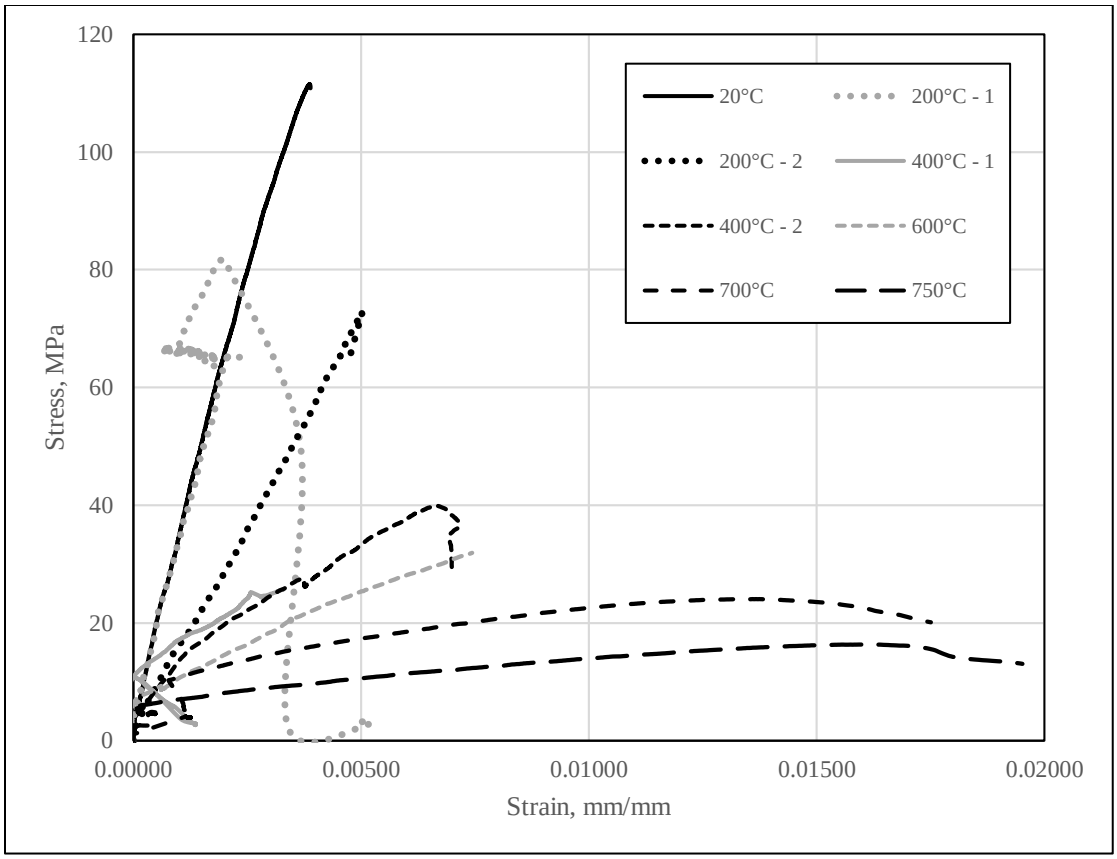

Figure 3.17: HSC-PP stress-strain relationships with respect to temperature

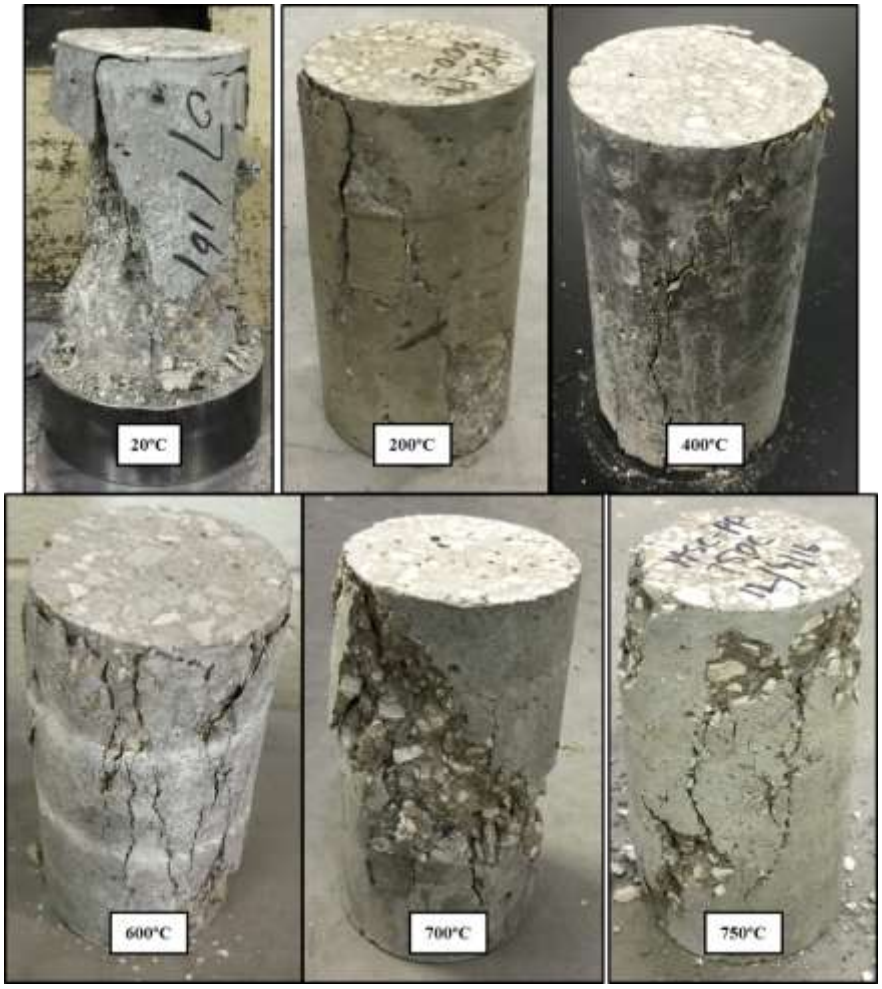

Figure 3.18: Failure modes of HSC – PP at respective temperatures

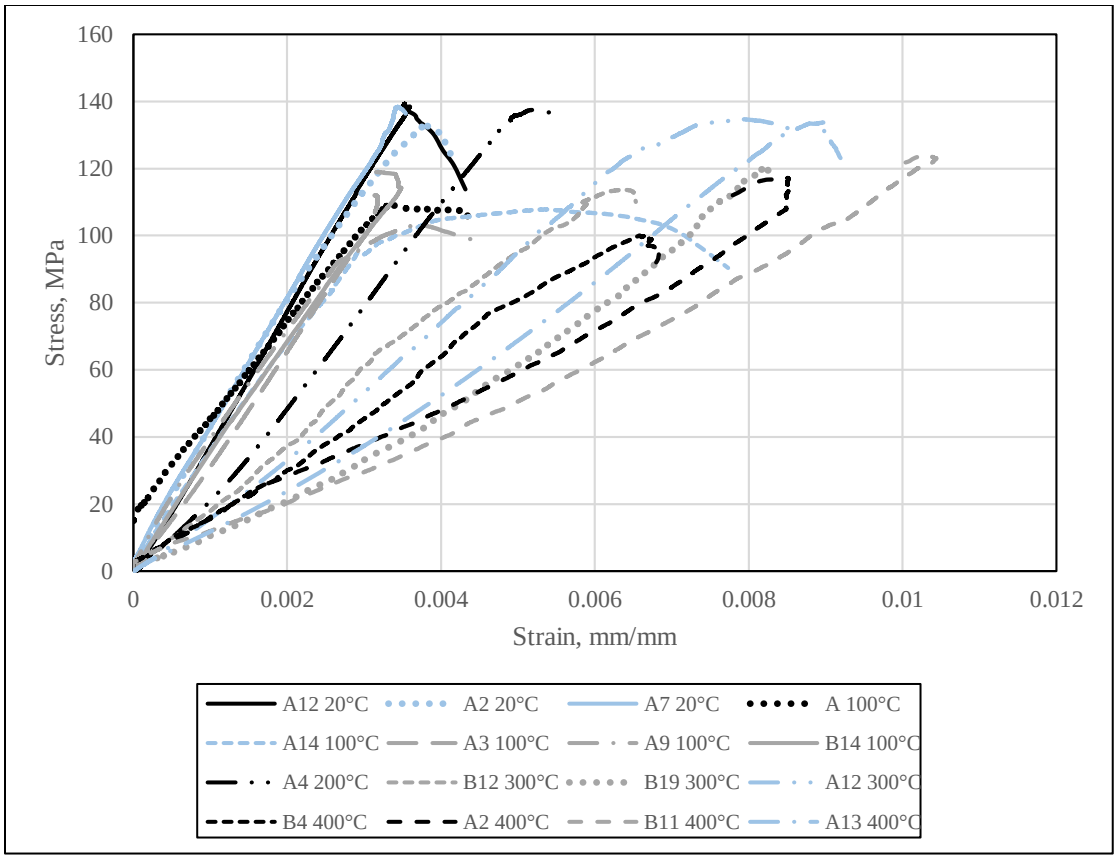

Figure 3.19: UHPC A & B stress-strain relationships with respect to temperature

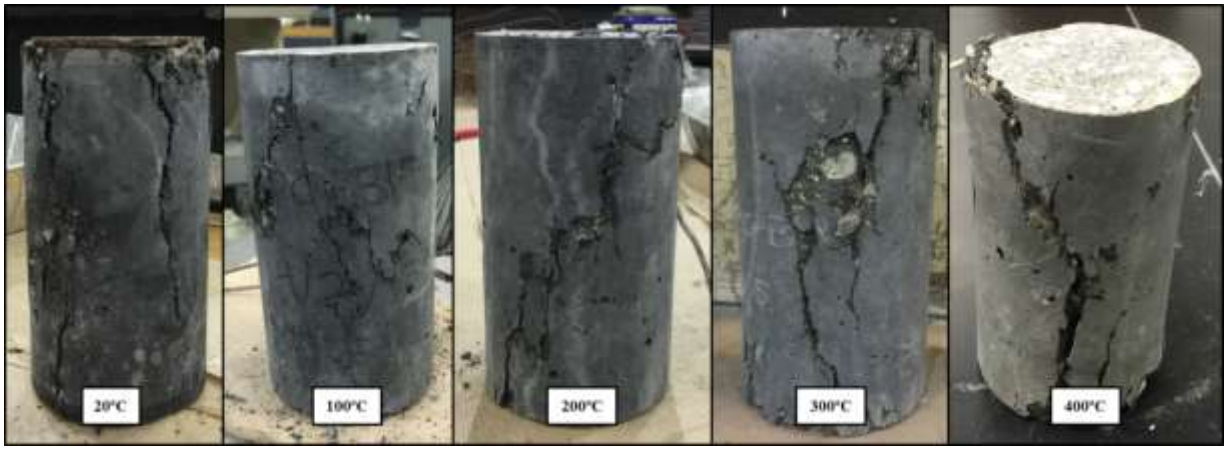

Figure 3.20: Failure modes of UHPC A & B at respective temperatures

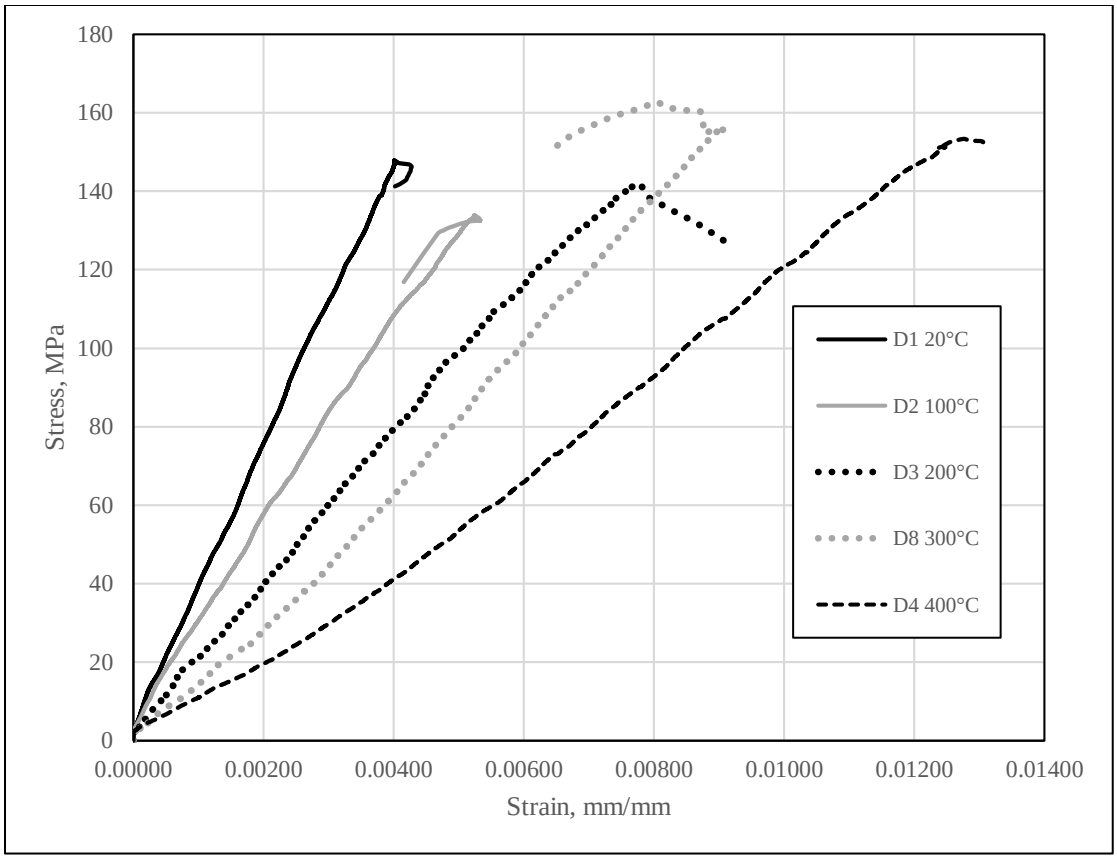

Figure 3.21: UHPC D stress-strain relationships with respect to temperature

Figure 3.22: Failure modes of UHPC D at respective temperatures

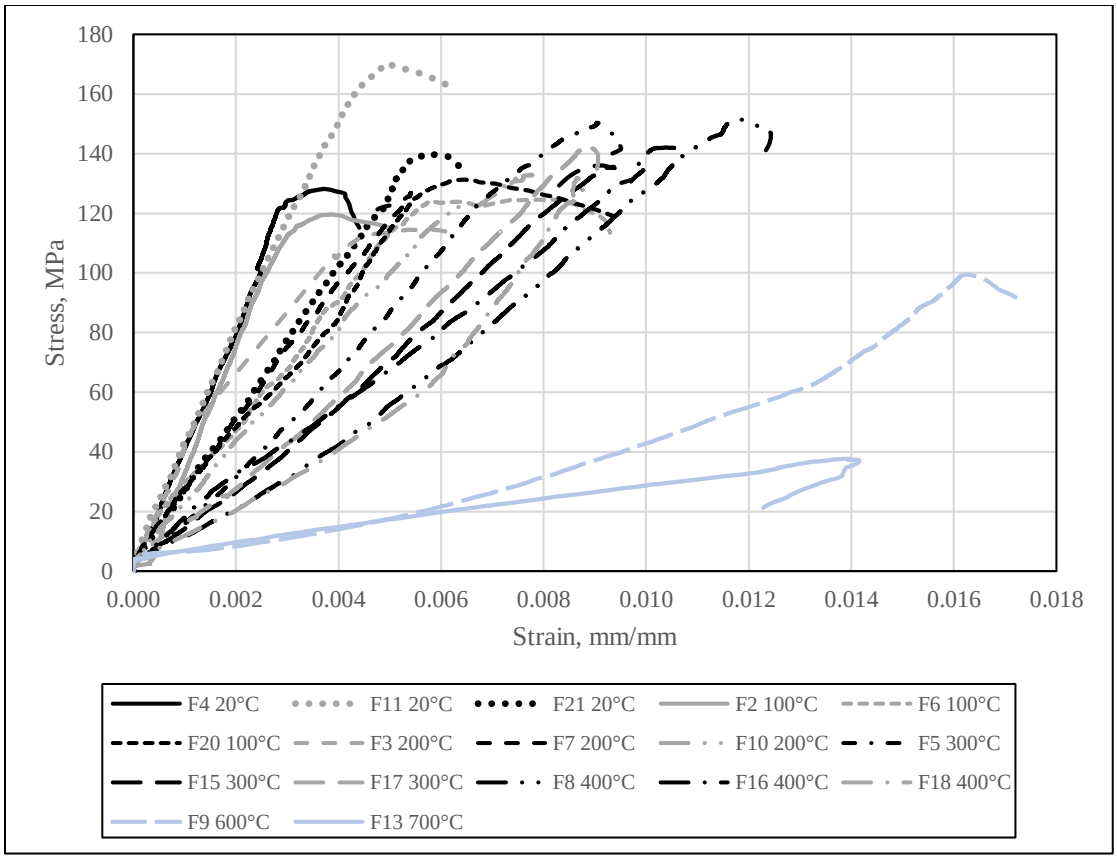

Figure 3.23: UHPC F stress-strain relationships with respect to temperature

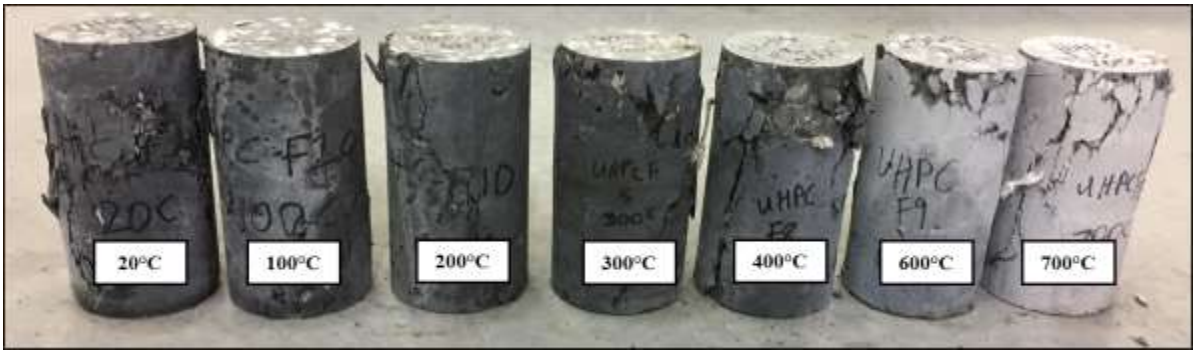

Figure 3.24: Failure modes of UHPC F at respective temperatures

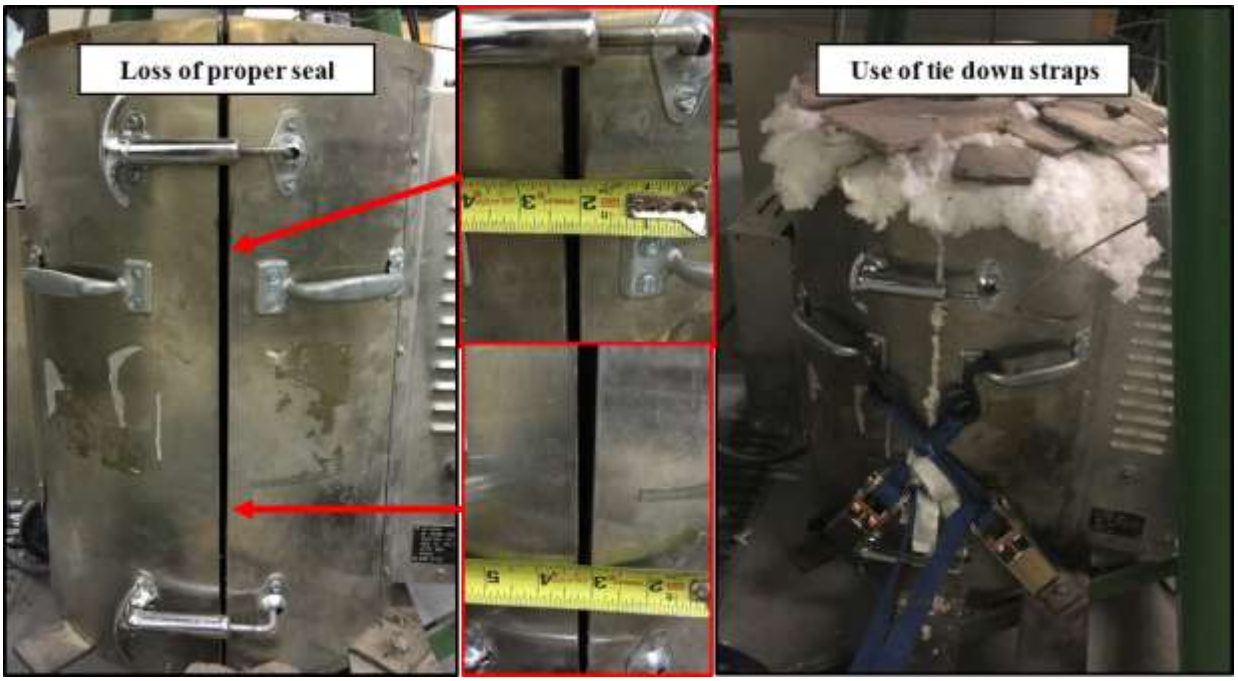

Figure 3.25: Damage to furnace due to explosive spalling

Figure 3.26: UHPC specimens following experiencing explosive spalling in electrical furnace

Figure 3.27: Specimen UHPC B5 displaying water escaping concrete following 300°C test

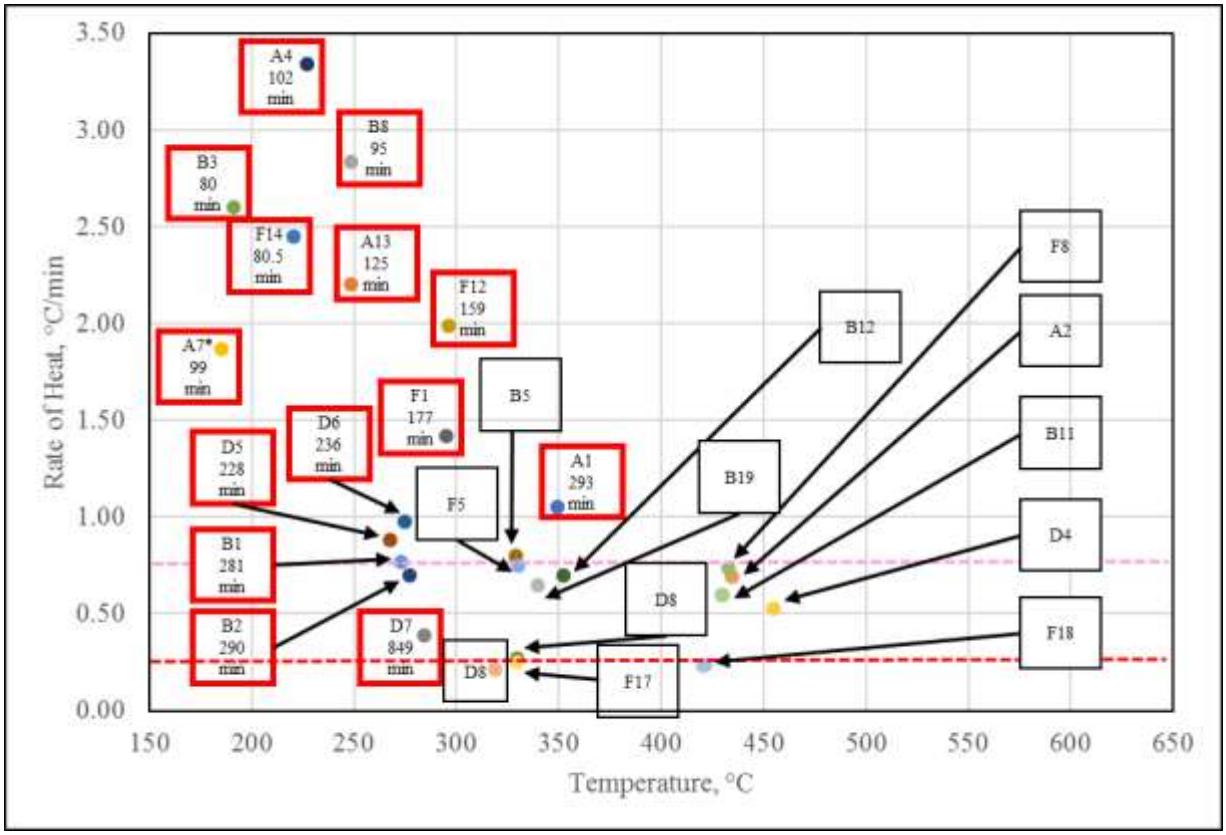

Figure 3.28: Relation between rate of heating with respect to either, (1) the spalling temperature, or (2) the maximum center temperature attained

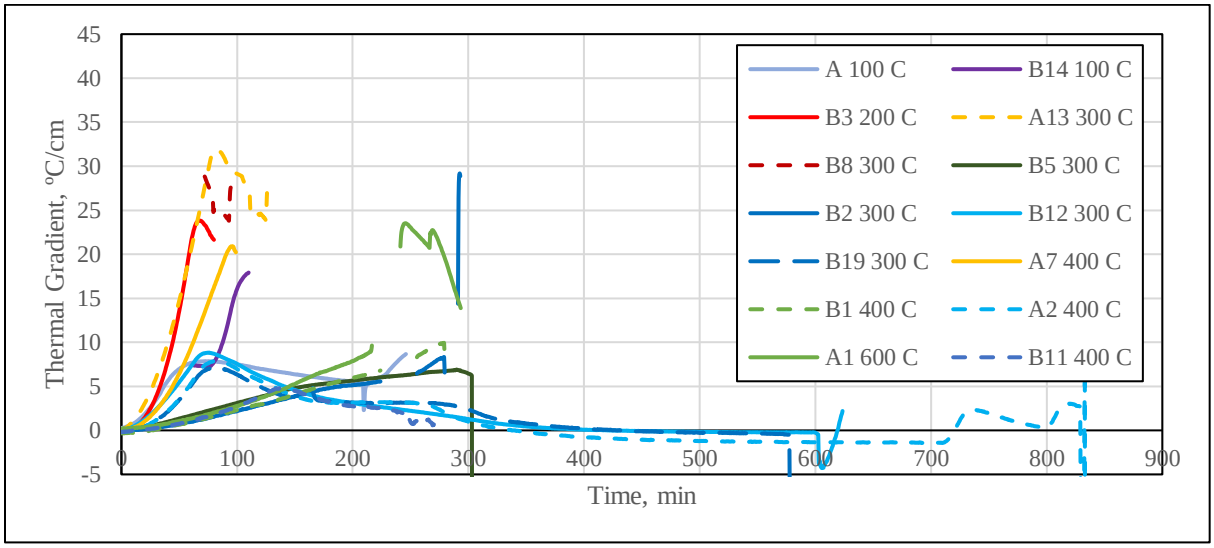

Figure 3.29: Thermal gradient with respect to time for UHPC A & B cylinders

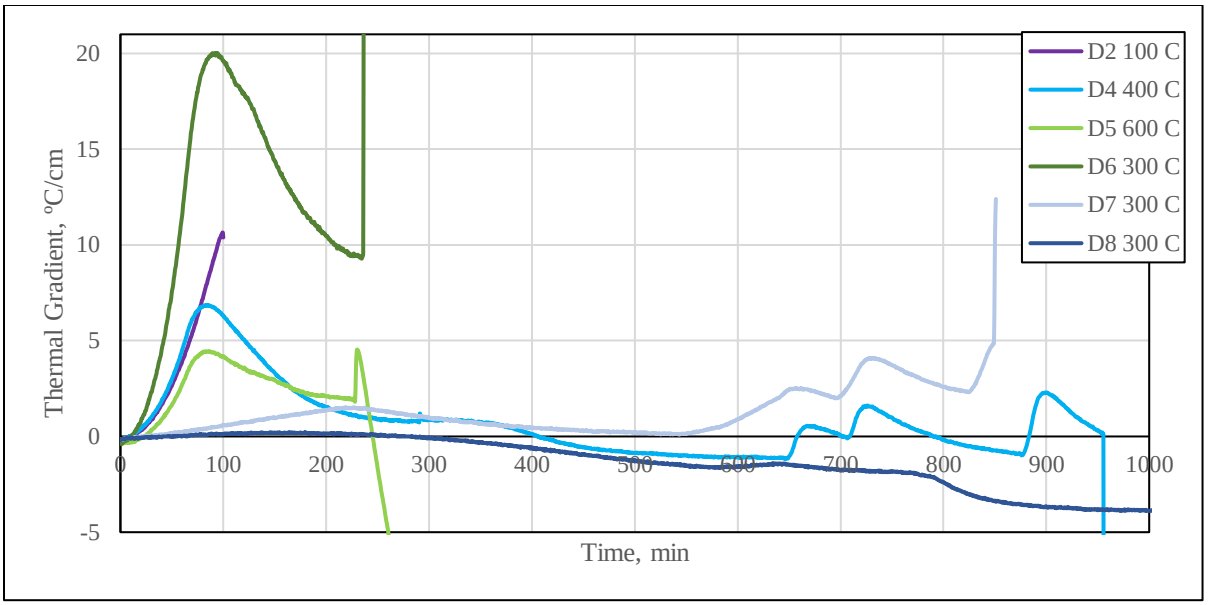

Figure 3.30: Thermal gradient with respect to time for UHPC D cylinders

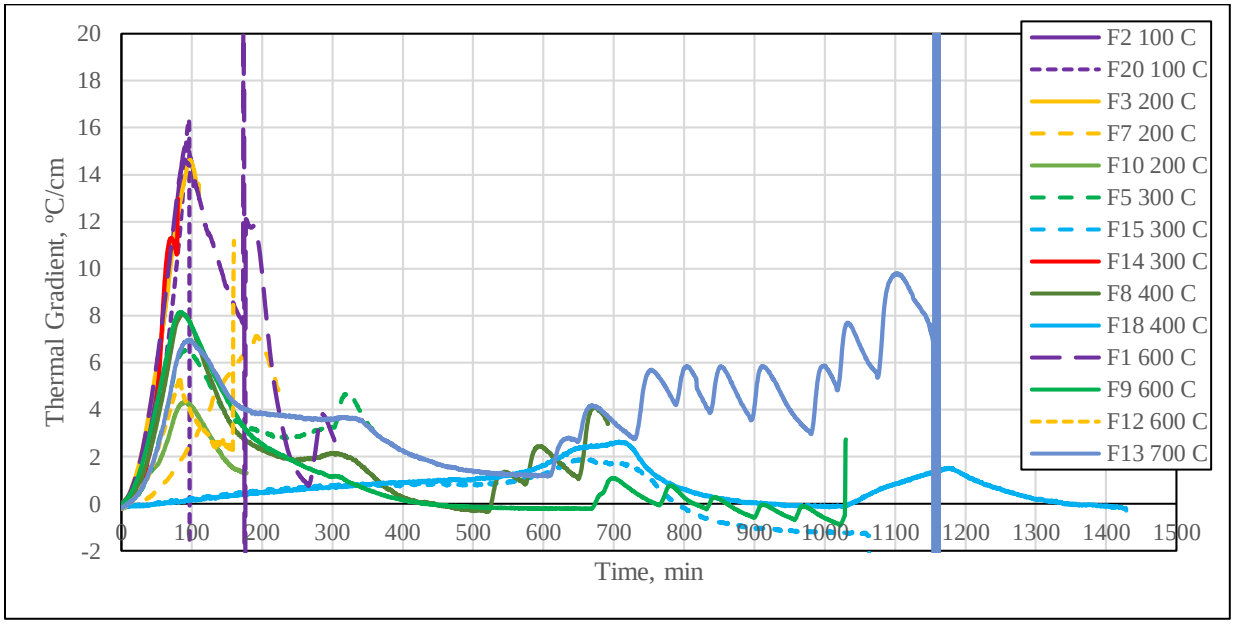

Figure 3.31: Thermal gradient with respect to time for UHPC F cylinders

3.5 Summary

Material tests were conducted to characterize the compressive strength, stiffness, and stress-strain relationship with increasing temperatures. All concretes evaluated underwent mechanical degradation with increasing temperatures, and to conduct successful tests of UHPC above 200°C, lower heating rates were utilized. Variables incorporated within the design mixes included, (1) addition of fibers (steel or polypropylene), (2) no fiber content, (3) varying the steel fiber content, and (4) a hybrid fiber mix (steel and polypropylene). The inclusion of fibers does not increase the strength. However, addition of steel fibers increases the ductility, and addition of polypropylene fibers influences the stiffness. Finally, all design mixes of UHPC experienced fire induced spalling, while none for conventional concretes. UHPC can sustain explosive spalling at temperatures less than 200°C, and minimizing the heating rate does not correspond to complete mitigation of explosive spalling.

CHAPTER FOUR

4. COMPARISON OF PROPERTIES OF UHPC WITH CONVENTIONAL CONCRETE AND BUILDING CODES

4.1 General

UHPC's design premise allows for excellent interfacial transition zones because it is developed upon minimal use of water, fine aggregate (limestone and silica sand), and profuse amount of silica fume and cement. These developmental qualities allow UHPC to have ambient condition mechanical properties superior to HSC and NSC. While at elevated temperatures, the rate of degradation of concrete is proportional to its strength or density. Consequently, the low permeability of UHPC, hailed for its mechanical properties and durability prowess, produces calamitous results with increasing temperatures. The compressive strength, stress-strain behavior, and elastic modulus of the three different design mixes of UHPC, A & B, D, and F, will be compared to the conventional concretes along with constitutive relationships provided as per ASCE (1992) and Eurocode 2 (2004). Initially the data will be compared at ambient conditions, followed by a comparison at elevated temperatures.

4.2 Comparison of room temperature properties

As compared to UHPC, the NSC evaluated as part of this study contains over 3.5 times the w/c ratio, coarse aggregate and contains no silica fume. While HSC's w/c ratio is 2 times more, it utilizes coarse aggregate and has 20% of the silica fume of UHPC. NSC and NSC-SF have the least compressive strength and elastic modulus due to their high w/c ratio. The two design mixes of NSC are on average only 30% and 60% of UHPC's compressive strength and stiffness, respectively. Concurrently, due to the higher w/c ratio and small amount of silica fume combined with coarse aggregate, HSC and HSC-PP possess mechanical properties less than the UHPC tested.

The two design mixes of HSC are on average 81% of UHPC. Moreover, the peak strain achieved for all concretes are within a 0.0035 to 0.0050 mm/mm range, with UHPC F displaying the greatest ductility, closely followed by NSC-SF and HSC. Similar to UHPC F, conventional concretes with fibers produce the superior ductility. Lastly, regarding stiffness UHPC A & B with the higher amount of steel fiber achieved the greatest value, and the inclusion of polypropylene fibers with HSC-PP and UHPC F proved to increase the stiffness as well.

4.3 Comparison of elevated temperature properties

4.3.1 Comparison of UHPC with conventional concretes tested

As seen in Figure 4.1, owing to each type of concrete's unique design, the rate of degradation is not consistent. Due to UHPC's maximized packing density, its compressive strength with increasing temperatures is quite different versus the conventional concretes tested. Moreover, due to implementing a heating rate that deviated from RILEM standard's recommendation, directly comparing UHPC's mechanical properties with the conventional concretes at and above temperatures of 200°C is abstruse. The comparison is further complicated by only UHPC F having successful tests conducted at 600 and 700°C. Given the above variables, the comparisons are as follows.

Regarding the relative compressive strength (Figure 4.1), tests conducted through 400°C, all UHPC design mixes remain relatively close to their respective original strengths. The expected strength loss from calcium-hydroxide at temperatures of 400°C is immensely reduced due to high contents of silica fume in each UHPC design mix. While the conventional concretes experience a steady degradation, HSC design mixes suffer a steeper decline. Beyond 500°C the quartz within UHPC will further exacerbate the degradation, and at temperatures greater than 700°C UHPC will encounter strength loss due to the decomposition of the cement paste. The conventional concretes'

strength suffers similarly to with the latter, however, UHPC's will be much higher due to the higher contents of cement. Another similarity seen in Figure 4.1 is that the inclusion or increasing the contents of steel fiber does not correlate to greater compressive strength. Lastly, as seen by UHPC F and HSC-PP, the addition of polypropylene fibers slightly compromises the compressive strength.

Contrary to the differences between the compressive strength, the relative modulus of elasticity (Figure 4.2) for all concretes tested, degrade in a similar fashion with increasing temperatures. Each type of concrete's elastic modulus drops to 50%, ranging from 200 to 250°C. Moreover, with respect to the concretes tested up to 300°C, the addition of steel fibers did not contribute to NSC's stiffness, while the inclusion of steel (UHPC A & B and D), polypropylene (HSC-PP), or polypropylene and steel fibers (UHPC F) did assist the modulus of elasticity. Although the relative elastic modulus for the various concrete degraded similarly, the relative stress-strain relationships (Figure 4.3) demonstrated differences.

At temperatures up to 400°C, the ductility of the tested conventional concretes was comparable to the UHPC design mixes (twice the ambient condition peak strain). UHPC D4 (400°C) withstood the greatest ductility amongst all design mixes of UHPC with 3.25 times its original peak strain. The addition of steel or polypropylene fibers with the UHPC and conventional concretes improved the ductility with increasing temperatures. Though UHPC F9 (600°C) displayed greater peak strain as compared to the conventional concretes, it was 20% less than UHPC D4. Furthermore, UHPC F13's (700°C) relative peak strain was 30% less than the tested conventional concretes. The drastic reduction in peak strain of UHPC F at 600 and 700°C may be attributed to the lengthy duration of fire exposure involved to reach the targeted temperatures.

4.3.2 Comparison of UHPC with building codes

Through 400°C, the relative compressive strengths (Figure 4.1) of the code conventional concretes display minimal degradation and behave comparably as the tested UHPC. Furthermore, UHPC F's relative strengths at 600 and 700°C are analogous to the constitutive relationships dictated by the codes as well. Along with the strengths, the elastic modulus (Figure 4.2), with increasing temperatures, displays minimal variation between the UHPC and code conventional concretes. However, the relative peak strain recommended by the codes is nearly 4.5 times the tested UHPC cylinders at a temperature range of 400 to 700°C.

4.4 Comparison of spalling

4.4.1 Comparison of UHPC with conventional concretes tested

Though the HSC investigated as part of this study contains 7% silica fume, as compared to cement weight, and no polypropylene fibers, it did not result in explosive spalling. In fact, no conventional concrete evaluated encountered fire induced spalling. Whereas all UHPC design mixes considered as part of this research experienced explosive spalling with heating rates as low as 0.40°C/min. The occurrence of explosive spalling at such minimal heating rates implies the principle cause is the pore pressure build-up due to the dense microstructure of UHPC.

4.4.2 Comparison of UHPC with building codes

Design mix UHPC F contains nearly 45% silica fume to cement weight ratio and as prescribed by Eurocode 2 (2004) for HSC, 2 kg/m^3 of polypropylene fiber were incorporated to mitigate fire induced spalling. However, three UHPC F cylinders suffered an explosion with heating rates as low as 1.40°C/min. Though the high content of silica fume lowered the C/S ratio, it gravely reduced the permeability and increased the main binder for UHPC, C-S-H.

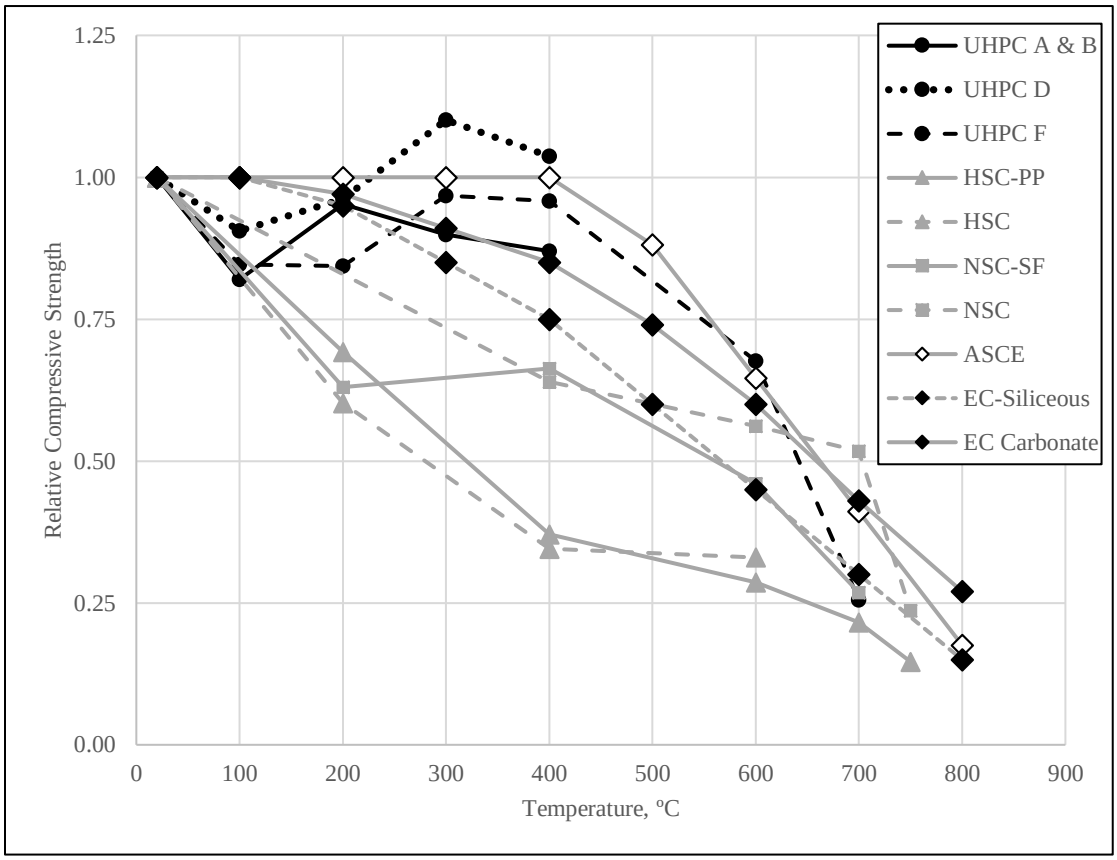

Figure 4.1: Relative compressive strength with respect to temperature of various concrete cylinders tested as part of research, and Eurocode 2 (2004) and ASCE (1992)

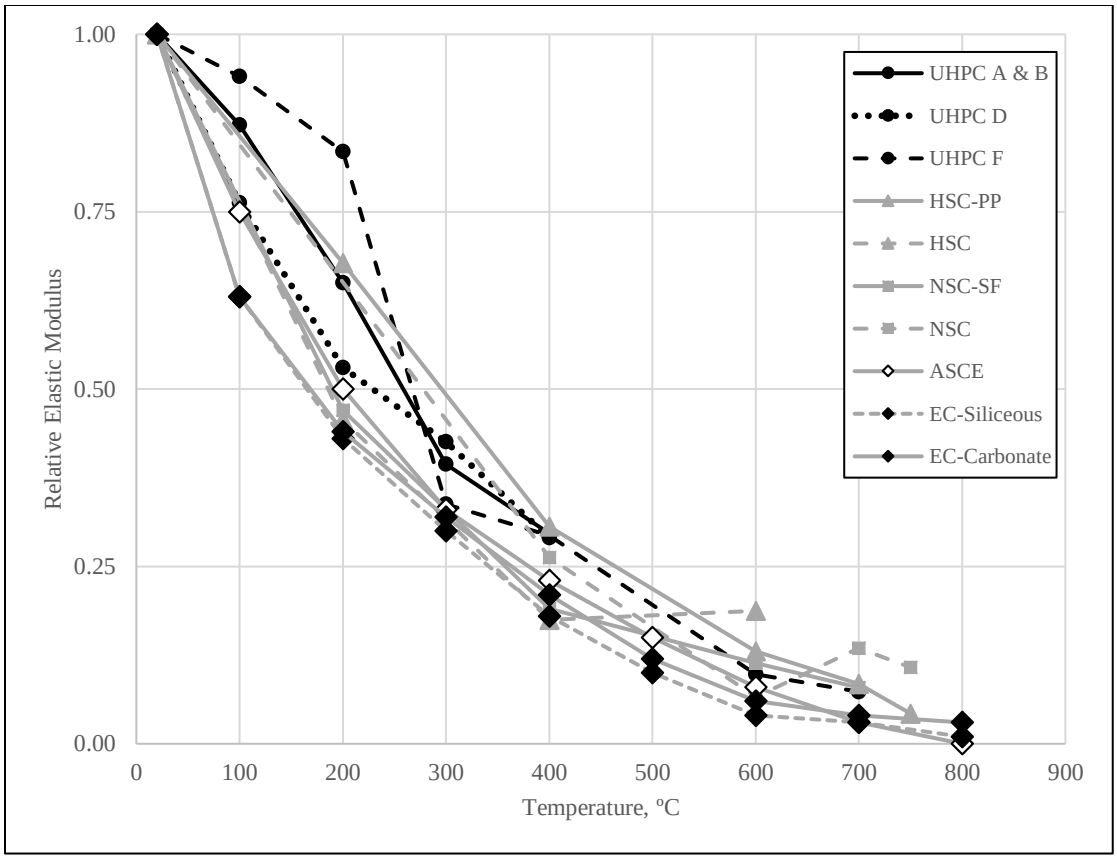

Figure 4.2: Relative elastic modulus with respect to temperature of various concrete cylinders tested as part of research, and Eurocode 2 (2004) and ASCE (1992)

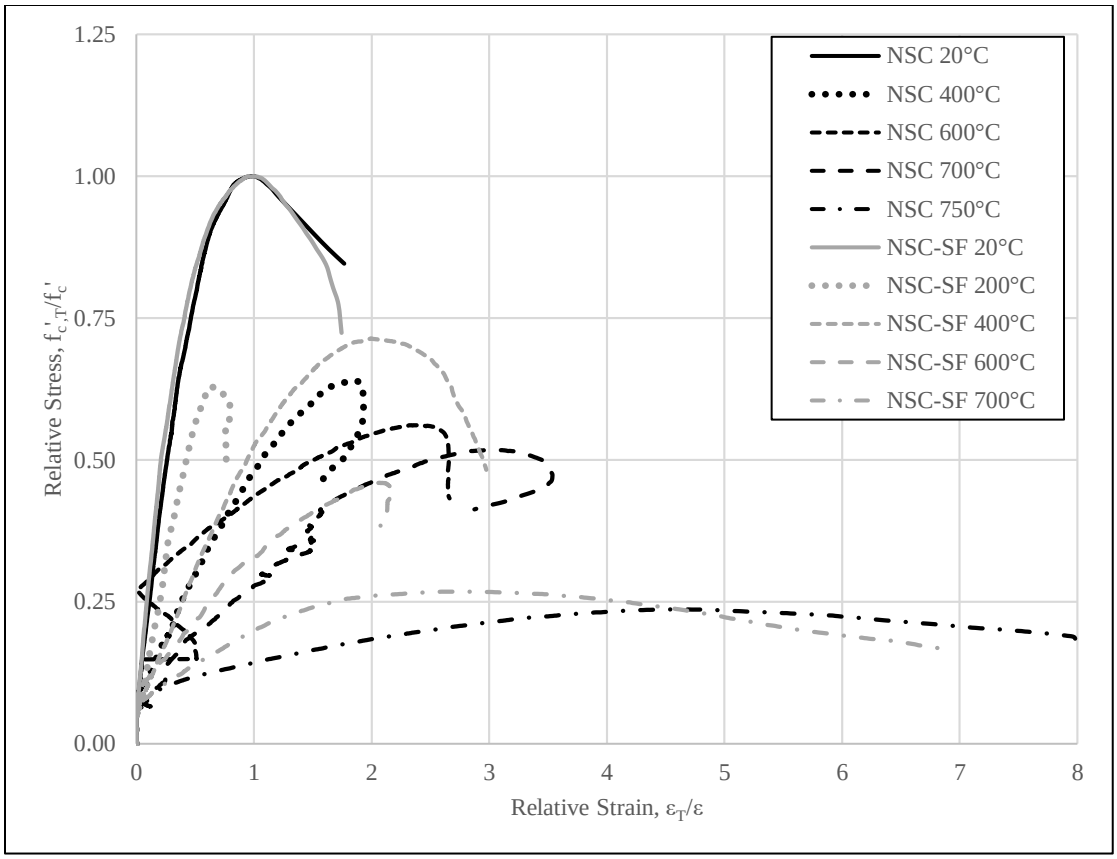

(a) Relative stress-strain relationship for NSC and NSC-SF concrete cylinders tested

Figure 4.3: Relative stress-strain relationships for concrete cylinders tested

Figure 4.3 (cont'd)

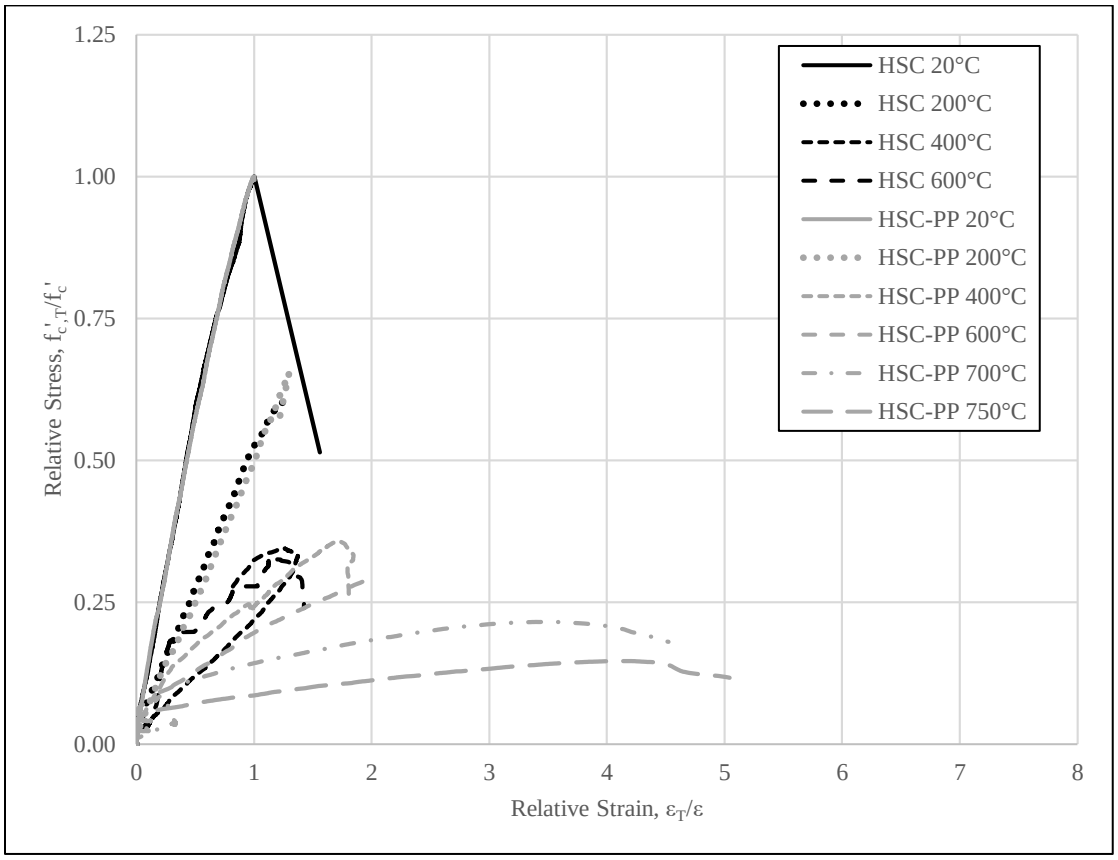

(b) Relative stress-strain relationship for HSC and HSC-PP concrete cylinders tested

Figure 4.3 (cont'd)

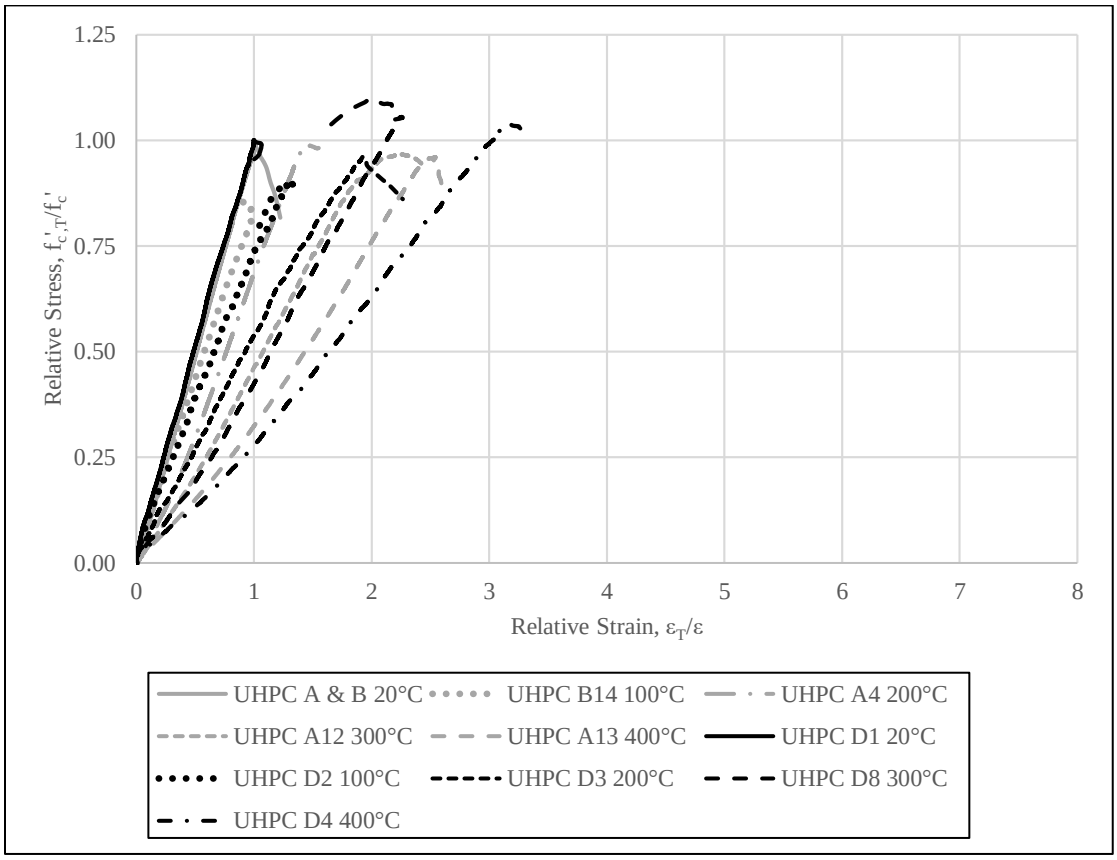

(c) Relative stress-strain relationship for UHPC A & B and D concrete cylinders tested

Figure 4.3 (cont'd)

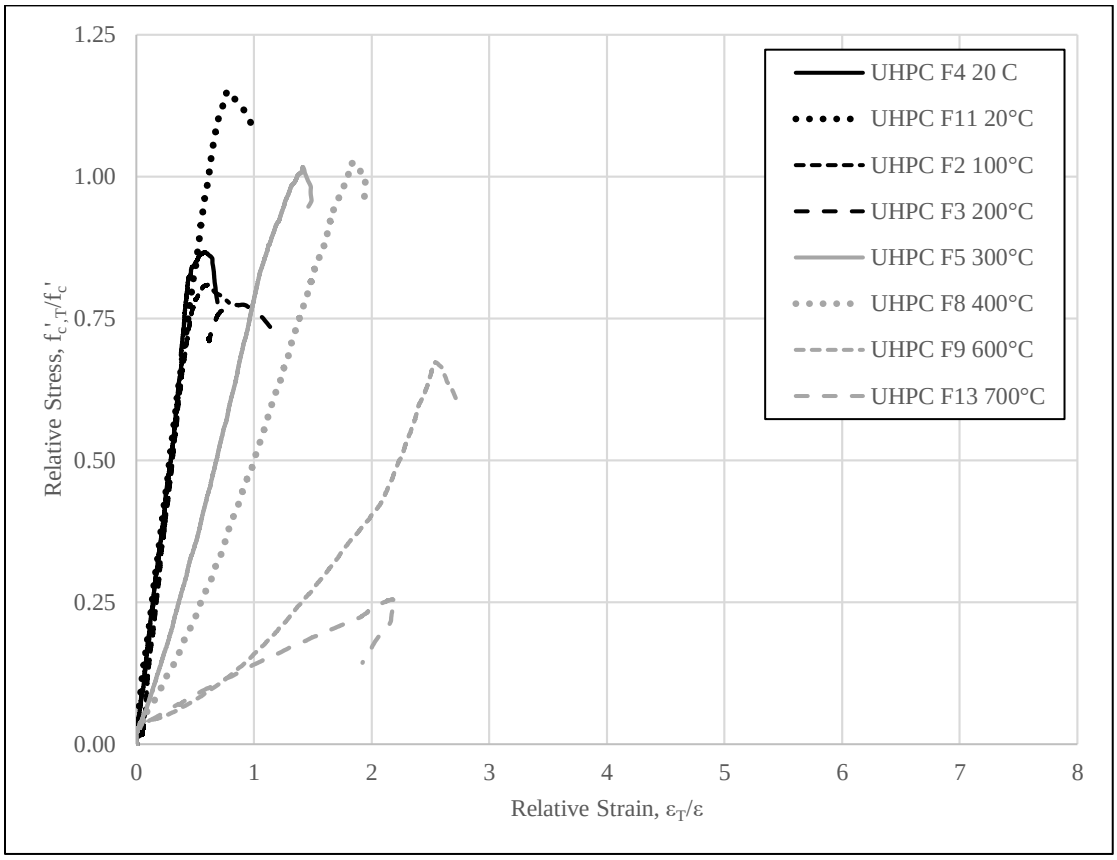

(d) Relative stress-strain relationship for UHPC F concrete cylinders tested

Figure 4.3 (cont'd)

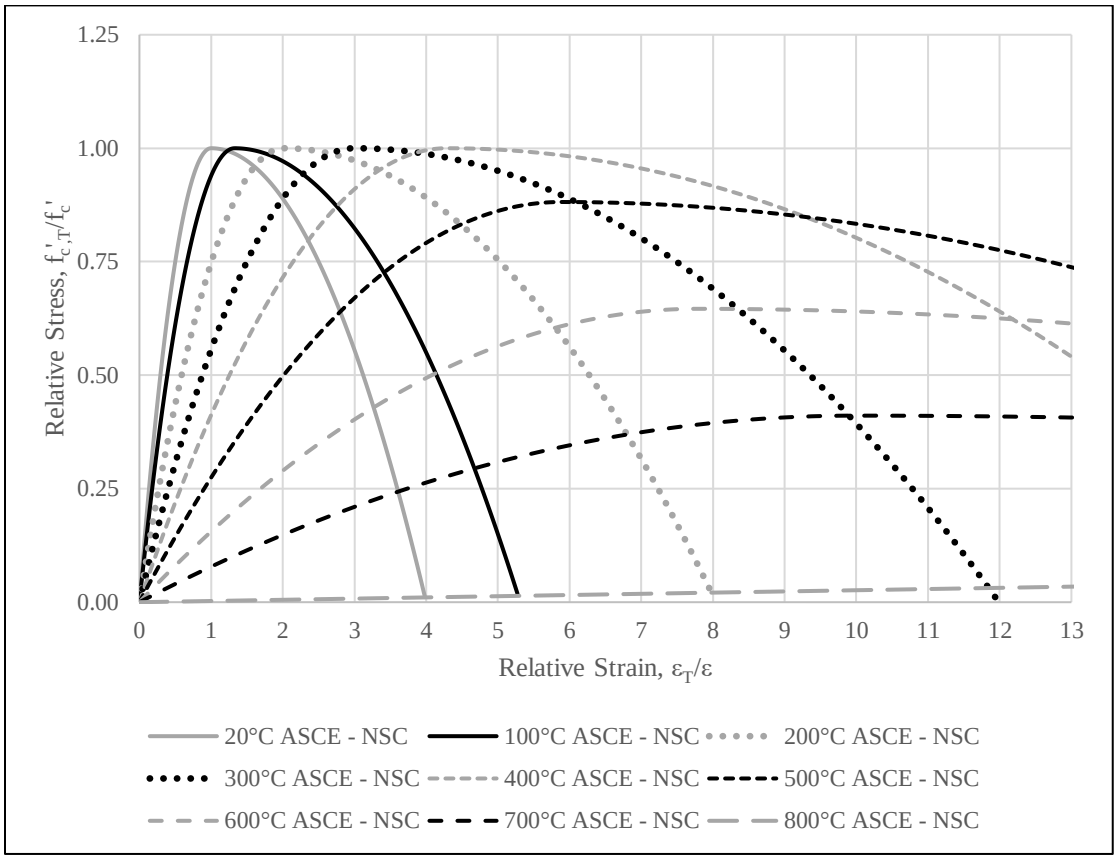

(e) Relative stress-strain relationship for NSC from ASCE (1992)

Figure 4.3 (cont'd)

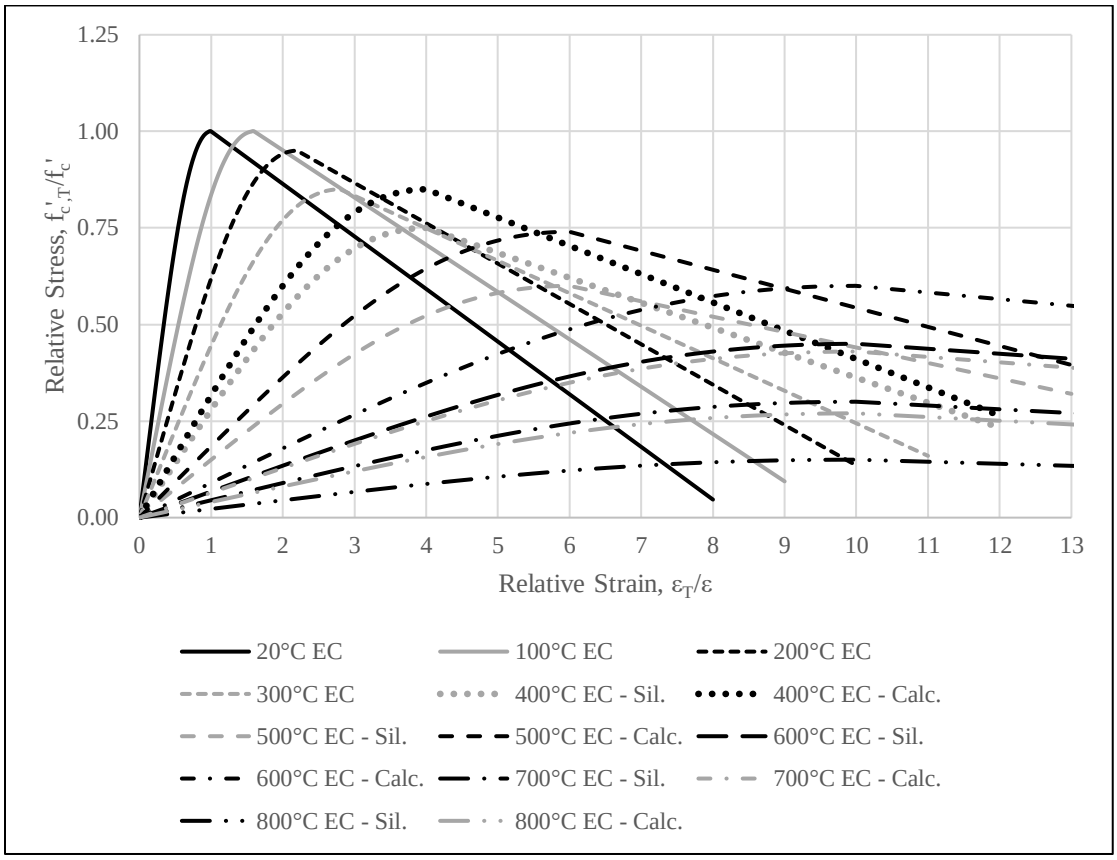

(e) Relative stress-strain relationship for siliceous and carbonate concrete from Eurocode 2 (2004)

4.5 Summary

Comparisons were presented from the experimental testing of UHPC and conventional concretes, and UHPC with the constitutive relationships recommended by ASCE (1992) and Eurocode 2 (2004). As expected due to UHPC's contrasting composition, there are differences regarding the properties of UHPC and conventional concretes. Furthermore, UHPC's strength degradation was comparable to the conventional concretes as prescribed by the codes. However, there is a vast variation of the peak strains between UHPC and code conventional concretes. Lastly, following the recommendations as prescribed by Eurocode 2 (2004) to mitigate fire induced spalling was not successful.

CHAPTER FIVE

5. CONCLUSIONS AND RECOMMENDATIONS

5.1 General

The experimental investigation conducted as part of this thesis provides data pertaining to the high temperature behavior of UHPC. Thereby providing the necessary data to evaluate the fire response of UHPC structural members. The mechanical properties tested from 20-700°C were compressive strength, stress-strain relationship, and elastic modulus of three different design mixes of UHPC consisting of varying fiber type and content, and four different conventional types of concrete were tested for comparative purposes. Furthermore, differing heating rates were employed to study the explosive spalling nature of UHPC. Empirical relations depicting the mechanical behavior with respect to temperature, and prominent data of fire induced spalling are presented.

5.2 Key findings

Based on the experimental research accumulated as part of this thesis, the following conclusions can be derived:

1. To conduct successful testing above 200°C of all UHPC design mixes heating rates less than 1°C/min were utilized, otherwise explosive spalling occurred. Furthermore, UHPC F sustained three explosive spalling occurrences, deeming 2.00 kg/m^3 of polypropylene fibers not sufficient to mitigate the abovementioned.
2. Fire induced spalling occurred with heating rates less than 0.50°C/min, implying the root cause of explosive spalling is the built-up pore pressure owing to UHPC's dense medium.

3. UHPC's compressive strength varies closely to its original strength up to 400°C, thereby degrading differently with temperature as compared to conventional concretes.
4. The steel fiber content does not influence the compressive strength of UHPC, but it does improve the ductility. Additionally, the combination of steel and polypropylene fibers (UHPC F) improves the stiffness up to 200°C
5. There is a vast disconnect for experimental data and recommendations prescribed in codes. Specifically, mechanical properties such as compressive strength and stress-strain behavior, displayed poorer fire performance as compared to their respective codes counterpart.

5.3 Recommendations for future research

Although all three design mixes of UHPC suffered explosive spalling, the literature contains various studies that prove contrary. Investigations have employed heating rates of 10°C/min and evaluated UHPC specimens up to 1000°C. Furthermore, UHPC mechanical properties considered at the respective elevated temperatures, as opposed to the residual-state, is quite scarce. Therefore, refinement of the design mix to be tested at the elevated temperature state is of the utmost importance. Below are the author's recommendations for future research:

- Formulate a design mix that would utilize a combination of silica fume, cement, and fly ash or GGBFS and evaluate the mechanical properties at elevated temperatures with varying heating rates
- Evaluate the mechanical properties at elevated temperatures with varying heating rates, utilizing a design mix with the above mentioned basic formula and vary the fiber content as follows:
    i. Steel fiber

ii. Steel and polypropylene fibers

iii. Steel and polypropylene fibers and vary the polypropylene fibers dimension

- Evaluate the thermal properties at elevated temperatures utilizing a design mix with the above mentioned basic formula
- Further investigation of fire induced spalling at differing heating rates

5.4 Research impact

It is evident that the data generated as part of this study is vital, and will provoke a swift impression upon the implementation of UHPC for infrastructure applications. By virtue of UHPC's microstructure, it possesses consummate mechanical and durability properties. However, the preceding properties cause UHPC to be susceptible to fire induced spalling, and such an occurrence can inhibit a structure reaching its fire resistance requirement. Through the course of testing, this limiting facet could not be minimized by additional steel fiber or inclusion of polypropylene fiber as recommended in codes, and results as such emphasize the continual evaluation of UHPC's properties at time of fire exposure. Therefore, to avoid further loss, supplementary research must be conducted evaluating high temperature properties of UHPC.

APPENDIX

Appendix High temperature properties of UHPC

Table A1: Additional notes pertaining to UHPC A & B specimen tests

Specimen	T	Average rate of heating	Comments
	°C	°C/min	
UHPC B9	20	N/A	None
UHPC A12	20	N/A	None
UHPC A2	20	N/A	None
UHPC A7	20	N/A	None
UHPC A	100	0.60 *	No data acquisition utilized. Average rate of heat is an estimation based off time
UHPC A	100	0.40	None
UHPC B14	100	1.37	None
UHPC A3	100	0.30*	None
UHPC A9	100	1.00*	None
UHPC A14	100	2.00*	None
UHPC A & B	200	0.70*	No data acquisition utilized. Average rate of heat is an estimation based off time
UHPC A6	200	0.54	None
UHPC A & B	200	0.75*	No data acquisition utilized. Average rate of heat is an estimation based off time
UHPC B12	300	0.70	Surface thermocouple readings were lower than center thermocouple; therefore for therm grad, utilized the average of the center and furnace for the surface temp
UHPC B19	300	0.65	None
UHPC A12	300	0.42	None
UHPC B4	400	0.60*	Data acquisition turned off; average rate of heat is an estimate based off a similar test
UHPC A2	400	0.69	None
UHPC A13	400	0.50	None
UHPC B11	400	0.60	Center thermocouple was not working

* – Denotes an estimate

Table A2: Additional notes pertaining to UHPC D specimen tests

Specimen	T	Average rate of heating	Comments
	°C	°C/min	
UHPC D-1	20	N/A	None
UHPC D-2	100	1.60	None
UHPC D-3	200	1.13	Surface and furnace thermocouples providing erroneous values
UHPC D-8	300	0.27	None
UHPC D-4	400	0.53	None

* – Denotes an estimate

Table A3: Additional notes pertaining to UHPC F specimen tests

Specimen	T	Average rate of heating	Comments
	°C	°C/min	
UHPC F-4	20	N/A	None
UHPC F-11	20	N/A	None
UHPC F-19	20	N/A	None
UHPC F-21	20	N/A	None
UHPC F-2	100	1.64	None
UHPC F-6	100	2.66	Center thermocouple values were void; data is regarding the surface thermocouple
UHPC F-20	100	1.65	None
UHPC F-3	200	1.89	Surface thermocouple readings were lower than expected; therefore, for thermal grad, utilized the average of the center and furnace for the surface temp
UHPC F-7	200	1.76	None
UHPC F-10	200	0.91	None
UHPC F-5	300	0.75	None
UHPC F-15	300	0.21	Testing the compressive strength with reduced rate of heating
UHPC F-17	300	0.25	Testing the compressive strength with reduced rate of heating
UHPC F-8	400	0.74	None
UHPC F-16	400	0.23	Testing the compressive strength with reduced rate of heating
UHPC F-18	400	0.24	Testing the compressive strength with reduced rate of heating
UHPC F-9	600	0.74	Surface thermocouple readings were lower than expected; therefore, for thermal grad, utilized the average of the center and furnace for the surface temp
UHPC F-13	700	0.69	None

* – Denotes an estimate

REFERENCES

REFERENCES

1. Abdul-Hussain, S.T. (2013). "Effect of Elevated Temperatures on Compressive and Tensile Strengths of Reactive Powder Concrete." Journal of Engineering and Development, vol. 17.4: pp. 259-278.

2. Abrams, D.A. (1919). “Design of concrete mixtures.” Structural Materials Research Laboratory, Lewis Institute.

3. Al-Jabri, K.S., Waris, M.B., Al-Saidy, A.H. (2016). "Effect of aggregate and water to cement ratio on concrete properties at elevated temperature: Effect of Aggregate and Water to Cement Ratio on Concrete Properties." Fire and Materials, vol. 40(7): pp. 913-925.

4. Ali, M.H., Dinkha, Y.Z., Haido J.H. (2016). "Mechanical properties and spalling at elevated temperature of high performance concrete made with reactive and waste inert powders." Engineering Science and Technology, an International Journal, vol. 2: pp. 536-541.

5. Alkaysi, M. (2016). “Strength and Durability of Ultra-High Performance Concrete Materials and Structures.” Doctoral dissertation, University of Michigan.

6. Arioz, O. (2007). "Effects of elevated temperatures on properties of concrete." Fire Safety Journal, vol. 42(8): pp. 516-522.

7. ASCE (1992). “Structural fire protection.” American Society of Civil Engineers Manuals and Reports on Engineering Practice, 78, New York.

8. Aslani, F., Bastami, M. (2011). "Constitutive Relationships for Normal- and High-Strength Concrete at Elevated Temperatures." ACI Materials Journal, vol. 108(4): pp, 355.

9. ASTM C39/C39M (2016). “Standard Test Method for Compressive Strength of Cylindrical Concrete Specimens.” American Society for Testing and Materials, West Conshohocken, PA.

10. ASTM C293/C293M (2016). “Standard Test Method for Flexural Strength of Concrete (Using Simple Beam with Center-point Loading.” American Society for Testing and Materials, West Conshohocken, PA.

11. ASTM C469/C469M (2014). “Standard Test Method for Static Modulus of Elasticity and Poisson’s Ratio of Concrete in Compression.” American Society for Testing and Materials, West Conshohocken, PA.

12. ASTM C496/C496M (2011). “Standard Test Method for Splitting Tensile Strength of Cylindrical Concrete Specimens.” American Society for Testing and Materials, West Conshohocken, PA.

13. ASTM C1113/C1113M (2013). “Standard Test Method for Thermal Conductivity of Refractories by Hot Wire (Platinum Resistance Thermometer Technique).” American Society for Testing and Materials, West Conshohocken, PA.

14. ASTM E119a (2008). “Standard Methods of Fire Test of Building Construction and Materials. ” American Society for Testing and Materials, West Conshohocken, PA.

15. ASTM E831 (2014). “Standard Test Method for Linear Thermal Expansion of Solid Materials by Thermomechanical Analysis.” American Society for Testing and Materials, West Conshohocken, PA.

16. ASTM E1269 (2011). “Standard Test for Determining Specific Heat Capacity by Differential Scanning Calorimetry.” American Society for Testing and Materials, West Conshohocken, PA.

17. ASTM E1530 (2016). “Standard Test Method for Evaluating the Resistance to Thermal Transmission of Materials by the Guarded Heat Flow Meter Technique.” American Society for Testing and Materials, West Conshohocken, PA.

18. ASTM E1868 (2015). “Standard Test Methods for Loss-On-Drying by Thermogravimetry.” American Society for Testing and Materials, West Conshohocken, PA.

19. Aydin, S., Baradan, B. (2013). “Engineering Properties of Reactive Powder Concrete without Portland Cement." ACI Materials Journal, vol. 110(6): pp. 619-627.

20. Aydin, S., Baradan, B. (2012). "High Temperature Resistance of Alkali-Activated Slag- and Portland Cement Based Reactive Powder Concrete." ACI Materials Journal, vol. 109(4): pp. 463-470.

21. Aziz, E.M. (2015). “Response of fire exposed steel bridge girders.” Doctoral dissertation, Michigan State University.

22. Bashandy, A.A. (2013). "Influence of elevated temperatures on the behavior of economical reactive powder concrete." Journal of Civil Engineering Research, vol. 3.3: pp. 89-97.

23. Behloul, M., Chanvillard, G., Casanova, P., Orange, G., France F.F. (2002). "Fire resistance of Ductal® ultra high performance concrete." 1st fib Congress, vol. 1: pp. 421-430.

24. Bei, S., Zhixiang, L. (2016). "Investigation on spalling resistance of ultra-high-strength concrete under rapid heating and rapid cooling." Case Studies in Construction Materials, vol. 4: pp. 146-153.

25. Buchanan, A.H., Abu, A.K. (2017). “Structural Design for Fire Safety.” John Wiley & Sons, Chichester, West Sussex, United Kingdom.

26. Burke, B.T. (2011). "Residual Strength of Ultra-High Performance Concrete After Exposure to Elevated Temperatures." Master thesis, University of Connecticut.

27. Canbaz, M. (2014). "The Effect of High Temperature on Reactive Powder Concrete." Construction and Building Materials, vol. 70: pp. 508-513.

28. Chang, Y.F., Chen, Y.H., Sheu, M.S., Yao, G.C. (2006). "Residual stress–strain relationship for concrete after exposure to high temperatures." Cement and Concrete Research, vol. 36(10): pp. 1999-2005.

29. Chen, G.M., Yang, H., Lin, C.J., Chen, J.F., He, Y.H., Zhang, H.Z. (2016). "Fracture behaviour of steel fibre reinforced recycled aggregate concrete after exposure to elevated temperatures." Construction and Building Materials, vol. 128: pp. 272-286.

30. Chen, X., Chen, W., Rougelot, T., Davy, C.A., Agostini, F., Skoczylas, F., Bourbon, X. (2009). "Experimental Evidence of a Moisture Clog Effect in Cement-Based Materials Under Temperature." Cement and Concrete Research, vol. 39(12): pp. 1139-1148.

31. Demirel, B., Keleştemur, O. (2010). "Effect of elevated temperature on the mechanical properties of concrete produced with finely ground pumice and silica fume." Fire Safety Journal, vol. 45(6): pp. 385-391.

32. Dehn, F. (2004). “Fire Resistance of Ultra High Performance Concrete (UHPC) – Testing of Laboratory Samples and Columns under Load.” International Symposium on Ultra High Performance Concrete, Kassel, Germany, September 13-15.

33. Dwaikat, M. B., Kodur, V.K.R. (2009). "Hydrothermal Model for Predicting Fire-Induced Spalling in Concrete Structural Systems." Fire Safety Journal, vol. 44(3): pp. 425-434.

34. Elwell, D.J., Fu, G. (1995). “Compression testing of concrete: cylinders vs. cubes”. No. FHWA/NY/SR-95/119.Albany, New York, NY, USA: Transportation Research and Development Bureau, New York State Department of Transportation.

35. Ergün, A., Kürklü, G., Serhat, M.B., Mansour, M.Y. (2013). "The effect of cement dosage on mechanical properties of concrete exposed to high temperatures." Fire Safety Journal, vol. 55: pp. 160-167.

36. EC2. (2004). “EN 1992-1-2: Design of concrete structures, Part 1-2: General Rules-Structural Fire Design.” European Committee for Standardization, Brussels, Belgium.

37. Felicetti R., Gambarova, P.G., Sora, M.N., Khoury, G.A. (2000). "Mechanical behaviour of HPC and UHPC in direct tension at high temperature and after cooling." Fifth RILEM symposium on fibre-reinforced concretes, vol. N: pp. 749-758.

38. Felicetti, R., Lo Monte, F. (2013). "Concrete Spalling: Interaction between Tensile Behaviour and Pore Pressure during Heating." MATEC Web of Conferences, vol. 6: pp. 3001.

39. Gesoglu, M., Güneyisi, E., Nahhab, A.H., Yazıcı, H. (2015). "Properties of Ultra-High Performance Fiber Reinforced Cementitious Composites made with Gypsum-Contaminated Aggregates and Cured at Normal and Elevated Temperatures." Construction and Building Materials, vol. 93: pp. 427-438.

40. Ghafari, E., Costa, H. and Júlio, E. (2015). "Statistical mixture design approach for eco-efficient UHPC." Cement and Concrete Composites, vol. 55: pp. 17-25.

41. Ghandehari, M., Behnood, A., Khanzadi, M. (2010). "Residual Mechanical Properties of High-Strength Concretes after Exposure to Elevated Temperatures." Journal of Materials in Civil Engineering, vol. 22(1): pp. 59-64.

42. Graybeal, B.A. (2015). "Compression Testing of Ultra-High-Performance Concrete." Advances in Civil Engineering Materials, vol. 4.2: pp. 102-112.

43. Graybeal, B.A. (2014). "Tensile Mechanical Response of Ultra-High-Performance Concrete." Advances in Civil Engineering Materials, vol. 4.2: pp. 62-74.

44. Graybeal, B., Davis, M. (2008). "Cylinder Or Cube: Strength Testing of 80 to 200 MPa (11.6 to 29 Ksi) Ultra-High-Performance Fiber-Reinforced Concrete." ACI Materials Journal, vol. 105(6): pp. 603-609.

45. Gu, C.P., Ye, G., Sun, W. (2015). "Ultrahigh Performance Concrete-Properties, Applications and Perspectives." Science China Technological Sciences, vol. 58(4): pp. 587-599.

46. Hager, I., Tracz, T., Śliwiński, J., Krzemień, K. (2016). "The influence of aggregate type on the physical and mechanical properties of high-performance concrete subjected to high temperature: Influence of aggregate type on HPC subjected to high temperature." Fire and Materials, vol. 40(5): pp. 668-682.

47. Hager, I., Zdeb, T., Krzemień, K. (2013). "The Impact of the Amount of Polypropylene Fibres on Spalling Behaviour and Residual Mechanical Properties of Reactive Powder Concretes." MATEC Web of Conferences, vol. 6: pp. 2003.

48. Hassan, A.M.T., Jones, S.W., Mahmud, G.H. (2012). "Experimental test methods to determine the uniaxial tensile and compressive behaviour of ultra high performance fibre reinforced concrete (UHPFRC)." Construction and Building Materials, vol. 37: pp. 874-882.

49. Heinz, D., Dehn, F., Urbonas, L. (2004). "Fire Resistance of Ultra High Performance Concrete (UHPC) – Testing of Laboratory Samples and Columns under Load." International Symposium on Ultra High Performance Concrete, Kassel, Germany, September 13-15.

50. Hertz, K.D. (2005). "Concrete Strength for Fire Safety Design." Magazine of Concrete Research, vol. 57(8): pp. 445-453.

51. Hertz, K.D. (2003). "Limits of Spalling of Fire-Exposed Concrete." Fire Safety Journal, vol. 38(2): pp. 103-116.

52. Hertz, K.D., Sørensen, L.S. (2005). "Test Method for Spalling of Fire Exposed Concrete." Fire Safety Journal, vol. 40(5): pp. 466-476.

53. Hertz, K. (1984). "Explosion of silica-fume concrete." Fire Safety Journal, vol. 8(1): pp. 77.

54. Ingason, H. (2004) "Fire development in catastrophic tunnel fires (CTF)." SP RAPPORT-STATENS PROVNINGSANSTALT, International Symposium on Catastrophic Tunnel Fires (CTF), Boras, Sweden, November 20-21, 2003: pp. 31-48.

55. Jagannathan, D. (2013). "Calcium-Silicate-Hydrate in cementitious systems: chemomechanical correlations, extreme temperature behavior, and kinetics and morphology of in-situ formation." Doctoral dissertation, Massachusetts Institute of Technology.

56. Jang, H., So, H., So, S. (2016). The properties of reactive powder concrete using PP fiber and pozzolanic materials at elevated temperature." Journal of Building Engineering, vol. 8: pp. 225-230.

57. Ju, Y., Wang, L., Liu, H., Tian, K. (2015). "An Experimental Investigation of the Thermal Spalling of Polypropylene-Fibered Reactive Powder Concrete Exposed to Elevated Temperatures." Science China Technological Sciences, vol. 23: pp. 2022-2053.

58. Ju, Y. Liu, H., Liu, J., Tian, K., Wei, S., Hao, S. (2011). "Investigation on Thermophysical Properties of Reactive Powder Concrete." Science China Technological Sciences, vol. 54(12): pp. 3382-3403.

59. Ju, Y., Liu, H., Tian, K., Wang, L., Ge, Z. (2013). "An Investigation on Micro Pore Structures and the Vapor Pressure Mechanism of Explosive Spalling of RPC Exposed to High Temperature." Science China Technological Sciences, vol. 56(2): pp. 458-470.

60. Kalifa, P., Menneteau, F.D., Quenard, D. (2000). "Spalling and Pore Pressure in HPC at High Temperatures." Cement and Concrete Research, vol. 30(12): pp. 1915-1927.

61. Kamen, A., Denarié, E., Brühwiler, E. (2007). "Thermal Effects on Physico-Mechanical Properties of Ultra-High-Performance Fiber-Reinforced Concrete." ACI Materials Journal, vol. 104(4): pp. 415-423.

62. Khaliq, W. (2012). "Performance characterization of high performance concretes under fire conditions." Doctoral dissertation, Michigan State University.

63. Khoury, G.A. (2000). "Effect of fire on concrete and concrete structures." Progress in Structural Engineering and Materials, vol. 2.4: pp. 429-447.

64. Kim, Y., Kim, G., Lee, T. (2009). "Mechanical properties of high-strength concrete subjected to high temperature by stressed test." Transactions of Nonferrous Metals Society of China, vol. 19: pp. s128-s133.

65. Klingsch, E. (2014). "Explosive spalling of concrete in fire." Doctoral dissertation, ETH Zurich.

66. Klingsch, E., Frangi, F. (2011). "Experimental analysis on changes of the porosity of ultrahigh performance concrete at elevated temperatures." 2nd International RILEM Workshop on Concrete Spalling due to Fire Exposure. RILEM Publications SARL.

67. Ko, J., Ryu, D., Noguchi, T. (2011). "The Spalling Mechanism of High-Strength Concrete Under Fire." Magazine of Concrete Research, vol. 63(5): pp. 357-370.

68. Kodur, V. (2014). "Properties of Concrete at Elevated Temperatures." ISRN Civ. Eng. pp. 1-15.

69. Kodur, V.K.R., Phan, L. (2007). "Critical Factors Governing the Fire Performance of High Strength Concrete Systems." Fire Safety Journal, vol. 42(6): pp. 482-488.

70. Khaliq, W., Kodur, V.K.R. (2011). "Effect of High Temperature on Tensile Strength of Different Types of High-Strength Concrete." ACI Materials Journal, vol. 108(4): pp. 394.

71. Kodur, V., Khaliq, W. (2011). "Effect of Temperature on Thermal Properties of Different Types of High-Strength Concrete." Journal of Materials in Civil Engineering, vol. 23(6): pp. 793-801.

72. Kosmatka, S.H. Wilson, M.L. (2011). "Design and Control of Concrete Mixtures." EB001, 15th edition, Portland Cement Association, Skokie, Illinois, USA, 460 pages.

73. Kusumawardaningsih, Y., Fehling, E., Ismail, M., Aboubakr, A.A.M. (2015). Tensile strength behavior of UHPC and UHPFRC. Procedia Engineering, vol. 125: pp. 1081-1086.

74. Li, H., Liu, G. (2016). "Tensile Properties of Hybrid Fiber-Reinforced Reactive Powder Concrete After Exposure to Elevated Temperatures." International Journal of Concrete Structures and Materials, vol. 10(1): pp. 29-37.

75. Li, Q., Yuan, G., Xu, Z., Dou, T. (2014). "Effect of elevated temperature on the mechanical properties of high-volume GGBS concrete." Magazine of Concrete Research, vol. 66(24): pp. 1277-1285.

76. Li, Z., Venkata, H.K., Rangaraju, P.R. (2015). "Influence of Silica flour–silica Fume Combination on the Properties of High Performance Cementitious Mixtures at Ambient Temperature Curing." Construction and Building Materials, vol. 100: pp. 225-233.

77. Lie, T.T., Kodur, V.K.R. (1996). "Thermal and mechanical properties of steel-fibre-reinforced concrete at elevated temperatures." Canadian Journal of Civil Engineering, vol. 23(2): pp. 511-517.

78. Lim, J., Moon, K., Falchetto, A.C., Jeong, J. (2016). "Testing and Modelling of Hygro-Thermal Expansion Properties of Concrete." KSCE Journal of Civil Engineering, vol. 20(2): pp. 709-717.

79. Liu, C.T., Huang, J.S. (2009). "Fire performance of highly flowable reactive powder concrete." Construction and Building Materials, vol. 23.5: pp. 2072-2079.

80. Magureanu, C., Sosa, I., Negrutiu, C., Heghes, B. (2012). "Mechanical Properties and Durability of Ultra-High-Performance Concrete." ACI Materials Journal, vol. 109(2): pp. 177.

81. Mindeguia, J., Carré, H., Pimienta, P., La Borderie, C. (2015). "Experimental Discussion on the Mechanisms Behind the Fire Spalling of Concrete." Fire and Materials, vol. 39(7): pp. 619-635.

82. Naser, M. Z., and Kodur, V.K.R. (2015). "A probabilistic assessment for classification of bridges against fire hazard." Fire Safety Journal, vol. 76: pp. 65-73.

83. National Fire Data Center (U.S.) (2017). "Fire in the United States, 2005-2014." Emmitsburg, MD: United States Fire Administration, National Fire Data Center.

84. Nazri, F.M., Jaya, R.P., Abu Bakar, B.H., Ahmadi, R. (2017). "Fire resistance of ultra-high performance fibre reinforced concrete due to heating and cooling." MATEC Web of Conferences. 87. EDP Sciences.

85. Nilson, A.H., Darwin, D., Dolan, C.W. (2010). “Design of Concrete Structures.” McGraw-Hill, New York, New York.

86. Peng, G.F., Yang, J., Long, Q.Q., Nin, X.J., Zeng, Q.P. (2016). “Comparison between Ultra-High-Performance Concretes with Recycled Steel Fiber and Normal Industrial Steel Fiber.” Fourth International Conference on Sustainable Construction Materials and Technologies, August 7-11, 2016.

87. Peng, G., Kang, Y., Huang, Y., Liu, X. & Chen, Q. (2012). "Experimental Research on Fire Resistance of Reactive Powder Concrete." Advances in Materials Science and Engineering, vol. 2012: pp. 1-6.

88. Phan, L.T. (1996). “Fire performance of high-strength concrete: A report of the state-of-the art.” US Department of Commerce, Technology Administration, National Institute of Standards and Technology, Office of Applied Economics, Building and Fire Research Laboratory, 1996.

89. Phan, L.T. (2008). "Pore Pressure and Explosive Spalling in Concrete." Materials and Structures, vol. 41(10): pp. 1623-1632.

90. Prem, P.R., Bharatkumar, B.H., Iyer, N.R. (2013). "Influence of Curing Regimes on Compressive Strength of Ultra High Performance Concrete." Sadhana, vol. 38(6): pp. 1421-1431.

91. Prem, P.R., Bharatkumar, B.H., Iyer, N.R. (2012). “Mechanical properties of Ultra High Performance Concrete.” International Journal of Civil, Environmental, Structural, Construction and Architectural Engineering, vol. 6(8): pp. 676-685.

92. Rahman, S., Molyneaux, T., Patnaikuni, I. (2005). "Ultra High Performance Concrete: Recent Applications and Research." Australian Journal of Civil Engineering, vol. 2(1): pp. 13.

93. Reda, M.M., Shrive, N.G., Gillott, J.E. (1999). "Microstructural investigation of innovative UHPC." Cement and Concrete Research, vol. 29(3): pp. 323-329.

94. Ren, W., Xu, J., Su, H. (2016). "Dynamic compressive behaviour of concrete after exposure to elevated temperatures." Materials and Structures, vol. 49(8): pp. 3321-3334.

95. Richard, P., Cheyrezy, M. (1995). "Composition of Reactive Powder Concretes." Cement and Concrete Research, vol. 25(7): pp. 1501-1511.

96. RILEM Technical Committee 200-HTC. (2007). “Recommendation of RILEM TC 200-HTC: mechanical concrete properties at high temperatures – modelling and applications: Part 1: Introduction-General presentation.” Mater. Struct., vol. 40: pp. 841-853.

97. RILEM Technical Committee 200-HTC. (2007). “Recommendation of RILEM TC 200-HTC: mechanical concrete properties at high temperatures—modelling and applications: Part 2: Stress–strain relation.” Mater. Struct., vol. 40: pp. 855–864.

98. Russell, H.G., Graybeal, B.A. (2013). “Ultra-High Performance Concrete: A State-Of-The-Art Report for the Bridge Community.” U.S. Department of Transportation, Federal Highway Administration, Research, Development, and Technology, Turner-Fairbank Highway Research Center, McLean, VA, 2013.

99. Sanchayan, S., Foster, S.J. (2016). "High Temperature Behaviour of Hybrid steel–PVA Fibre Reinforced Reactive Powder Concrete." Materials and Structures, vol. 49(3): pp. 769-782.

100. Sarhat, S.R., Sherwood, E.G. (2013). "Residual Mechanical Response of Recycled Aggregate Concrete after Exposure to Elevated Temperatures." Journal of Materials in Civil Engineering, vol. 25(11): pp. 1721-1730.

101. Schrefler, B.A., Majorana, C.E., Khoury, G.A., Gawin, D. (2002). "Thermo-hydro-mechanical modelling of high performance concrete at high temperatures." Engineering Computations, vol. 19.7: pp. 787-819.

102. So, H., Jang, H., Khulgadai, J., So, S. (2015). "Mechanical Properties and Microstructure of Reactive Powder Concrete using Ternary Pozzolanics Materials at Elevated Temperature." KSCE Journal of Civil Engineering, vol. 19(4): pp. 1050-1057.

103. So, H., Yi, J., Khulgadai, J., So, S. (2014). "Properties of Strength and Pore Structure of Reactive Powder Concrete Exposed to High Temperature." ACI Materials Journal, vol. 111(3): pp. 335.

104. Soliman, A.M., Nehdi, M.L. (2011). "Effect of Drying Conditions on Autogenous Shrinkage in Ultra-High Performance Concrete at Early-Age." Materials and Structures, vol. 44(5): pp. 879-899.

105. Sultan, M.A., Kodur, V.K.R. (2003). "Effect of Temperature on Thermal Properties of High-Strength Concrete." Journal of Materials in Civil Engineering, vol. 15(2): pp. 101-107.

106. Tai, Y.S., Pan, H.H., Kung, Y.N. (2011). "Mechanical Properties of Steel Fiber Reinforced Reactive Powder Concrete Following Exposure to High Temperature Reaching 800 °C." Nuclear Engineering and Design, vol. 241(7): pp. 2416-2424.

107. Ulm, F.J. (2008). “What's the matter with concrete?” Atti del XX Convegno Nazionale del Gruppo Italiano Frattura, vol. 3.

108. Voit, K., Kirnbauer, J. (2014). "Tensile Characteristics and Fracture Energy of Fiber Reinforced and Non-Reinforced Ultra High Performance Concrete (UHPC)." International Journal of Fracture, vol. 188(2): pp. 147-157.

109. Wang, D., Shi, C., Wu, Z., Xiao, J., Huang, Z., Fang, Z. (2015). "A review on ultra high performance concrete: Part II. Hydration, microstructure and properties." Construction and Building Materials, vol. 96: pp. 368-377.

110. Wang, J.J., Ren, F., DiPaolo, B.P. (2013). "Thermal Expansion Study and Microstructural Characterization of High-Performance Concretes." Journal of Materials in Civil Engineering, vol. 25.10: pp. 1574-8.

111. Wang, R., Gao, X. (2016). "Relationship between Flowability, Entrapped Air Content and Strength of UHPC Mixtures Containing Different Dosage of Steel Fiber." Applied Sciences, vol. 6(8): pp. 216.

112. Watanabe, K., Bangi, M.R., Horiguchi, T. (2013). "The effect of testing conditions (hot and residual) on fracture toughness of fiber reinforced high-strength concrete subjected to high temperatures." Cement and Concrete Research, vol. 51: pp. 6-13.

113. Way, R.T., Wille, K. (2015). "Effect of Heat-Induced Chemical Degradation on the Residual Mechanical Properties of Ultrahigh-Performance Fiber-Reinforced Concrete." Journal of Materials in Civil Engineering, vol. 28.4.

114. Wille, K., Naaman, A.E., Parra-Montesinos, G.J. (2011). "Ultra-High Performance Concrete with Compressive Strength Exceeding 150 MPa (22 ksi): A Simpler Way." ACI Materials Journal, vol. 108(1): pp. 46-54.

115. Xiao, R., Deng, Z., Shen, C. (2014). "Properties of Ultra High Performance Concrete Containing Superfine Cement and without Silica Fume." Journal of Advanced Concrete Technology, vol. 12(2): pp. 73-81.

116. Xiong, M.X., Liew, R.Y.J. (2015). "Spalling behavior and residual resistance of fibre reinforced Ultra-High performance concrete after exposure to high temperatures." Mater. Construction, vol. 65: pp. e071.

117. Yang, S.L., Millard, S.G., Soutsos, M.N., Barnett, S.J., Le, T.T. (2009). "Influence of aggregate and curing regime on the mechanical properties of ultra-high performance fibre reinforced concrete (UHPFRC)." Construction and Building Materials, vol. 23(6): pp. 2291-2298.

118. Yazıcı, H., Yardımcı, M.Y., Yiğiter, H., Aydın, S., Türkel, S. (2010). "Mechanical Properties of Reactive Powder Concrete Containing High Volumes of Ground Granulated Blast Furnace Slag." Cement and Concrete Composites, vol. 32(8): pp. 639-648.

119. Yazıcı, H., Yardımcı, M.Y., Aydın, S., Karabulut, A.Ş. (2009). "Mechanical Properties of Reactive Powder Concrete Containing Mineral Admixtures Under Different Curing Regimes." Construction and Building Materials, vol. 23(3): pp. 1223-1231.

120. Ye, H., Feng, N., Ling-hu, Y., Ran, Z., Lin, L., Qi, S., Dong, Y. (2012). "Research on Fire Resistance of Ultra-High-Performance Concrete." Advances in Materials Science and Engineering, vol. 2012: pp. 1-7.

121. Youssef, M.A., Moftah, M. (2007). "General stress–strain relationship for concrete at elevated temperatures." Engineering Structures, vol. 29(10): pp. 2618-2634.

122. Yu, K., Yu, J., Lu, Z., Chen, Q. (2016) "Fracture properties of high-strength/high-performance concrete (HSC/HPC) exposed to high temperature." Materials and Structures, vol. 49(11): pp. 4517-4532.

123. Zdeb, T. (2013). "Ultra-high performance concrete – properties and technology." Bull. Pol. Acad. Sci. Tech. Sci., vol. 61: pp. 183–193.

124. Zdeb, T. (2017). "An Analysis of the Steam Curing and Autoclaving Process Parameters for Reactive Powder Concretes." Construction and Building Materials, vol. 131: pp. 758-766.

125. Zheng, W., Luo, B., Lu, S. (2014a). "Rezistenta La Compresiune Si Încovoiere a Betoanelor Cu Continut De Pulberi Reactive Si Fibre Hibride La Temperaturi înalte/compressive and Tensile Strengths of Reactive Powder Concrete with Hybrid Fibres at Elevated Temperatures." Revista Romana de Materiale, vol. 44(1): pp. 36.

126. Zheng, W., Luo, B., Wang, Y. (2013). "Compressive and Tensile Properties of Reactive Powder Concrete with Steel Fibres at Elevated Temperatures." Construction and Building Materials, vol. 41: pp. 844-851.

127. Zheng, W., Luo, B., Wang, Y. (2014b). "Microstructure and Mechanical Properties of RPC Containing PP Fibres at Elevated Temperatures." Magazine of Concrete Research, vol. 66(8): pp. 397-408.

128. Zheng, W., Luo, B., Wang, Y. (2015). "Stress–strain Relationship of Steel-Fibre Reinforced Reactive Powder Concrete at Elevated Temperatures." Materials and Structures, vol. 48(7): pp. 2299-2314.

129. Zheng, W., Li, H., Wang, Y. (2012). "Compressive stress–strain Relationship of Steel Fiber-Reinforced Reactive Powder Concrete After Exposure to Elevated Temperatures." Construction and Building Materials, vol. 35: pp. 931-940.